DESY 94–115
CERN–TH. 7339/94
IC/94/154
July 1994

Model independent QED corrections to the process $ep \longrightarrow eX$ †

Arif Akhundov [1,2], Dima Bardin [3,4], Lida Kalinovskaya [4], Tord Riemann [5]

[1] International Centre for Theoretical Physics, Strada Costiera, 11, I–34014 Trieste, Italy

[2] Institute of Physics, Academy of Sciences of Azerbaijan, pr. Azizbekova 33, AZ–370143 Baku, Azerbaijan

[3] Theoretical Physics Division, CERN, CH–1211 Geneva 23, Switzerland

[4] Laboratory for Theoretical Physics, JINR, ul. Joliot-Curie 6, RU–141980 Dubna, Russia

[5] DESY – Institut für Hochenergiephysik, Platanenallee 6, D–15738 Zeuthen, Germany

ABSTRACT

We give an exhaustive presentation of the semi-analytical approach to the model independent leptonic QED corrections to deep inelastic neutral current lepton-nucleon scattering. These corrections include photonic bremsstrahlung from and vertex corrections to the lepton current of the order $\mathcal{O}(\alpha)$ with soft photon exponentiation. A common treatment of these radiative corrections in several variables – leptonic, hadronic, mixed, Jaquet-Blondel variables – has been developed and double differential cross-sections are calculated. In all sets of variables we use some structure functions, which depend on the hadronic variables and which do not have to be defined in the quark parton model. The remaining numerical integrations are twofold (for leptonic variables) or onefold (for all other variables). For the case of hadronic variables, all phase space integrals have been performed analytically. Numerical results are presented for a large kinematical range, covering fixed target as well as collider experiments at HERA or LEP⊗LHC, with a special emphasis on HERA physics.

† Supported by the Heisenberg-Landau fund.

Emails: AKHUNDOV@CERNVM.CERN.CH, BARDINDY@CERNVM.CERN.CH,
lika@thsun1.jinr.dubna.su, RIEMANN@CERNVM.CERN.CH

To the memory of our colleague and friend

Oleg Fedorenko

1951–1994

Contents

1 Introduction

The first deep inelastic scattering experiments have been performed at SLAC in 1968 and lead to the discovery of the parton structure of nucleons [1]. The cross-section of the reaction of figure 1,

$$e(k_1) + p(p_1) \to e(k_2) + X(p_2), \tag{1.1}$$

was determined at a transferred momentum of $\sqrt{Q^2} \sim 3$ GeV. The measurements were based on the registration of the scattered electron's energy and angle. The physical interpretation of the data took into account contributions from two important competing processes: the bremsstrahlung contribution to (1.1) of figure 2 with non-observed photon(s),

$$e(k_1) + p(p_1) \to e(k_2) + X(p_2) + n\gamma(k), \tag{1.2}$$

and also the elastic radiative tail, i.e. photonic bremsstrahlung in the elastic channel:

$$e(k_1) + p(p_1) \to e(k_2) + p(p_2) + n\gamma(k). \tag{1.3}$$

Analytical expressions for the cross-sections of these radiative corrections to (1.1) had been calculated in the classical work of Mo and Tsai [2]. They were of considerable importance for the interpretation of the data. In the long period between the SLAC experiment and the start-up of HERA, the experimental devices for the study of deep inelastic lepton-nucleon scattering had a relatively simple structure. Therefore, there was little need to radically improve the treatment of the radiative corrections as developed in [2]. On the other hand, rising experimental accuracy and considerably higher beam energies had to be met with corresponding improvements in the treatment of radiative corrections.

Originally motivated by the needs of the BCDMS experiment [3], a series of papers [4]–[9] was published by the Dubna group in the seventies and eighties. They all are devoted to the model independent semi-analytical calculation of QED corrections arising from the reactions (1.2) and (1.3). The QED corrections connected with the electrons are treated for processes with the virtual exchange of a photon between the lepton and the hadronic system. Applications to high energy muon scattering were first published in [5]. In [6], a technique was developed for a covariant treatment of the corrections, thus preventing the introduction of an unphysical parameter $\bar{\omega}$; this parameter was used in [2] to divide the contribution from (1.2) into two parts which describe soft and hard photons separately. A covariant form of the peaking approximation of [2] and of the soft photon exponentiation have been introduced in [7]. With the momentum transfer of $\sqrt{Q^2} \sim 10$ GeV in the BCDMS experiment, the Z-boson exchange had to be taken into account in the Born cross-section. Therefore, the structure functions became modified, and a new one describing parity violation had to be introduced [10]. All these developments, together with the contributions from QED lepton pair production [8] and the $\mathcal{O}(\alpha^2)$ corrections of the process (1.3) [9] have been included in the analytical program `TERAD86` [11]. A detailed comparison of the Mo and Tsai program with `TERAD86` may be found in [12].

So far, the theoretical description of deep inelastic scattering relied on a picture, where leptons with some couplings (electrical charge, weak neutral couplings) interact via a neutral current with a hadronic system, being described by structure functions. These contain the quark couplings and distributions. In this sense, a *factorization* of the matrix element into a leptonic and a hadronic part occured.

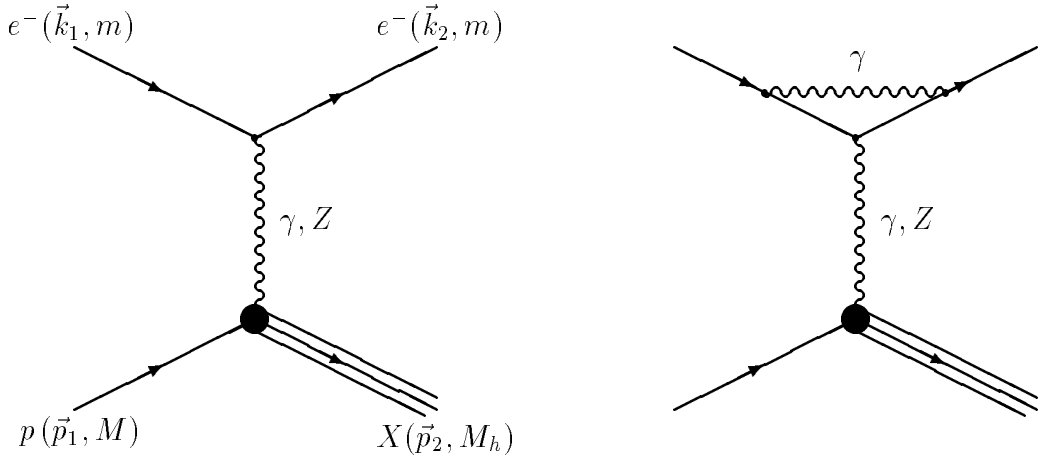

Figure 1: *Deep inelastic scattering of electrons off protons: (a) Born diagram, (b) leptonic vertex correction.*

In a next step, the complete treatment of electroweak Standard Model corrections to deep inelastic lepton-nucleon scattering was performed in [13], thereby covering both the complete $\mathcal{O}(\alpha)$ photonic corrections with soft photon exponentiation and the full set of weak one loop insertions. Such a complete treatment of the weak corrections unavoidably spoils the factorization between the electronic and the hadronic part of the cross section formula, which is the spiritual basis of the introduction of structure functions. See [14] for details. Therefore, the model independent approach to the radiative corrections has to be given up in favor of the quark parton model. The calculations in [13] go beyond the model independent approach in a second respect: A complete treatment of the photonic corrections includes photonic radiation from the hadronic state, containing as a part the electron-quark interference. The numerical calculations in the quark parton model approach were realized in the Fortran program `ASYMETR` [13]. At that time, the sophisticated treatment of these tiny effects which are covered in `ASYMETR` but not in `TERAD86` was not justified by experimental needs so that the program `ASYMETR` did not find a broader attention. The same happened with the early study published in [15], where a leading logarithmic calculation of leptonic QED corrections for *ep* scattering at HERA energies was performed. Recently, initiated by the HERA Physics Workshops, the Dubna-Zeuthen group updated the treatment of the weak one loop corrections and the renormalization scheme used in `ASYMETR`. Further, the QED part was recalculated, carefully checked, and considerably compactified [14], [16]; the related programs are `DISEPNC` and `DISEPCC`. The latter two programs use the weak library `DIZET` [17].

Recently, the experimental techniques have been improved considerably and much higher beam energies are reached. In deep inelastic fixed target experiments, transferred momenta of $\sqrt{Q^2} \sim 10$ GeV and $\sqrt{Q^2} \sim 17$ GeV were obtained at CERN [18] and Fermilab [19]. At HERA [20, 21, 22], the mass scale of the weak gauge bosons is in reach, $\sqrt{Q^2} \sim 100$ GeV. Moreover, the HERA detectors are much more sophisticated. As did the SLAC experiment, the recent fixed target experiments rely on the observation of the scattered electrons (muons) (with the notable exclusion of the neutral current neutrino scattering experiments [23]). By comparison, the HERA detectors H1 [24] and ZEUS [25] represent a new generation. They allow to detect the scattered electrons, the hadronic final state, and also photons with high

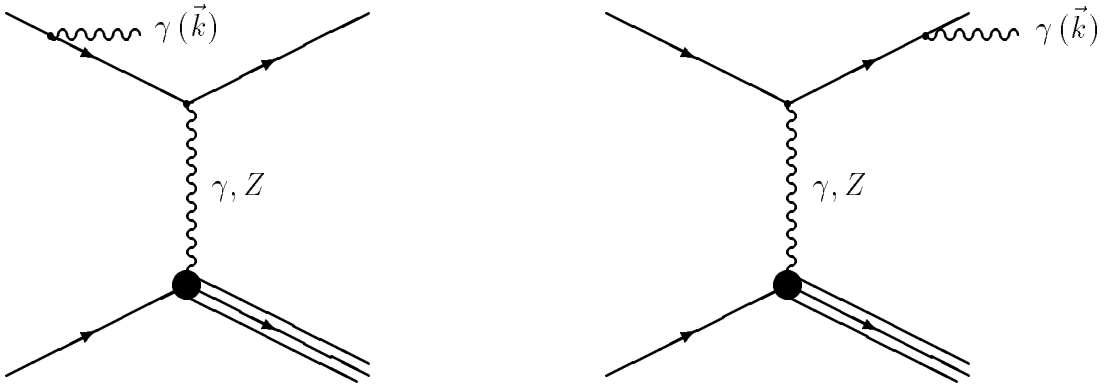

Figure 2: *The two leptonic bremsstrahlung diagrams.*

precision. Thus, for the physical analysis of the ep collisions at HERA one can use not only the familiar electron variables,

$$Q_l^2 = (k_1 - k_2)^2, \qquad y_l = \frac{p_1(k_1 - k_2)}{p_1 k_1}, \qquad x_l = \frac{Q_l^2}{y_l S}, \tag{1.4}$$

where

$$s = -(k_1 + p_1)^2 = S + m^2 + M^2 \approx 4E_e E_p, \tag{1.5}$$

but also the kinematical variables from the hadron measurement,

$$Q_h^2 = (p_2 - p_1)^2, \qquad y_h = \frac{p_1(p_2 - p_1)}{p_1 k_1}, \qquad x_h = \frac{Q_h^2}{y_h S}, \tag{1.6}$$

or some composition of both, the so-called mixed variables [26, 27]:

$$Q_m^2 = Q_l^2, \qquad y_m = y_h, \qquad x_m = \frac{Q_l^2}{y_h S}. \tag{1.7}$$

Here E_e, m and E_p, M are the energies and masses of incident electron and proton (see figure 1).

Another useful set of hadronic variables has been introduced by Jaquet and Blondel [28]:

$$Q_{\mathrm{JB}}^2 = \frac{(\vec{p}_2^{\perp})^2}{1 - y_h}, \qquad y_{\mathrm{JB}} = y_h, \qquad x_{\mathrm{JB}} = \frac{Q_{\mathrm{JB}}^2}{y_h S}. \tag{1.8}$$

Different choices of variables make no difference for the determination of the cross-section of reaction (1.1) in the Born approximation. Although, there are huge differences in the predictions for the radiative corrections, because the kinematics becomes quite different. This may be seen from the tetrahedron of momenta which is shown in figure 3. For vanishing photon momentum k, the simple Born kinematics is recovered. The differences concern the *calculation* of the corrections, but also, and maybe more important, their *numerical values.* In addition, the advanced HERA detectors allow the application of dedicated experimental cuts in the event selection which represent further potential problems for the calculation of radiative corrections. A satisfactory treatment relies almost exclusively on the use of the

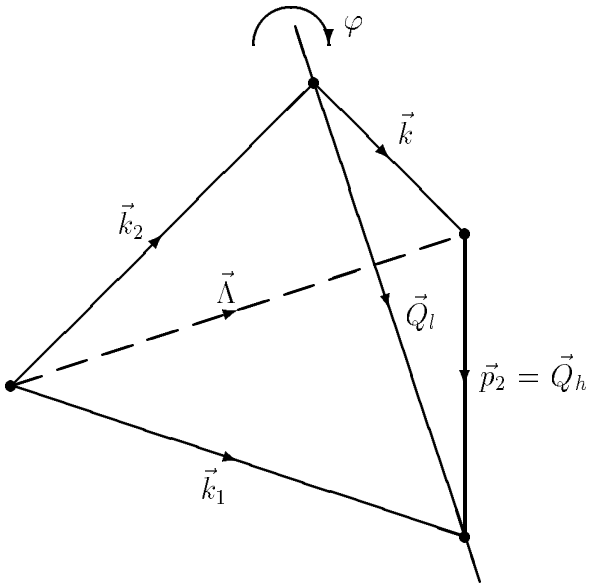

Figure 3: *Spatial configuration of the momenta in reaction (1.2) in the proton rest system.*

Monte-Carlo technique. Nevertheless, from the data with sometimes complicated cuts, it is usually possible to reconstruct some sufficiently inclusive and smooth cross-sections. These cross-sections then may be the subject of further study by a semi-analytical approach as is advocated here.

The HERA physics workshops in 1987 [21] and 1991 [22] lead to an enhanced activity both in the search for new results and in the comparison between the results of different authors [29]. Several authors obtained new results for the radiative corrections using quite different techniques, which we quote here for completeness: leading logarithmic calculations [30]–[34], Monte-Carlo approaches [35]–[37], and semi-analytical approaches [14, 16, 38, 39, 40, 41] for both the neutral current and the charged current reactions at HERA. Eventually, all groups were able to reproduce the numerical results of the above mentioned series of papers of the Dubna-Zeuthen group with reasonable precision [42] and, of course, to go beyond in many other aspects [29].

In the following, we will restrict ourselves to neutral current scattering. The Born cross-section is:

$$\frac{d^2\sigma_{\rm B}}{dydQ^2} = \frac{2\pi\alpha^2}{S}\sum_{i=1}^{3}\mathcal{A}_i(x,Q^2)\frac{1}{Q^4}\,\mathcal{S}_i^{\rm B}(y,Q^2),$$

with the kinematical factors

$$\begin{aligned}
\mathcal{S}_1^{\rm B}(y,Q^2) &= Q^2,\\
\mathcal{S}_2^{\rm B}(y,Q^2) &= 2(1-y)S^2,\\
\mathcal{S}_3^{\rm B}(y,Q^2) &= 2Q^2(2-y)S.
\end{aligned}$$

The generalized structure functions $\mathcal{A}_i(x,Q^2)$ describe the electroweak interactions of the electrons with the protons via the exchange of a photon or Z boson and will be defined later.

It is well-known from the above mentioned earlier studies, e.g. from [14], that a treatment of the leptonic photonic corrections covers the bulk of the complete corrections to this cross-section. Fortunately, both types of corrections – weak loop insertions and QED corrections related to the hadronic current – are relatively small. For a large part of the kinematical region they are below the experimental accuracy. If the experimental intention is a study of the hadronic current, one may be interested in a model independent description of the cross-section which not necessarily uses the quark parton model. With the last remarks, the line of thought which we will follow from now on in this article is indicated:
This article is devoted to complete, model independent, semi-analytical calculations of leptonic corrections to neutral current deep inelastic lepton-nucleon scattering in different kinematical variables. By *complete* we mean the full $\mathcal{O}(\alpha)$ corrections with soft photon exponentiation which are not restricted to the leading logarithmic approximation. By *semi-analytical* we understand that the Monte-Carlo technique is not used. We perform as many analytical integrations as is possible for a given set of kinematical variables instead. In order to get a double differential cross-section, one has to perform three phase space integrations. In principle, one is interested to describe the cross-sections with structure functions which may have an arbitrary dependence on the variables x_h, Q_h^2. Then, for the case of *leptonic* variables, only one analytical integration, for the case of *Jaquet-Blondel* variables or for *mixed* variables – two integrations, and for *hadronic* variables all three phase space integrations may be performed analytically.

In the above discussion, the characteristic elements of the calculation of real bremsstrahlung corrections have been introduced:

- Choice of a reasonable phase space parameterization with a practical set of internal variables which are to be integrated over;
- Choice of the order of integration and complete understanding of the corresponding kinematical boundaries, by necessity without neglect of masses;
- Separation of the infrared singular part of the bremsstrahlung integral with use of a special rest system which has to be chosen appropriately;
- Dedicated performance of the various hard bremsstrahlung integrations which are regulated or finite in the soft photon part of the phase space;
- Calculation of the infrared divergent correction with a reasonable regularization procedure. Consecutively, compensation of the infrared singularity with that of the virtual corrections and elimination of the soft and hard photon separation with establishment of the lorentz invariance of the net correction.

In order to give an impression of the spirit of the approach we quote here an expression which contains the complete leptonic QED corrections to order $\mathcal{O}(\alpha)$ with soft-photon exponentiation to the Born cross-section (1.9):

$$\frac{d^2\sigma}{dy_h dQ_h^2} = \frac{d^2\sigma_{\rm B}}{dy_h dQ_h^2} \exp\left[\frac{\alpha}{\pi}\delta_{\rm inf}(y_h, Q_h^2)\right] + \frac{2\alpha^3}{S}\sum_{i=1}^{3}\frac{1}{Q_h^4}\mathcal{A}_i(x_h, Q_h^2)\mathcal{S}_i(y_h, Q_h^2).$$

The soft photon corrections factorize with the Born cross-section. They are exponentiated in order to take into account the multiple soft photon emission:

$$\delta_{\rm inf}(y_h, Q_h^2) = \left(\ln\frac{Q_h^2}{m^2} - 1\right)\ln(1-y_h). \tag{1.9}$$

The hard bremsstrahlung corrections are taken into account to order $\mathcal{O}(\alpha)$. They do not factorize but lead to modifications of the functions $\mathcal{S}_i^{\rm B}$ while the generalized structure functions $\mathcal{A}_i(x,Q^2)$ remain unchanged:

$$\begin{aligned}
\mathcal{S}_1(y_h,Q_h^2) &= Q_h^2\Bigg[\frac{1}{4}\ln^2 y_h - \frac{1}{2}\ln^2(1-y_h) - \ln y_h\ln(1-y_h) - \frac{3}{2}{\rm Li}_2(y_h) + \frac{1}{2}{\rm Li}_2(1) \\
&\quad -\frac{1}{2}\ln y_h {\rm L_h} + \frac{1}{4}\left(1+\frac{2}{y_h}\right){\rm L_{h_1}} + \left(1-\frac{1}{y_h}\right)\ln y_h - \left(1+\frac{1}{4y_h}\right)\Bigg], \\
\mathcal{S}_2(y_h,Q_h^2) &= S^2\Bigg[-\frac{1}{2}y_h\ln^2 y_h - (1-y_h)\ln^2(1-y_h) - 2(1-y_h)\ln y_h\ln(1-y_h) - y_h{\rm Li}_2(1) \\
&\quad -(2-3y_h){\rm Li}_2(y_h) + y_h\ln y_h {\rm L_h} + \frac{y_h}{2}(1-y_h){\rm L_{h_1}} - \frac{y_h}{2}(2-y_h)\ln y_h\Bigg], \\
\mathcal{S}_3(y_h,Q_h^2) &= SQ_h^2\Bigg\{-(2-y_h)\Bigg[-\frac{1}{2}\ln^2 y_h + \ln^2(1-y_h) + 2\ln y_h\ln(1-y_h) + 3{\rm Li}_2(y_h) \\
&\quad -{\rm Li}_2(1) + \ln y_h + \ln y_h {\rm L_h}\Bigg] + \frac{3}{2}y_h{\rm L_{h_1}} + y_h - \frac{7}{2} + 2\ (1-2y_h)\ln y_h\Bigg\},
\end{aligned} \tag{1.10}$$

with ${\rm L_h} = \ln(Q_h^2/m^2)$ and ${\rm L_{h_1}} = {\rm L_h} + \ln[y_h/(1-y_h)]$.

Since the structure functions depend on the hadronic variables and are hardly to be integrated over together with radiative corrections, such a compact result may be obtained only in hadronic variables.

The purpose of the present article is fourfold:

- We give a systematic presentation of the model independent approach to the leptonic QED corrections in terms of leptonic variables, thereby compactifying known results and transforming them into a modern terminology.
- The complicated kinematics of deep inelastic scattering is explained in great detail for leptonic, mixed, hadronic, and Jaquet-Blondel variables. We systematically retain both the electron and the proton masses if needed. This is necessary for many intermediate steps of the calculation of QED corrections.
- The complete leptonic QED corrections to order $\mathcal{O}(\alpha)$ with soft photon exponentiation in terms of mixed, hadronic, and Jaquet-Blondel variables are reviewed here for the first time[1].

[1] With the exception of [43] which contains a short communication about QED corrections with the use of Jaquet-Blondel variables.

- The contents of this article is the theoretical framework for the Fortran program `TERAD91` [38][2]. This program is used here for a systematic numerical study of the QED corrections for a wide kinematical range: fixed target deep inelastic μp scattering, ep scattering at HERA, and ep scattering at LEP$\otimes$LHC [45]. Naturally, the main emphasis will be on applications to HERA physics.

The article is organized as follows. After an introduction of notations and of the Born cross-section the radiative process (1.2) is described in section 2. In section 3, the phase space is parameterized such that the analytical integrations we aim at may be performed. A first integration will be carried out there. After this, the further treatment of the phase space will depend on the choice of kinematical variables. In section 4, we isolate and handle the infrared singularity, thereby defining soft and hard cross-section parts in a covariant way. The soft photon exponentiation is performed. All this will be done separately for leptonic, mixed, and hadronic variables. The integrated cross-section in the three above-mentioned variables is derived in section 5. There, for the case of mixed and hadronic variables, a second analytical integration is performed. Numerical results for the QED corrections at three different accelerator scenarios will be compared. In section 6, we introduce the necessary modifications for an accurate treatment of the photoproduction region. Section 7 contains a parameterization of the phase space, which deviates from that introduced in section 3. This parameterization will allow us to derive compact formulae for the QED corrections in terms of Jaquet-Blondel and hadronic variables. For the case of hadronic variables we perform all three phase space integrations analytically, thus obtaining a double differential cross-section formula for the QED corrections without any integration being left. Section 8 contains a discussion. It includes a comparison with estimates which are based on the leading logarithmic approximation, a study of the influence of different choices of structure functions on the relative size of the radiative corrections, an example of cuts on the photon kinematics, and an outlook. In appendix A, we derive several phase space parameterizations, which are used in the calculations. In appendix B, the kinematical boundaries for the different variable sets are studied. The photons are treated totally inclusively in the main body of this article. Appendix B.1.2 is an exclusion to this. It contains some formulae with cuts on the photonic variables. Several tables of integrals which have to be used in order to perform the many integrations are listed in appendices D and E for the different phase space parameterizations. For completeness, we collect the cross-sections in leading logarithmic approximation which have been used for comparisons in appendix F.

2 Matrix elements and differential cross-sections

2.1 The Born process $ep \to eX$

In order to define the notations, we collect some basic formulae for the Born process (1.1). The matrix element which corresponds to the diagram shown in figure 1a is

$$\mathcal{M}^{\mathrm{B}} = \frac{s_e e^2}{(2\pi)^2}(2\pi)^3\langle p_2|\mathcal{J}_\mu|p_1\rangle\frac{1}{Q^2}\bar{u}(k_2)\left\{|Q_e|\gamma_\mu + \chi\gamma_\mu\left(v_e + a_e\gamma_5\right)\right\}u(k_1), \qquad (2.1)$$

[2] A short collection of some of the main formulae, though in an old notation, may be found in [44].

where v_e and a_e are the vector and axial-vector couplings of the electron to the Z boson:

$$v_e = 1 - 4|Q_e| \sin^2 \theta_W, \qquad a_e = 1. \tag{2.2}$$

Here, θ_W is the weak mixing angle $\sin^2 \theta_W = 1 - M_W^2/M_Z^2$ and $s_e|Q_e| = Q_e = -1$ is the electron charge. Further,

$$\chi = \chi(Q^2) = \frac{G_\mu}{\sqrt{2}} \frac{M_Z^2}{8\pi\alpha} \frac{Q^2}{Q^2 + M_Z^2}, \tag{2.3}$$

with the finestructure constant $\alpha = 1/137.06$, the Fermi constant $G_\mu = 1.16637 \cdot 10^{-5}$ GeV^{-2}, and the Z boson mass M_Z. In the numerical examples, we will use the following values: $\sin^2 \theta_W = 0.228$, $M_Z = 91.173$ GeV.

The cross-section of the reaction (1.1),

$$d\sigma_{\rm B} = 2\frac{(2\pi)^2 p_1^0}{\sqrt{\lambda_S}} \sum_{\rm spins} \left|\mathcal{M}^{\rm B}\right|^2 \frac{d\vec{k}_2}{2k_2^0} \prod_i \frac{d\vec{p}_i}{2p_i^0} \delta^4(k_1 + p_1 - k_2 - \sum_i p_i), \tag{2.4}$$

$$\lambda_S = S^2 - 4m^2 M^2, \tag{2.5}$$

depends on three variables, e.g. on S, the momentum transfer Q, and the energy transfer ν:

$$S = -2p_1 k_1, \qquad Q^2 = (p_2 - p_1)^2, \qquad \nu = -2p_1 Q. \tag{2.6}$$

In the following, we will use also the Bjorken scaling variables y and x, the parton momentum fraction,

$$y = \frac{\nu}{S}, \qquad x = \frac{Q^2}{\nu}, \tag{2.7}$$

with

$$Q^2 = xyS. \tag{2.8}$$

The phase space element of the Born process is:

$$\begin{aligned} d\Gamma_{\rm B} &= \frac{d\vec{k}_2}{2k_2^0} \prod_i \frac{d\vec{p}_i}{2p_i^0} \delta^4(k_1 + p_1 - k_2 - \sum_i p_i) \\ &= \frac{d\vec{k}_2}{2k_2^0} \frac{d\vec{p}_2}{2p_2^0} dM_h^2 \delta^4(k_1 + p_1 - k_2 - p_2) d\Gamma_h \\ &= \frac{\pi S}{2\sqrt{\lambda_S}} dy dQ^2 d\Gamma_h. \end{aligned} \tag{2.9}$$

In the last step, the integral over p_2 has been performed with the aid of the δ-function. The integral over k_2 is performed in appendix A.4.1. Further, we introduced the phase space element of the hadron system in the final state $d\Gamma_h$ and its invariant mass M_h:

$$d\Gamma_h = \prod_i \frac{d\vec{p}_i}{2p_i^0} \delta^4(p_2 - \sum_i p_i), \qquad M_h^2 = -p_2^2. \tag{2.10}$$

In the following, the $d\Gamma_h$ will become part of the definition of the hadronic structure functions.

With our definitions we follow [46],

$$\frac{p_1^0}{M}\sum_{\text{spins}}\left|\mathcal{M}^{\rm B}\right|^2 = \frac{e^4}{(2\pi)^4 Q^4}\left(\mathcal{S}^{{\rm B}\gamma}_{\mu\nu}W^{\gamma}_{\mu\nu} + 2\chi\mathcal{S}^{\rm BI}_{\mu\nu}W^{I}_{\mu\nu} + \chi^2\mathcal{S}^{\rm BZ}_{\mu\nu}W^{Z}_{\mu\nu}\right), \tag{2.11}$$

where $\mathcal{S}^{\rm BA}_{\mu\nu}$ and $W^A_{\mu\nu}$, $A = \gamma, I, Z$, are the corresponding components of the leptonic and hadronic tensors.

The phenomenological hadronic tensors $W^A_{\mu\nu}$ [10],

$$\begin{aligned} W^A_{\mu\nu} &= (2\pi)^6\frac{p_1^0}{M}\sum\int\langle p_1|\mathcal{J}^{\gamma,Z}_{\mu}|p_2\rangle\langle p_2|\mathcal{J}^{\gamma,Z}_{\nu}|p_1\rangle d\Gamma_h \\ &\equiv W^A_1(\delta_{\mu\nu}-\frac{Q_\mu Q_\nu}{Q^2}) + \frac{W^A_2}{M^2}(p_{1\mu}-\frac{p_1Q}{Q^2}Q_\mu)(p_{1\nu}-\frac{p_1Q}{Q^2}Q_\nu) + \frac{W^A_3}{2M^2}e_{\mu\nu\rho\sigma}p_{1\rho}Q_\sigma, \end{aligned} \tag{2.12}$$

describe the deep inelastic interactions of unpolarized nucleons with a photon and a Z boson. The real scalar functions W^A_a depend on the invariants Q^2 and ν.

After neglecting in the contractions in (2.11) those terms from the squared Z exchange, which are proportional to $a_e^2m^2$, one observes a factorization of the leptonic and hadronic parts of the Born cross-section:

$$\frac{d^2\sigma_{\rm B}}{dydQ^2} = \frac{2\pi\alpha^2}{\lambda_S}S\sum_{i=1}^{3}\mathcal{A}_i(x,Q^2)\frac{1}{Q^4}\,\mathcal{S}^{\rm B}_i(y,Q^2). \tag{2.13}$$

The factorized functions $\mathcal{S}^{\rm B}_i$ are:

$$\mathcal{S}^{\rm B}_1(y,Q^2) = Q^2-2m^2, \tag{2.14}$$
$$\mathcal{S}^{\rm B}_2(y,Q^2) = 2[(1-y)S^2-M^2Q^2], \tag{2.15}$$
$$\mathcal{S}^{\rm B}_3(y,Q^2) = 2Q^2(2-y)S. \tag{2.16}$$

The factorized hadronic functions $\mathcal{A}_i(x,Q^2)$ describe the electroweak interactions of leptons with beam charge Q_e and a lepton beam polarization ξ via the exchange of a photon or Z boson with unpolarized nucleons:

$$\begin{aligned} \mathcal{A}_1(x,Q^2) &\equiv (2MW_1) &&= 2\mathcal{F}^{\rm NC}_1(x,Q^2), \\ \mathcal{A}_2(x,Q^2) &\equiv \frac{1}{yS}(\nu W_2) &&= \frac{1}{yS}\mathcal{F}^{\rm NC}_2(x,Q^2), \\ \mathcal{A}_3(x,Q^2) &\equiv \frac{1}{2Q^2}(\nu W_3) &&= \frac{1}{2Q^2}\mathcal{F}^{\rm NC}_3(x,Q^2). \end{aligned} \tag{2.17}$$

The generalized structure functions $\mathcal{F}^{\rm NC}_i(x,Q^2)$ are:

$$\begin{aligned} \mathcal{F}^{\rm NC}_{1,2}(x,Q^2) &= F_{1,2}(x,Q^2) + 2|Q_e|\,(v_e+\lambda a_e)\,\chi(Q^2)G_{1,2}(x,Q^2) \\ &\quad + 4\left(v_e^2+a_e^2+2\lambda v_e a_e\right)\chi^2(Q^2)H_{1,2}(x,Q^2), \end{aligned} \tag{2.18}$$

$$\begin{aligned} \mathcal{F}^{\rm NC}_3(x,Q^2) &= -2\ \mathrm{sign}(Q_l)\Big\{|Q_e|\,(a_e+\lambda v_e)\,\chi(Q^2)xG_3(x,Q^2) \\ &\quad +2\left[2v_ea_e+\lambda\left(v_e^2+a_e^2\right)\right]\chi^2(Q^2)xH_3(x,Q^2)\Big\}, \end{aligned} \tag{2.19}$$

with $\lambda = \xi\,\mathrm{sign}(Q_l)$. In the above formulae, the Q_l is the charge of the lepton beam.

The contribution of the weak loop corrections to (1.1) is not within the scope of the present article. We only mention that these corrections may be covered by an inclusion of real-valued weak form factors into the definitions of the weak neutral couplings (2.2). Such a program has been carried through first in [14], and was described and updated also in [47].

The generalized structure functions $\mathcal{F}_i^{\mathrm{NC}}(x,Q^2)$ may also be used to describe some new phenomena, e.g. the virtual exchange of an additional heavy gauge boson Z' [48].

The running of the QED coupling α may be taken into account by a real form factor:

$$\alpha(Q^2) = \frac{\alpha}{1-\sum_f Q_f^2 N_f \Delta F_f(Q^2)}, \tag{2.20}$$

$$\Delta F_f(Q^2) = \frac{\alpha}{\pi}\left[-\frac{5}{9}+\frac{4}{3}\frac{m_f^2}{Q^2}+\frac{1}{3}\beta_f\left(1-\frac{2m_f^2}{Q^2}\right)\ln\frac{\beta_f+1}{\beta_f-1}\right], \tag{2.21}$$

$$\beta_f = \sqrt{1+\frac{4m_f^2}{Q^2}}. \tag{2.22}$$

The sum in (2.20) extends over all charged fermions f, Q_f is the corresponding electric charge, and N_f the color factor: $N_f = 3, 1$ for quarks and leptons, respectively. The heavy fermions practically decouple in (2.20). For light fermions, with $m_f^2 << Q^2$, the following approximate formula is valid:

$$\Delta F_f(Q^2) = \frac{\alpha}{3\pi}\left(\ln\frac{Q^2}{m_f^2}-\frac{5}{3}\right). \tag{2.23}$$

The numerical factors in (2.18)–(2.19) are chosen such that some often used definitions of the structure functions in the quark parton model are matched. Assuming here the Callan-Gross relation, it is

$$\begin{aligned}
2xF_1(x,Q^2) &= F_2(x,Q^2) &&= x\sum_q |Q_q|^2\,[q(x,Q^2)+\bar q(x,Q^2)],\\
2xG_1(x,Q^2) &= G_2(x,Q^2) &&= x\sum_q |Q_q|\,v_q\,[q(x,Q^2)+\bar q(x,Q^2)],\\
2xH_1(x,Q^2) &= H_2(x,Q^2) &&= x\sum_q \tfrac{1}{4}\left(v_q^2+a_q^2\right)[q(x,Q^2)+\bar q(x,Q^2)],\\
&\quad xG_3(x,Q^2) &&= x\sum_q |Q_q|\,a_q\,[q(x,Q^2)-\bar q(x,Q^2)],\\
&\quad xH_3(x,Q^2) &&= x\sum_q \tfrac{1}{2}\,v_q a_q\,[q(x,Q^2)-\bar q(x,Q^2)].
\end{aligned} \tag{2.24}$$

These definitions should help the reader to find a link to other articles on the subject, which often prefer the use of a slightly different notation (remind that we use the definition $a_f = 1$ for all fermions). A comprehensive presentation of the basic formulae for the description of deep inelastic scattering may be found in [49].

The allowed region of the variables y and Q^2 is derived in appendix B.2.1 and shown in figure 4. In the following, sometimes the exact expressions in the electron and the proton masses are needed. So, in the figures with kinematics we will not apply the ultra-relativistic approximation.

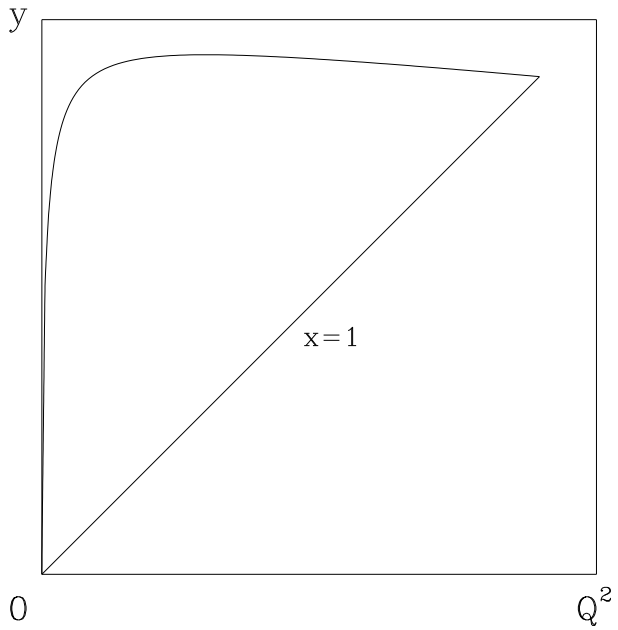

Figure 4: *Physical region of the variables y and Q^2.*

In figure 5, we show the Born cross-section (2.13), rewritten as a function of x and Q^2:

$$\frac{d^2\sigma_{\rm B}}{dxdQ^2} = \frac{2\pi\alpha^2}{xQ^4}\Bigg\{2\left(1-y-xy\frac{M^2}{S}\right)\mathcal{F}_2^{\rm NC}(x,Q^2)+2xy^2\left(1-2\frac{m^2}{Q^2}\right)\mathcal{F}_1^{\rm NC}(x,Q^2) + y(1-y)\mathcal{F}_3^{\rm NC}(x,Q^2)\Bigg\}. \tag{2.25}$$

At small Q^2 the neglect of the Z exchange is a good approximation:

$$\frac{d^2\sigma_{\rm B}^{\gamma}}{dxdQ^2} = \frac{2\pi\alpha^2}{xQ^4}\left[2\left(1-y\right)-2xy\frac{M^2}{S}+\left(1-2\frac{m^2}{Q^2}\right)\left(1+4x^2\frac{M^2}{Q^2}\right)\frac{y^2}{1+R}\right]\mathcal{F}_2^{\gamma}(x,Q^2), \tag{2.26}$$

where R is the ratio of the cross-sections with virtual exchange of longitudinal and transverse photons, respectively:

$$R(x,Q^2)=\frac{\sigma_L}{\sigma_T}=\left(1+4x^2\frac{M^2}{Q^2}\right)\frac{\mathcal{F}_2^{\gamma}(x,Q^2)}{2x\mathcal{F}_1^{\gamma}(x,Q^2)}-1. \tag{2.27}$$

This cross-section formula becomes in the ultra-relativistic approximation:

$$\frac{d^2\sigma_{\rm B}^{\gamma}}{dxdQ^2}=\frac{2\pi\alpha^2}{xQ^4}\left[Y_+\mathcal{F}_2^{\gamma}(x,Q^2)-y^2\mathcal{F}_L^{\gamma}(x,Q^2)\right], \tag{2.28}$$

where the notations

$$\begin{aligned}\mathcal{F}_L^{\gamma}(x,Q^2) &= \mathcal{F}_2^{\gamma}(x,Q^2)-2x\mathcal{F}_1^{\gamma}(x,Q^2)\\ &= 2x\mathcal{F}_1^{\gamma}(x,Q^2)R(x,Q^2)\end{aligned} \tag{2.29}$$

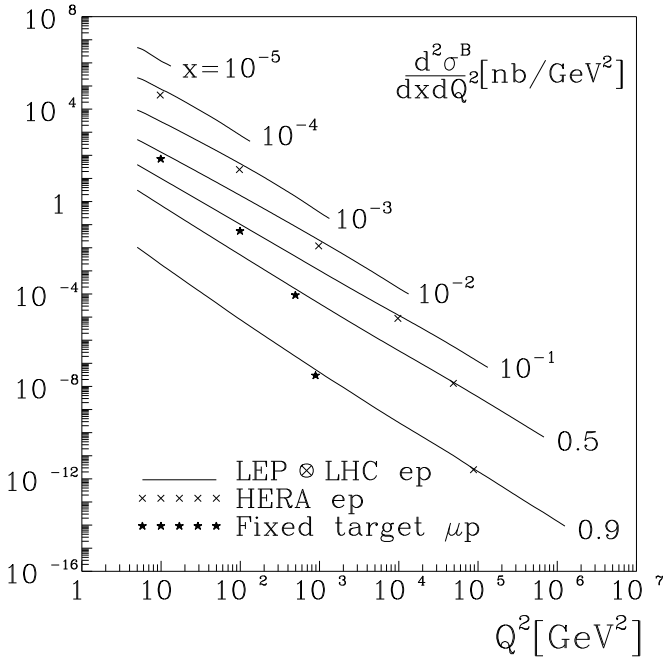

Figure 5: *Born cross-section $d^2\sigma^{\rm B}/dxdQ^2$ for deep inelastic neutral current scattering as function of* $\ln Q^2$ *with x as a parameter.*

and

$$Y_\pm = 1 \pm (1-y)^2 \tag{2.30}$$

are introduced. The cross-section (2.25) becomes in the ultra-relativistic approximation:

$$\frac{d^2\sigma_{\rm B}}{dxdQ^2} = \frac{2\pi\alpha^2}{xQ^4}\left[Y_+\mathcal{F}_2^{\rm NC}(x,Q^2) + Y_-\mathcal{F}_3^{\rm NC}(x,Q^2)\right]. \tag{2.31}$$

Here, we additionally assume the validity of the Callan-Gross relation [50]:

$$\mathcal{F}_2^{\rm NC}(x,Q^2) = 2x\mathcal{F}_1^{\rm NC}(x,Q^2). \tag{2.32}$$

In the numerical examples, we will cover three typical kinematical regions: that of fixed target muon scattering ($S = 1000$ GeV^2), of the ep collider HERA ($S = 4\cdot 30\cdot 820$ GeV^2), and of the ep collider project LEP$\otimes$LHC ($S = 4\cdot 50\cdot 7000$ GeV^2). The solid curves in figure 5 are calculated for LEP$\otimes$LHC. They start at $Q^2 = 5$ GeV^2, the approximate lower limit of applicability of the structure functions which are derived from the available data. For a given value of x, the highest value of Q^2 depends on S. This boundary derives from (2.8), taken at $y = 1$, and is seen in the figure. Further, the actual value of S has an influence on the cross-sections (2.31) via the functions $Y_\pm$. This leads to different predictions for the fixed target and HERA kinematics. The stars (for fixed targets) and crosses (for HERA) in the figure indicate the corresponding cross-section values at the maximal allowed Q^2 for given x. The first curve which shows a prediction for the fixed target case, e.g., is that for $x = 10^{-2}$. Smaller values of x are outside the kinematical range for $Q^2 > 5$ GeV^2. The influence of S

on the predictions is minor (in the variables and scales, which are chosen here). In the double logarithmic representation, the cross-sections are nearly linear functions over the complete kinematical region. The cross-section behaviour is determined by the characteristic $1/(xQ^4)$ dependence. The $1/Q^4$ arises from the photon propagator (and, at very high energies, also from the Z propagator). The event rates are highest for the smallest values of x and Q^2. With the lower bound on Q^2 being fixed, the accessible kinematical range in x and Q^2 rises considerably with the available beam energies, although the event rates at the highest values of x and Q^2 are substantially suppressed.

In sum, the ep collider with the highest accessible beam energies will open the field not only for a study of very deep inelastic scattering, but also, at high rates, the study of the region of very small x.

The cross-section predictions may depend crucially on the choice of structure functions. For the illustrational purposes, we decided to use the MRS D$'_-$ parameterization in the DIS scheme [51] as it is compiled in [52]. The influence of the structure functions on the theoretical predictions, including the numerical values of the QED corrections, will be a subject of the discussion.

2.2 The radiative process $ep \to eX\gamma$

The differential cross-section for the scattering of electrons off protons (1.2), originating from the Feynman diagrams of figure 2, may be derived from the following matrix element:

$$\begin{aligned}\mathcal{M}^{\mathrm{R}} &= \frac{s_e Q_e e^3}{(2\pi)^{7/2}}\epsilon_\alpha(k)(2\pi)^3\langle p_2|\mathcal{J}_\mu|p_1\rangle\frac{1}{Q_h^2}\\ &\times\ \bar{u}(k_2)\Bigg\{|Q_e|\left[\frac{1}{z_1}\gamma_\mu\left(2k_{1\alpha}-\hat{k}\gamma_\alpha\right)-\frac{1}{z_2}\left(2k_{2\alpha}+\gamma_\alpha\hat{k}\right)\gamma_\mu\right]\\ &+\ \chi\left[\frac{1}{z_1}\gamma_\mu\left(v_e+a_e\gamma_5\right)\left(2k_{1\alpha}-\hat{k}\gamma_\alpha\right)-\frac{1}{z_2}\left(2k_{2\alpha}+\gamma_\alpha\hat{k}\right)\gamma_\mu\left(v_e+a_e\gamma_5\right)\right]\Bigg\}u(k_1),\end{aligned} \tag{2.33}$$

where the electron propagators have the denominators z_1 or z_2:

$$z_1 = -2k_1k, \qquad z_2 = -2k_2k. \tag{2.34}$$

The corresponding cross-section[3],

$$d\sigma_{\mathrm{R}} = 2\frac{(2\pi)^2p_1^0}{\sqrt{\lambda_S}}\sum_{\text{spins}}\left|\mathcal{M}^{\mathrm{R}}\right|^2\delta^4(k_1+p_1-k_2-\sum_i p_i-k)\frac{d\vec{k}_2}{2k_2^0}\frac{d\vec{k}}{2k^0}\prod_i\frac{d\vec{p}_i}{2p_i^0}, \tag{2.35}$$

may be rewritten as follows:

$$d\sigma_{\mathrm{R}} = \frac{8\alpha^3}{\pi^2\sqrt{\lambda_S}}\frac{1}{Q_h^4}\mathcal{S}d\Gamma, \tag{2.36}$$

[3]The squaring of the Feynman diagrams has been performed with the program for algebraic manipulations SCHOONSCHIP [53].

where

$$\mathcal{S} = \frac{1}{2} M \left(\mathcal{S}^{\gamma}_{\mu\nu} W^{\gamma}_{\mu\nu} + 2\chi \mathcal{S}^{\mathrm{I}}_{\mu\nu} W^{I}_{\mu\nu} + \chi^2 \mathcal{S}^{\mathrm{Z}}_{\mu\nu} W^{Z}_{\mu\nu} \right), \tag{2.37}$$

and

$$d\Gamma \;=\; \frac{d\vec{k}_2}{2k_2^0} \frac{d\vec{p}_2}{2p_2^0} \frac{d\vec{k}}{2k^0} dM_h^2 \delta^4(k_2 + p_2 + k - k_1 - p_1). \tag{2.38}$$

The sum (2.37) may be treated exactly in the masses of electron m and proton M. As mentioned above, the Born cross-section (2.13) exhibits a nice factorization property. We have shown explicitly, that the same is true for the radiative cross-section after a neglection of the tiny terms proportional to $\chi^2 a_e^2 m^2 / z_{1(2)}$ and $\chi^2 a_e^2 m^4 / z_{1(2)}^2$:

$$\mathcal{S} \equiv \mathcal{S}(\mathcal{E}, \mathcal{I}, z_1, z_2) = \sum_{i=1}^{3} \mathcal{A}_i(x_h, Q_h^2) \mathcal{S}_i(\mathcal{E}, \mathcal{I}, z_1, z_2). \tag{2.39}$$

The neglected terms are due to the Z exchange. They are vanishing at small Q^2 since the Z propagator is suppressed there compared to the photon propagator. So, the corresponding approximation is sufficiently well even in the photoproduction region. In that region one has to retain, however, all particle masses in the cross-section contributions from photon exchange. We should mention in addition that certain bremsstrahlung corrections, which are proportional to $m^2/z_{1(2)}^2$ yield finite contributions to the cross-section even at larger Q^2; this may be seen from an inspection of the tables of integrals in appendix D.

Besides on z_1 and z_2, the radiator functions $\mathcal{S}_i(\mathcal{E}, \mathcal{I}, z_1, z_2)$ depend on two additional two-dimensional sets of variables $\mathcal{E}$ and $\mathcal{I}$:

$$\begin{aligned}
\mathcal{S}_1(\mathcal{E}, \mathcal{I}, z_1, z_2) \;=\;& 1 + \frac{1}{z_1 z_2}(Q_h^4 - 4m^4) + \left(\frac{1}{z_1} - \frac{1}{z_2} \right) \left[\frac{1}{2}(Q_h^2 + Q_l^2) - 2m^2 \right] \\
& - m^2 (Q_h^2 - 2m^2) \left(\frac{1}{z_1^2} + \frac{1}{z_2^2} \right),
\end{aligned} \tag{2.40}$$

$$\begin{aligned}
\mathcal{S}_2(\mathcal{E}, \mathcal{I}, z_1, z_2) \;=\;& -2M^2 + \frac{1}{z_1 z_2} \Big\{ Q_h^2 [(1 - y_h) S^2 + (1 - y_l)(1 - y_l + y_h) S^2 \\
& - 2M^2 (Q_h^2 + 2m^2)] + 2m^2 \Big[2(1 - y_l) + y_h (y_l - y_h) \Big] S^2 \Big\} \\
& - \frac{1}{z_1} \Big[y_h S^2 + M^2 (Q_h^2 + Q_l^2) \Big] - \frac{1}{z_2} \Big[y_h (1 - y_l) S^2 - M^2 (Q_h^2 + Q_l^2) \Big] \\
& - 2m^2 \frac{1}{z_1^2} \Big[(1 - y_l)(1 - y_l + y_h) S^2 - M^2 Q_h^2 \Big] \\
& - 2m^2 \frac{1}{z_2^2} \Big[(1 - y_h) S^2 - M^2 Q_h^2 \Big],
\end{aligned} \tag{2.41}$$

$$\begin{aligned}
\mathcal{S}_3(\mathcal{E}, \mathcal{I}, z_1, z_2) \;=\;& S \Big\{ 2Q_h^2 \frac{1}{z_1 z_2} (Q_h^2 + 2m^2)(2 - y_l) \\
& + \frac{1}{z_1} \Big[2Q_h^2 - y_h (Q_h^2 + Q_l^2) \Big] - \frac{1}{z_2} \Big[2(1 - y_l) Q_h^2 + y_h (Q_h^2 + Q_l^2) \Big] \\
& - 2m^2 Q_h^2 \left[\frac{1}{z_1^2} (2 - 2y_l + y_h) + \frac{1}{z_2^2} (2 - y_h) \right] \Big\}.
\end{aligned} \tag{2.42}$$

The first two of the functions $\mathcal{S}_i$ are the result of an exact calculation in both the masses m and M for the case of photon exchange. For Z exchange, they contain certain harmless approximations in the electron mass, which were mentioned before (2.39). The same is with the $\mathcal{S}_3$.

These radiators $\mathcal{S}_i$ will be the central objects of the derivations in the following sections. In their arguments, the symbol $\mathcal{E}$ stands for two *external* variables, which will not be integrated over, while $\mathcal{I}$ denotes two *internal* variables. These latter two become, together with z_2 (or z_1), part of the integration measure. In the first part of the paper, the variable sets $\mathcal{E}$ and $\mathcal{I}$ will be selected out of the following set of variables:

$$\begin{aligned} Q_l^2 &= (k_1-k_2)^2, & y_l &= \frac{-2p_1Q_l}{S}, & x_l &= \frac{Q_l^2}{y_lS}, \\ Q_h^2 &= (p_2-p_1)^2, & y_h &= \frac{-2p_1Q_h}{S}, & x_h &= \frac{Q_h^2}{y_hS}. \end{aligned} \tag{2.43}$$

The radiators $\mathcal{S}_i$ are the main ingredient of the subsequent integration over the radiative phase space. The functions $\mathcal{S}_1$ and $\mathcal{S}_2$ agree analytically with expressions obtained earlier (the second reference in [5]). Further, the Monte Carlo program `HERACLES` [35] is based on formulae, which are equivalent to our functions $\mathcal{S}_i$ (i=1,2,3) [54].

The following sections will be devoted to a number of analytical integrations, aiming at semi-analytical, compact expressions for the QED corrections.

2.3 The elastic radiative tail $ep \to ep\gamma$

A possible background process for deep inelastic scattering is the *elastic* scattering (1.3) from which the so-called elastic radiative tail originates. The corresponding formulae have been derived in [39]. They may be obtained from the formulae for reaction (1.2) applying the following relations between the generalized structure functions $\mathcal{A}_i(x_h,Q_h^2)$ (i=1,2,3) and the generalized elastic form factors $\mathcal{A}_i(Q_h^2)$:

$$\mathcal{A}_1(x_h,Q_h^2) = x_h\,\mathcal{A}_1(Q_h^2)\,\delta(1-x_h), \tag{2.44}$$

$$\mathcal{A}_{2,3}(x_h,Q_h^2) = \frac{x_h}{Q_h^2}\,\mathcal{A}_{2,3}(Q_h^2)\,\delta(1-x_h), \tag{2.45}$$

where $\mathcal{A}_i(Q_h^2)$ are defined by formulae (20)–(22) of [39].

Further, from (3.13)–(3.16) of the subsequent section, one may get formulae (26)–(28) of [39], the expressions for $\mathcal{S}^{\rm el}_{1,2,3}$ in the ultra-relativistic approximation. The exact in m and M expressions for $\mathcal{S}^{\rm el}_{1,2}$ may be found in the first reference in [5], equation (37).

3 A covariant treatment of the phase space

3.1 Phase space parameterization

The cross-section of reaction (1.2) is characterized by six independent invariants which may be taken as follows:

$$S,\ y_l,\ Q_l^2,\ y_h,\ Q_h^2,\ z_2. \tag{3.1}$$

In addition, we use

$$z_1 \;=\; z_2 + Q_h^2 - Q_l^2. \tag{3.2}$$

We will now rewrite the phase space of process (1.2) such that it is expressed by these variables. The phase space is defined as follows:

$$d\Gamma \;=\; \frac{d\vec{k}_2}{2k_2^0}\frac{d\vec{k}}{2k^0}\frac{d\vec{p}_2}{2p_2^0} dM_h^2\, \delta^4(k_1 + p_1 - k_2 - k - p_2), \tag{3.3}$$

where the $d\Gamma_h$ is already split away. After rewriting $d\vec{p}_2/2p_2^0 = d^4p_2\, \delta(p_2^2 + M_h^2)$ and taking the integral over d^4p_2 using the δ function, we arrive at

$$d\Gamma \;=\; \frac{d\vec{k}_2}{2k_2^0}\frac{d\vec{k}}{2k^0}\, \delta[(p_1 + Q_h)^2 + M_h^2]\, dM_h^2. \tag{3.4}$$

With a trivial calculation, which is explained in appendix A.4.1, one gets

$$\frac{d\vec{k}_2}{2k_2^0} \;=\; \frac{\pi S}{2\sqrt{\lambda_S}} dy_l dQ_l^2. \tag{3.5}$$

Introducing the notation

$$d\Gamma_k = \frac{d\vec{k}}{2k^0}\delta[(p_1 + Q_h)^2 + M_h^2]\delta[Q_h^2 - (p_2 - p_1)^2)], \tag{3.6}$$

we arrive at:

$$d\Gamma = \frac{\pi S}{2\sqrt{\lambda_S}}\, dy_l\, dQ_l^2\, dM_h^2\, dQ_h^2\, d\Gamma_k. \tag{3.7}$$

With $M_h^2 = -p_2^2 = M^2 + y_h S - Q_h^2$, the differential $dM_h^2 dQ_h^2$ may be replaced by $S dy_h dQ_h^2$. In appendix A.4.2, we derive the following parameterization, which will be used for the subsequent integrations:

$$d\Gamma_k \;=\; \frac{dz_2}{2\sqrt{R_z}}, \tag{3.8}$$

where R_z is a quadratic polynomial in z_2.

In sum, the phase space in terms of the invariants y_l, Q_l^2, y_h, Q_h^2, together with one additional variable z_2 (or z_1), is:

$$\Gamma = \frac{\pi S^2}{4\sqrt{\lambda_S}} \int dy_l\, dQ_l^2\, dy_h\, dQ_h^2 \frac{dz_{1(2)}}{\sqrt{R_z}}. \tag{3.9}$$

3.2 An analytical integration

Taking into account (2.39) and (3.9), the differential cross-section (2.36) for the process (1.2) can be written as follows:

$$d\sigma_{\rm R} = \frac{2\alpha^3 S^2}{\pi\lambda_S}\mathcal{S}(\mathcal{E}, \mathcal{I}, z_1, z_2)\, d\mathcal{E}\, d\mathcal{I} \frac{dz_{1(2)}}{Q_h^4\sqrt{R_z}}. \tag{3.10}$$

Here and henceforth we use the following variables:

$$\begin{array}{rrcccrrcccl}
\text{leptonic variables}: & \mathcal{E} & = & \mathcal{E}_l & = & (y_l, Q_l^2), & \mathcal{I} & = & \mathcal{I}_l & = & (y_h, Q_h^2); \\
\text{mixed variables}: & \mathcal{E} & = & \mathcal{E}_m & = & (y_h, Q_l^2), & \mathcal{I} & = & \mathcal{I}_m & = & (y_l, Q_h^2); \\
\text{hadronic variables}: & \mathcal{E} & = & \mathcal{E}_h & = & (y_h, Q_h^2), & \mathcal{I} & = & \mathcal{I}_h & = & (y_l, Q_l^2).
\end{array} \tag{3.11}$$

For the case of mixed variables, we define in addition:

$$x_m = \frac{Q_l^2}{y_h S}. \tag{3.12}$$

The physical regions of $\mathcal{E}_a$ and $\mathcal{I}_a$, $a = l, m, h$, are determined in appendix B. Here, we would only like to mention that the variable x_m may not be restricted to the interval [0,1]; see the discussion in appendix B.3.

For the calculation of the double differential cross section (1.2) one has to perform a threefold integration over the squared matrix element (2.36) with the following integration variables: z_2 (or z_1), and the two invariants in $\mathcal{I}_a$, $a = l, m, h$, respectively.

The first integration is that over z_2. Since the generalized structure functions $\mathcal{A}_i(x_h, Q_h^2)$ are independent of $z_{1(2)}$, it is sufficient to integrate the kinematical functions $\mathcal{S}_i(\mathcal{E}, \mathcal{I}, z_1, z_2)$ of (2.40)–(2.42). The integration limits may be found in (B.9), and the necessary table of integrals in appendix D.1.

The following expressions are the result of the integration:

$$\mathcal{S}(\mathcal{E},\mathcal{I}) \;=\; \frac{1}{\pi}\int \frac{dz_{1(2)}}{\sqrt{R_z}} \mathcal{S}(\mathcal{E},\mathcal{I},z_1,z_2) \equiv \sum_{i=1}^{3} \mathcal{A}_i(x_h,Q_h^2)\mathcal{S}_i(\mathcal{E},\mathcal{I})\;, \tag{3.13}$$

where the $\mathcal{S}_i(\mathcal{E},\mathcal{I})$ are

$$\begin{aligned}
\mathcal{S}_1(\mathcal{E},\mathcal{I}) \;=\; & \left\{ \frac{1}{\sqrt{C_2}} \left[2m^2 - \frac{1}{2}\,(Q_h^2 + Q_l^2) + \frac{Q_h^4 - 4m^4}{Q_h^2 - Q_l^2} \right] \right. \\
& \left. - \; m^2 (Q_h^2 - 2m^2) \frac{B_2}{C_2^{3/2}} \right\} + \frac{1}{\sqrt{A_2}} - \Big\{ (1) \leftrightarrow -(1 - y_l) \Big\},
\end{aligned} \tag{3.14}$$

$$\begin{aligned}
\mathcal{S}_2(\mathcal{E},\mathcal{I}) \;=\; & \left\{ \frac{1}{\sqrt{C_2}} \Big[M^2 (Q_h^2 + Q_l^2) - y_h (1 - y_l) S^2 \Big] \right. \\
& + \; \frac{1}{(Q_h^2 - Q_l^2)\sqrt{C_2}} \Big[Q_h^2 \Big[(1)\,[(1) - y_h]\, S^2 \\
& + \; (1 - y_l)\,[(1 - y_l) + y_h]\, S^2 - 2M^2 (Q_h^2 + 2m^2) \Big] \\
& + \; 2m^2 S^2 \Big[[(1) - y_h]\,[(1 - y_l) + y_h] + (1)(1 - y_l) \Big] \Big] \\
& \left. - \; 2m^2 \frac{B_2}{C_2^{3/2}} \Big[(1)\,[(1) - y_h]\, S^2 - M^2 Q_h^2 \Big] \right\} - \frac{2M^2}{\sqrt{A_2}} \\
& - \Big\{ (1) \leftrightarrow -(1 - y_l) \Big\},
\end{aligned} \tag{3.15}$$

$$\begin{aligned}
\mathcal{S}_3(\mathcal{E},\mathcal{I}) \;=\; & \left\{ \frac{S}{\sqrt{C_2}} \left[\frac{2Q_h^2 (Q_h^2 + 2m^2)\,[(1) + (1 - y_l)]}{Q_h^2 - Q_l^2} - 2(1 - y_l) Q_h^2 - y_h (Q_h^2 + Q_l^2) \right] \right. \\
& \left. - \; 2m^2 S Q_h^2 \frac{B_2}{C_2^{3/2}} [2(1) - y_h] \right\} + \Big\{ (1) \leftrightarrow -(1 - y_l) \Big\},
\end{aligned} \tag{3.16}$$

where

$$
\begin{aligned}
A_2 &= \lambda_q, \\
B_2 &= \left\{2M^2Q_l^2(Q_l^2-Q_h^2)+(1-y_l)(y_lQ_h^2-y_hQ_l^2)S^2+S^2(1)Q_l^2(y_l-y_h)\right\} \\
&\equiv -B_1\left\{(1)\leftrightarrow -(1-y_l)\right\}, \\
C_2 &= \left\{(1-y_l)Q_h^2-Q_l^2\left[(1)-y_h\right]\right\}^2S^2+4m^2\left[(y_l-y_h)(y_lQ_h^2-y_hQ_l^2)S^2-M^2(Q_h^2-Q_l^2)^2\right\} \\
&\equiv C_1\left\{(1)\leftrightarrow -(1-y_l)\right\}.
\end{aligned}
$$

The kinematical function λ_q and the coefficients A_i, B_i, C_i, i=1,2, are derived in appendix A. Again, for the photon exchange and the γZ interference cross-sections, the radiators are exact in the masses m, M.

Formulae (3.13)–(3.16) describe the contribution of the radiative process to neutral current deep inelastic scattering without applying a cut on the photon kinematics. In (3.13), an integration over the azimuthal angle φ of the emitted photon [as introduced in (A.21)] is already performed. In principle, one could proceed here in a different way and apply some simple photonic cuts. This is done in section 8.3 and appendix B.1.2.

Further, we should indicate that the resulting expressions are singular at $k \to 0$. There, z_1 and z_2 vanish. It may be seen from (3.2) which relates z_1 and z_2 that Q_h^2 and Q_l^2 become equal in this limit. The same happens with y_h and y_l [see (2.43)]. This reflects the infrared singularity of the radiative cross-section which deserves a special treatment before we can perform additional numerical or analytical integrations.

4 Removal of the infrared divergence

4.1 The infrared divergence

In the last section, it has been shown that the double differential cross-section of the process (1.2) can be written in the following form:

$$
\frac{d\sigma_{\mathrm{R}}}{d\mathcal{E}} = \frac{2\alpha^3S^2}{\lambda_S}\int d\mathcal{I}\sum_{i=1}^{3}\mathcal{A}_i(x_h,Q_h^2)\frac{1}{Q_h^4}\,\mathcal{S}_i(\mathcal{E},\mathcal{I}). \tag{4.1}
$$

As was mentioned at the end of the foregoing section, the integrand of (4.1) diverges if the kinematics is such that the photon momentum vanishes. Then the kinematical functions $\mathcal{S}_i(\mathcal{E},\mathcal{I})$ become infrared singular as may be seen from formulae (3.14)–(3.16). Usually, in complete $\mathcal{O}(\alpha)$ QED calculations the infrared singularity is treated as follows. One introduces an (artificial) infrared cut-off parameter ϵ, which divides the photon phase space into two parts: In the soft photon part, the photon momentum may become infinitesimal, while in the other, the hard photon part, it is enforced to remain finite. The soft photon contribution to the cross-section is treated analytically; it depends on the cut-off which is introduced in a specially chosen lorentz frame. Thereby the lorentz invariance is spoiled intermediary in the calculation. The soft photon contribution contains the infrared singularity, which is compensated by the vertex correction of figure 1b. The hard photon contribution is calculated by some dedicated integration method and depends also on the cut-off ϵ. Finally, the compensation of the various occurrences of the infinitesimal parameter ϵ is performed numerically, often with the need of an adjustment of it to the kinematical situation. Examples of such an approach are [2] and [40].

For the calculations, which are aiming at the leading logarithmic approximation, the soft photon problem may be solved completely by an analytical calculation of all the contributions. This implies both an explicit analytical compensation of the infrared cut-off parameter ϵ and the semi-analytical integration of the hard photon bremsstrahlung.

Here, the infrared problem will be treated with a *covariant* method [6] with similar features as that used in the leading logarithmic calculations. As mentioned above, a cut-off parameter ϵ will be invented. Then, from the exact squared matrix element the terms, which contain the infrared singularity are extracted. These are *of much simpler structure than the exact expression*. The resulting simplified cross-section part will be integrated analytically over the *full* phase space, thereby compensating the infrared singularity with the vertex correction and, more complicated, eliminating the cut-off parameter ϵ. By construction, the infrared divergent bremsstrahlung cross-section part contains hard and soft photon contributions. This is quite similar to the leading logarithmic approximation.

The rest of the bremsstrahlung contribution is free of the soft photon problem. The integrand is quite complicated. Nevertheless, one may perform analytical integrations over all those internal variables, which are not an argument of the structure functions.

One may represent (4.1) in the following form:

$$\frac{d^2\sigma_{\rm R}}{d\mathcal{E}} = \left(\frac{d^2\sigma_{\rm R}}{d\mathcal{E}} - \frac{d^2\sigma_{\rm R}^{\rm IR}}{d\mathcal{E}}\right) + \frac{d^2\sigma_{\rm R}^{\rm IR}}{d\mathcal{E}} \equiv \frac{d^2\sigma_{\rm R}^{\rm F}}{d\mathcal{E}} + \frac{d^2\sigma_{\rm R}^{\rm IR}}{d\mathcal{E}}, \tag{4.2}$$

where $d\sigma_{\rm R}^{\rm IR}/d\mathcal{E}$ is the infrared divergent part to be defined below and $d\sigma_{\rm R}^{\rm F}/d\mathcal{E}$ is finite at $k \to 0$. Such a separation is not unique. The essentials of the approach will be the same for all the different ways of integrations over sets $\mathcal{I}$ of invariants, although certain details of the specific calculations will differ.

Going back to (2.36) and (3.7), the fully differential cross-section may be written as

$$d\sigma_{\rm R} = \frac{4\alpha^3 S^2}{\pi\lambda_S}\frac{1}{Q_h^4}\mathcal{S}(\mathcal{E},\mathcal{I},z_1,z_2)\,d\mathcal{E}\,d\mathcal{I}\,d\Gamma_k. \tag{4.3}$$

From (2.40)–(2.42), one may get the limit of $\mathcal{S}(\mathcal{E},\mathcal{I},z_1,z_2)/Q_h^4$ at $k \to 0$:

$$\lim_{k\to 0}\frac{1}{Q_h^4}\mathcal{S}(\mathcal{E},\mathcal{I},z_1,z_2) = \sum_{i=1}^{3}\mathcal{A}_i(x,Q^2)\frac{1}{Q^4}\mathcal{S}_i^{\rm B}(y,Q^2)\mathcal{F}^{\rm IR}(Q^2,z_1,z_2), \tag{4.4}$$

where

$$\mathcal{F}^{\rm IR}(Q^2,z_1,z_2) = \frac{Q^2+2m^2}{z_1z_2} - m^2\left(\frac{1}{z_1^2}+\frac{1}{z_2^2}\right), \tag{4.5}$$

and x, y and Q^2 are variables as defined in the Born kinematics. The factorized universal function $\mathcal{F}^{\rm IR}$ is the well-known Low factor [55],

$$\mathcal{F}^{\rm IR} = \left(\frac{k_1}{2k_1k} - \frac{k_2}{2k_2k}\right)^2, \tag{4.6}$$

and contains the infrared singularities of the photonic bremsstrahlung from the electron line.

Now, we define the infrared part of the cross-section as follows:

$$\frac{d^2\sigma_{\rm R}^{\rm IR}}{d\mathcal{E}} = \frac{4\alpha^3 S^2}{\pi\lambda_S}\int d\mathcal{I}\,d\Gamma_k\sum_{i=1}^{3}\mathcal{A}_i(x,Q^2)\frac{1}{Q^4}\mathcal{S}_i^{\rm B}(y,Q^2)\mathcal{F}^{\rm IR}(Q^2,z_1,z_2)$$

$$
\begin{aligned}
&= \frac{d^2\sigma_{\rm B}}{d\mathcal{E}}\frac{2\alpha S}{\pi^2}\int d\mathcal{I}\, d\Gamma_k \mathcal{F}^{\rm IR}(Q^2,z_1,z_2) \\
&\equiv \frac{d^2\sigma_{\rm B}}{d\mathcal{E}}\frac{\alpha}{\pi}\delta_{\rm R}^{\rm IR}(\mathcal{E}). \qquad (4.7)
\end{aligned}
$$

The integration range in (4.7) will be split into two parts:

$$
\begin{aligned}
\delta_{\rm R}^{\rm IR}(\mathcal{E}) &= \frac{2S}{\pi}\int d\mathcal{I}\, d\Gamma_k \mathcal{F}^{\rm IR}(Q^2,z_1,z_2)\theta(\epsilon-k_0) \\
&\quad + \frac{2S}{\pi}\int d\mathcal{I}\, d\Gamma_k \mathcal{F}^{\rm IR}(Q^2,z_1,z_2)\theta(k_0-\epsilon) \\
&\equiv \delta_{\rm soft}^{\rm IR}(\mathcal{E},\epsilon)+\delta_{\rm hard}^{\rm IR}(\mathcal{E},\epsilon). \qquad (4.8)
\end{aligned}
$$

Here, the k_0 is chosen to be the energy of the emitted photon in the proton rest frame (A.4),

$$
k^0 = \frac{S}{2M}(y_l - y_h), \qquad (4.9)
$$

and ϵ is an infinitesimal parameter, $\epsilon > 0, \epsilon \to 0$. The first term will constitute the soft photon contribution to $\delta_{\rm soft}^{\rm IR}(\mathcal{E})$:

$$
\begin{aligned}
\delta_{\rm soft}^{\rm IR}(\mathcal{E},\epsilon) &= \frac{2S}{\pi}\int d\mathcal{I}\frac{d\vec{k}}{2k_0}\delta\left[(p_1+Q_h)^2+M_h^2\right]\,\delta\left[Q_h^2-(p_2-p_1)^2\right]\mathcal{F}^{\rm IR}(Q^2,z_1,z_2)\theta(\epsilon-k_0) \\
&= \frac{2}{\pi}\int\frac{d\vec{k}}{2k_0}\mathcal{F}^{\rm IR}(Q^2,z_1,z_2)\theta(\epsilon-k_0). \qquad (4.10)
\end{aligned}
$$

The second part contains an integration over nearly the complete phase space and implies also contributions from hard photons, but with a considerably simplified integrand compared to the complete bremsstrahlung integral. It will also be dependent on the infrared cut-off ϵ, but is infrared finite for finite ϵ:

$$
\delta_{\rm hard}^{\rm IR}(\mathcal{E},\epsilon) = \frac{S}{\pi}\int d\mathcal{I}\frac{dz_{1(2)}}{\sqrt{R_z}}\mathcal{F}^{\rm IR}(Q^2,z_1,z_2)\theta(k_0-\epsilon). \qquad (4.11)
$$

With the additional notation

$$
\begin{aligned}
\mathcal{F}^{\rm IR}(\mathcal{E},\mathcal{I}) &= \frac{S}{\pi}\int\frac{dz_{1(2)}}{\sqrt{R_z}}\mathcal{F}^{\rm IR}(Q^2,z_1,z_2) \\
&= \frac{Q^2+2m^2}{Q_l^2-Q_h^2}\Big(\frac{1}{\sqrt{C_1}}-\frac{1}{\sqrt{C_2}}\Big) - m^2\Big(\frac{B_1}{C_1^{3/2}}+\frac{B_2}{C_2^{3/2}}\Big), \qquad (4.12)
\end{aligned}
$$

the hard part of the infrared divergent correction becomes:

$$
\delta_{\rm hard}^{\rm IR}(\mathcal{E},\epsilon) = \int d\mathcal{I}\,\mathcal{F}^{\rm IR}(\mathcal{E},\mathcal{I})\theta(k_0-\epsilon). \qquad (4.13)
$$

The integration of (4.5) over z_2 has been performed with the table of integrals D.1. The coefficients B_i, C_i, i=1,2 are introduced in appendix A.

For later use, the infrared divergent part of the corrections is quoted also in a slightly more general notation:

$$
\delta_{\rm R}^{\rm IR}(\mathcal{E}) = \frac{4}{\pi^2}\frac{\sqrt{\lambda_S}}{S}\int\frac{d\Gamma}{d\mathcal{E}}\mathcal{F}^{\rm IR}(Q^2,z_1,z_2), \qquad (4.14)
$$

where the Q^2 on the right hand side is, by definition, one of the external variables and the $\mathcal{F}^{\rm IR}(Q^2,z_1,z_2)$ is defined in (4.5).

4.2 The soft and hard parts of $\delta_{\rm R}^{\rm IR}$

The soft photon contribution $\delta_{\rm soft}^{\rm IR}(\mathcal{E},\epsilon)$ will be considered first. The integration region is limited to photons with an energy, which is smaller than ϵ. After inserting $\mathcal{F}^{\rm IR}$ as defined in (4.5) into (4.10), one gets

$$\delta_{\rm soft}^{\rm IR}(\mathcal{E},\epsilon) = 2(2\pi)^2 \int \frac{d^3k}{(2\pi)^3 k^0} \theta(\epsilon - k^0) \left[\frac{Q^2+2m^2}{(-2k_1k)(-2k_2k)} - \frac{m^2}{(-2k_1k)^2} - \frac{m^2}{(-2k_2k)^2} \right]. \tag{4.15}$$

The expression (4.15) will be regularized now by changing into the $(n-1)$-dimensional space [56]. After an integration over $(n-3)$ azimuthal angles, two integrations remain to be performed: one over the polar angle ϑ of the photon and the other over the photon energy k^0:

$$\begin{aligned} \delta_{\rm soft}^{\rm IR}(\mathcal{E},\epsilon) \to & \frac{2(2\pi)^2}{(2\sqrt{\pi})^n \Gamma(n/2-1)} \int_0^1 d\alpha \frac{1}{\mu^{n-4}} \int_0^\epsilon (k^0)^{n-5} dk^0 \int_0^\pi (\sin\vartheta)^{n-3} d\vartheta \\ & \left[\frac{Q^2+2m^2}{(k_\alpha^0)^2(1-\beta_\alpha \cos\vartheta_\alpha)^2} - \frac{m^2}{(k_1^0)^2(1-\beta_1\cos\vartheta_1)^2} - \frac{m^2}{(k_2^0)^2(1-\beta_2\cos\vartheta_2)^2} \right]. \end{aligned} \tag{4.16}$$

In order to simplify the angular integration, in the first term a Feynman parameter integration is inserted, which linearizes the angular dependence of the denominator:

$$\frac{1}{(-2k_1k)(-2k_2k)} = \int_0^1 \frac{d\alpha}{[(-2k_1k)\alpha + (-2k_2k)(1-\alpha)]^2}, \tag{4.17}$$

$$k_\alpha = k_1\alpha + k_2(1-\alpha). \tag{4.18}$$

Further, the relations

$$-k_ik = k_i^0 k^0 (1 - \beta_i \cos\vartheta_i), \tag{4.19}$$

$$\beta_i = \frac{|\vec{k}_i|}{k_i^0}, \qquad i = 1,2,\alpha, \tag{4.20}$$

are used where the β_i are $(n-1)$ dimensional velocities, and the ϑ_i the corresponding spatial angles between the photon three-momentum and $\vec{k}_i$. We now go into the rest system of the proton, where it is $\vec{p}_1 = 0$. In this system, the β_i are expressed in terms of the invariants (A.4).

We get:

$$\begin{aligned} \frac{1}{\mu^{n-4}} \int_0^\epsilon dk^0 (k^0)^{n-5} &= \frac{(\epsilon/\mu)^{n-4}}{n-4} \\ &= \frac{1}{n-4} \left[1 + (n-4)\ln\frac{\epsilon}{\mu} + \cdots \right]. \end{aligned} \tag{4.21}$$

Soft photon emission is isotropic. For any of the three terms under the integral, one has the freedom to choose a coordinate frame in the proton rest system with the $(n-1)^{st}$ axis being

parallel to $\vec{k}_i$, i.e. $\vartheta_i = \vartheta$. After a trivial change of variable, $\cos\vartheta = \xi$,

$$\begin{aligned}\int_0^\pi \frac{(\sin\vartheta)^{n-3}d\vartheta}{(1-\beta_i\cos\vartheta)^2} &= \int_{-1}^1 \frac{(1-\xi^2)^{n/2-2}d\xi}{(1-\beta_i\xi)^2} \\ &= \int_{-1}^1 \frac{d\xi}{(1-\beta_i\xi)^2}\left[1+\frac{1}{2}(n-4)\ln(1-\xi^2)+\cdots\right]. \qquad (4.22)\end{aligned}$$

From the above substitutions, one obtains the following expression for $\delta^{\rm IR}_{\rm soft}(\mathcal{E},\epsilon)$:

$$\delta^{\rm IR}_{\rm soft}(\mathcal{E},\epsilon) = \left[\mathcal{P}^{\rm IR}+\ln\frac{2\epsilon}{\mu}\right]\frac{1}{2}\int_0^1 d\alpha\int_{-1}^1 d\xi\ \mathcal{F}(\alpha,\xi)+\frac{1}{4}\int_0^1 d\alpha\int_{-1}^1 d\xi\ \ln(1-\xi^2)\ \mathcal{F}(\alpha,\xi). \qquad (4.23)$$

Here, it is

$$\mathcal{F}(\alpha,\xi) = \frac{Q^2+2m^2}{(k^0_\alpha)^2(1-\beta_\alpha\xi)^2}-\frac{m^2}{(k^0_1)^2(1-\beta_1\xi)^2}-\frac{m^2}{(k^0_2)^2(1-\beta_2\xi)^2}, \qquad (4.24)$$

and

$$\mathcal{P}^{\rm IR} = \frac{1}{n-4}+\frac{1}{2}\gamma_E+\ln\frac{1}{2\sqrt{\pi}} \equiv -\frac{1}{2\bar{\epsilon}}, \qquad (4.25)$$

where the $\bar{\epsilon}$ is a parameter, which is often used in the $\overline{\rm MS}$ subtraction scheme. The $\mathcal{P}^{\rm IR}$ contains the pole term, which corresponds to the infrared divergence, as well as the Euler constant γ_E. The arbitrary parameter μ has the dimension of a mass.

After the integration over ξ and α with the aid of the integrals of appendix D.2 one gets:

$$\delta^{\rm IR}_{\rm soft}(\mathcal{E},\epsilon) = 2\Big[\mathcal{P}^{\rm IR}+\ln\frac{2\epsilon}{\mu}\Big]\Big[(Q^2+2m^2){\rm L_m}-1\Big]+\ \mathcal{S}_\Phi+\frac{1}{2\beta_1}\ln\frac{1+\beta_1}{1-\beta_1}+\frac{1}{2\beta_2}\ln\frac{1+\beta_2}{1-\beta_2}, \qquad (4.26)$$

with $\mathcal{S}_\Phi$ defined in (D.22) and (4.31). Further,

$$\begin{aligned}\beta_1 &= \frac{\sqrt{\lambda_S}}{S} = \sqrt{1-\frac{4m^2M^2}{S^2}}, &(4.27)\\ \beta_2 &= \frac{\sqrt{\lambda_l}}{(1-y_l)S} = \sqrt{1-\frac{4m^2M^2}{(1-y_l)^2S^2}}, &(4.28)\\ {\rm L_m} &= \frac{1}{\sqrt{\lambda_m}}\ln\frac{\sqrt{\lambda_m}+Q^2}{\sqrt{\lambda_m}-Q^2}, &(4.29)\\ \lambda_m &= Q^2(Q^2+4m^2). &(4.30)\end{aligned}$$

The equation (4.26) with $\mathcal{S}_\Phi$ defined in (D.22) is exact. In the ultra-relativistic limit it is

$$\mathcal{S}_\Phi = -\frac{1}{2}\ln^2\left(\frac{Q^2}{m^2}\frac{1}{1-y}\right)-\ln\frac{Q^2}{m^2}\ln\frac{S^2(1-y)^2}{M^2Q^2}-{\rm Li}_2(1), \qquad (4.31)$$

and one gets the following short expression:

$$\begin{aligned}\delta^{\rm IR}_{\rm soft}(\mathcal{E},\epsilon) &= \left[2\mathcal{P}^{\rm IR}+2\ln\frac{2\epsilon}{\mu}-\ln\frac{(1-y)S^2}{m^2M^2}\right]\left(\ln\frac{Q^2}{m^2}-1\right)\\ &\quad+\frac{1}{2}\ln^2\frac{Q^2}{m^2}-\ \frac{1}{2}\ln^2(1-y)-{\rm Li}_2(1), \qquad (4.32)\end{aligned}$$

where

$$\mathrm{Li}_2(x) = -\int_0^1 \frac{\ln(1-xy)}{y} dy. \tag{4.33}$$

The infrared pole $\mathcal{P}^{\rm IR}$ in $\delta^{\rm IR}_{\rm soft}(\mathcal{E},\epsilon)$ has to cancel against a corresponding contribution from the QED vertex correction:

$$\delta_{\rm vert}(\mathcal{E}) = -2\left(\mathcal{P}^{\rm IR} + \ln\frac{m}{\mu}\right)\left(\ln\frac{Q^2}{m^2} - 1\right) - \frac{1}{2}\ln^2\frac{Q^2}{m^2} + \frac{3}{2}\ln\frac{Q^2}{m^2} + \mathrm{Li}_2(1) - 2. \tag{4.34}$$

This cancellation may be seen explicitly from the above expressions.

The parameter ϵ in (4.32) has to be compensated by corresponding terms from $\delta^{\rm IR}_{\rm hard}(\mathcal{E},\epsilon)$.

In order to obtain the $\delta^{\rm IR}_{\rm hard}(\mathcal{E},\epsilon)$, one has to perform the integration of $\mathcal{F}^{\rm IR}(\mathcal{E},\mathcal{I})$ over the physical regions of the variable sets $\mathcal{I}_a (a = l,m,h)$ as derived in appendix B, but with the exclusion of a small region around the infrared point $\mathcal{F}$; see also the figures in that appendix. These integrations are tedious and will be commented on in appendix D.3.

In the ultra-relativistic approximation, one gets the following expression for $\delta^{\rm IR}_{\rm hard}$ in *leptonic* variables:

$$\begin{aligned}\delta^{\rm IR}_{\rm hard}(\mathcal{E}_l,\epsilon) &= \left[-2\ln\frac{2\epsilon}{m} + \ln\frac{(1-y_l)y_l^2(1-x_l)^2S^2}{(1-y_lx_l)(1-y_l(1-x_l))m^2M^2}\right]\left(\ln\frac{Q_l^2}{m^2}-1\right)\\ &+ \frac{1}{2}\ln^2(1-y_l) - \frac{1}{2}\ln^2\left[\frac{1-y_l(1-x_l)}{1-y_lx_l}\right]\\ &+ \mathrm{Li}_2\left[\frac{(1-y_l)}{(1-y_lx_l)(1-y_l(1-x_l))}\right] - \mathrm{Li}_2(1).\end{aligned} \tag{4.35}$$

In *mixed* variables, it is:

$$\begin{aligned}\delta^{\rm IR}_{\rm hard}(\mathcal{E}_m,\epsilon) &= \left[-2\ln\frac{2\epsilon}{m} + \ln\frac{(1-y_h)^2(1-x_m)S^2}{m^2M^2}\right]\left(\ln\frac{Q_l^2}{m^2}-1\right)\\ &- \frac{1}{2}\ln^2(1-x_m) + \ln(1-y_h)\ln(1-x_m) - \mathrm{Li}_2\left[\frac{x_m(1-y_h)}{x_m-1}\right].\end{aligned} \tag{4.36}$$

Finally, in *hadronic* variables:

$$\delta^{\rm IR}_{\rm hard}(\mathcal{E}_h,\epsilon) = \left[-2\ln\frac{2\epsilon}{m} + \ln\frac{(1-y_h)^2S^2}{m^2M^2}\right]\left(\ln\frac{Q_h^2}{m^2}-1\right) + \ln y_h + \mathrm{Li}_2(1-y_h) - \mathrm{Li}_2(1) + 1. \tag{4.37}$$

At this intermediate state of the calculation, we would only like to remark that the dependencies of $\delta^{\rm IR}_{\rm hard}$ on the $\ln(2\epsilon/m)$, $\ln(S/m^2)$, and $\ln(S/M^2)$ are fictitious. They are compensated by corresponding dependencies of $\delta^{\rm IR}_{\rm soft}$ completely; see (4.32). At the other hand, the $\ln(Q^2/m^2)$ becomes part of the final results.

4.3 The net correction $\delta^{\rm IR}_{\rm R}$ and the soft photon exponentiation

For applications, it is convenient to define a dimensionless radiative correction factor,

$$\delta_a \equiv \delta(\mathcal{E}_a) = \frac{d^2\sigma_{\rm theor}/d\mathcal{E}_a}{d^2\sigma_{\rm B}/d\mathcal{E}_a} - 1, \qquad a = l,m,h, \tag{4.38}$$

where $d^2\sigma_{\rm B}/d\mathcal{E}$ is the Born cross-section of the process (1.1) and $d^2\sigma_{\rm theor}/d\mathcal{E}$ is the theoretical prediction for the measured cross-section,

$$\frac{d^2\sigma_{\rm theor}}{d\mathcal{E}} = \left(1+\frac{\alpha}{\pi}\,\delta_{\rm vert}\right)\frac{d^2\sigma_{\rm B}}{d\mathcal{E}} + \frac{d^2\sigma_{\rm R}}{d\mathcal{E}}. \tag{4.39}$$

One may collect within one expression all the terms, which are explicitly proportional to the Born cross-section; we call it the *factorized part* $\delta^{\rm VR}$ of the total radiative corrections and introduce it in the following way:

$$\begin{aligned}\frac{d^2\sigma_{\rm theor}}{d\mathcal{E}} &= \left[1+\frac{\alpha}{\pi}\,\delta_{\rm vert}(\mathcal{E})\right]\frac{d^2\sigma_{\rm B}}{d\mathcal{E}} + \frac{d^2\sigma^{\rm IR}_{\rm soft}}{d\mathcal{E}} + \frac{d^2\sigma^{\rm IR}_{\rm hard}}{d\mathcal{E}} + \frac{d^2\sigma^{\rm F}_{\rm R}}{d\mathcal{E}} \\ &\equiv \left[1+\frac{\alpha}{\pi}\,\delta^{\rm VR}(\mathcal{E})\right]\frac{d^2\sigma_{\rm B}}{d\mathcal{E}} + \frac{d^2\sigma^{\rm F}_{\rm R}}{d\mathcal{E}},\end{aligned} \tag{4.40}$$

with

$$\begin{aligned}\delta_{\rm VR}(\mathcal{E}) &= \delta_{\rm vert}(\mathcal{E}) + \delta^{\rm IR}_{\rm soft}(\mathcal{E},\epsilon) + \delta^{\rm IR}_{\rm hard}(\mathcal{E},\epsilon) \\ &\equiv \delta_{\rm vert}(\mathcal{E}) + \delta^{\rm IR}_{\rm R}(\mathcal{E}).\end{aligned} \tag{4.41}$$

The net radiative correction factor (4.38) becomes to order $\mathcal{O}(\alpha)$:

$$\begin{aligned}\delta_a &= \frac{\alpha}{\pi}\,\delta_{\rm VR}(\mathcal{E}_a) + \frac{d^2\sigma^{\rm F}_{\rm R}}{d\mathcal{E}_a}\Big/\frac{d^2\sigma_{\rm B}}{d\mathcal{E}_a} \\ &\equiv \frac{\alpha}{\pi}\left[\delta_{\rm VR}(\mathcal{E}_a) + \delta^{\rm F}_{\rm R}(\mathcal{E}_a)\right].\end{aligned} \tag{4.42}$$

In $\delta_{\rm VR}(\mathcal{E}_a)$, a dilogarithmic term $\delta_{\rm inf}(\mathcal{E}_a)$ may be found, which controls the multiple soft photon emission in the bremsstrahlung process (1.2). An exponentiation of this term leads to a significant numerical improvement of the QED predictions [7]:

$$\frac{\alpha}{\pi}\,\delta_{\rm VR}(\mathcal{E}) \to \frac{\alpha}{\pi}\,\delta^{\rm exp}_{\rm VR}(\mathcal{E}) = \exp\left[\frac{\alpha}{\pi}\delta_{\rm inf}(\mathcal{E})\right] - 1 + \frac{\alpha}{\pi}\Big[\delta_{\rm VR}(\mathcal{E}) - \delta_{\rm inf}(\mathcal{E})\Big]. \tag{4.43}$$

Finally, the radiative correction factor (4.38) with soft photon exponentiation becomes:

$$\delta^{\rm exp}_a = \frac{\alpha}{\pi}\left[\delta^{\rm exp}_{\rm VR}(\mathcal{E}_a) + \delta^{\rm F}_{\rm R}(\mathcal{E}_a)\right]. \tag{4.44}$$

The factorized correction (4.41) follows from (4.32), (4.34), and (4.35)–(4.37) and is different for the different sets of variables.

In *leptonic* variables, it is:

$$\begin{aligned}\delta_{\rm VR}(\mathcal{E}_l) &= \delta_{\rm inf}(\mathcal{E}_l) - \frac{1}{2}\ln^2\left[\frac{1-y_l(1-x_l)}{1-y_lx_l}\right] + {\rm Li}_2\left[\frac{1-y_l}{(1-y_lx_l)[1-y_l(1-x_l)]}\right] \\ &\quad + \frac{3}{2}\ln\frac{Q_l^2}{m^2} - {\rm Li}_2(1) - 2\ ,\end{aligned} \tag{4.45}$$

where

$$\delta_{\rm inf}(\mathcal{E}_l) = \left(\ln\frac{Q_l^2}{m^2} - 1\right)\ln\left[\frac{y_l^2(1-x_l)^2}{(1-y_lx_l)[1-y_l(1-x_l)]}\right]. \tag{4.46}$$

In *mixed* variables, we can write (4.43) as follows:

$$\delta_{\rm VR}(\mathcal{E}_m) \;=\; \delta_{\rm inf}(\mathcal{E}_m) - \frac{1}{2}\ln^2\left(\frac{1-y_h}{1-x_m}\right) - \;{\rm Li}_2\left[\frac{x_m(1-y_h)}{x_m-1}\right] + \frac{3}{2}\ln\frac{Q_l^2}{m^2} - 2\;, \qquad (4.47)$$

where

$$\delta_{\rm inf}(\mathcal{E}_m) = \left(\ln\frac{Q_l^2}{m^2} - 1\right)\ln[(1-y_h)(1-x_m)]. \qquad (4.48)$$

In *hadronic* variables, finally:

$$\delta_{\rm VR}(\mathcal{E}_h) \;=\; \delta^{\rm inf}(\mathcal{E}_h) - \frac{1}{2}\ln^2(1-y_h) + {\rm Li}_2(1-y_h) + \;\ln y_h + \frac{3}{2}\ln\frac{Q_h^2}{m^2} - {\rm Li}_2(1) - 1\;, \qquad (4.49)$$

where

$$\delta_{\rm inf}(\mathcal{E}_h) = \left(\ln\frac{Q_h^2}{m^2} - 1\right)\ln(1-y_h). \qquad (4.50)$$

5 The net radiative correction $\delta_{\rm R} = \delta_{\rm VR}^{\rm exp} + \delta_{\rm R}^{\rm F}$

In this section, the net correction will be discussed:

$$\delta_a^{\rm exp} \;=\; \frac{\alpha}{\pi}\left[\delta_{\rm VR}^{\rm exp}(\mathcal{E}_a) + \delta_{\rm R}^{\rm F}(\mathcal{E}_a)\right]. \qquad (5.1)$$

We will use the following abbreviations: $\delta_{\rm lep} = \delta_l^{\rm exp}$, $\delta_{\rm mix} = \delta_m^{\rm exp}$, $\delta_{\rm had} = \delta_h^{\rm exp}$.

Before the discussion of the numerical results, some preparations will be performed with the infrared finite, hard part of the corrections. This hard part of the cross-section has been defined in (4.2):

$$\begin{aligned}\frac{d^2\sigma_{\rm R}^{\rm F}}{d\mathcal{E}} \;&\equiv\; \frac{d^2\sigma_{\rm R}}{d\mathcal{E}} - \frac{d^2\sigma_{\rm R}^{\rm IR}}{d\mathcal{E}} \qquad (5.2)\\ &=\; \frac{2\alpha^3 S^2}{\lambda_S}\int d\mathcal{I}\sum_{i=1}^{3}\Big[\,\mathcal{A}_i(x_h,Q_h^2)\frac{1}{Q_h^4}\mathcal{S}_i(\mathcal{E},\mathcal{I}) - \mathcal{A}_i(x,Q^2)\frac{1}{Q^4}\;\mathcal{S}_i^{\rm B}(y,Q^2)\;\mathcal{F}^{\rm IR}(\mathcal{E},\mathcal{I})\Big]\\ &\equiv\; \frac{\alpha}{\pi}\delta_{\rm R}^{\rm F}\frac{d^2\sigma_{\rm B}}{d\mathcal{E}}.\end{aligned}$$

From the explicit expressions (3.14)–(3.16) and (4.12) one may see that both terms under the integral contain a remnant of the soft photon singularity at $Q_l^2 = Q_h^2$, while their difference is finite by construction.

The subsequent calculations in this section will be organized in such a way that the integrations over Q_l^2 or Q_h^2 remain the last ones, respectively. Thus, the compensation of the harmless rests of the infrared singularity appears to be quite transparent. In the case of non-leptonic variables, in the analytical integrations of the hard bremsstrahlung no special care has to be devoted to the soft photon problems.

In the following subsections, formulae will be presented for the infrared free part of the cross-section in the different sets of variables.

5.1 Leptonic variables

For the case of leptonic variables, the generalized structure functions $\mathcal{A}_i(x_h, Q_h^2)$ (i=1,2,3) depend on the integration variables y_h and Q_h^2 and the structure functions become part of the integrand for the remaining twofold integral, which has to be performed numerically. For the variables $\mathcal{E}_l = (y_l, Q_l^2)$ and $\mathcal{I}_l = (y_h, Q_h^2)$, the expression (5.2) is the final result:

$$\begin{aligned}\frac{d^2\sigma_{\rm R}^{\rm F}}{dy_l dQ_l^2} &= \frac{2\alpha^3 S^2}{\lambda_S}\int dy_h dQ_h^2 \sum_{i=1}^{3}\Bigg[\mathcal{A}_i(x_h,Q_h^2)\frac{1}{Q_h^4}\mathcal{S}_i(y_l,Q_l^2,y_h,Q_h^2) \\ &\quad - \mathcal{A}_i(x_l,Q_l^2)\frac{1}{Q_l^4}\,\mathcal{S}_i^B(y_l,Q_l^2)\,\mathcal{L}^{\rm IR}(y_l,Q_l^2,y_h,Q_h^2)\Bigg], \qquad (5.3)\end{aligned}$$

where the radiators $\mathcal{S}_i(y_l, Q_l^2, y_h, Q_h^2)$ are given by (3.14) –(3.16).

The expression for $\mathcal{L}^{\rm IR}(y_l, Q_l^2, y_h, Q_h^2)$ is defined by (4.12) with $Q^2 = Q_l^2$; it is exact in both masses m and M:

$$\begin{aligned}\mathcal{L}^{\rm IR}(y_l,Q_l^2,y_h,Q_h^2) &\equiv \mathcal{F}^{\rm IR}(y_l,Q_l^2,y_h,Q_h^2)|_{Q^2=Q_l^2} \\ &= \frac{Q_l^2+2m^2}{Q_l^2-Q_h^2}\Big(\frac{1}{\sqrt{C_1}}-\frac{1}{\sqrt{C_2}}\Big) - m^2\Big(\frac{B_1}{C_1^{3/2}}+\frac{B_2}{C_2^{3/2}}\Big). \qquad (5.4)\end{aligned}$$

The two-dimensional numerical integration in (5.3) has to be performed over the physical region (B.34); see figure 35. In the ultra-relativistic approximation, the boundaries are:

$$\begin{aligned} 0 \;\le\; y_h \;&\le\; y_l, \\ \frac{y_h}{y_l}Q_l^2 \;\le\; Q_h^2 \;&\le\; \min\left[y_h S, Q_l^2\left(1+\frac{y_l-y_h}{x_l}\frac{S}{M^2}\right)\right]. \end{aligned} \qquad (5.5)$$

In the numerical integrations, one has to leave out a small region around the phase space points with $Q_l^2 = Q_h^2$. There, the integrand is finite but occurs as the difference of two divergent terms.

5.1.1 Discussion

The radiative corrections in leptonic variables are shown in figures 6–8 for a fixed target experiment, HERA, and LEP⊗LHC. At HERA and LEP⊗LHC, the corrections are very similar. For small x, the range of y is reduced due to the condition $Q^{2\,\rm min} = 5$ GeV^2 at a given value of x. This tendency is more pronounced for the fixed target experiments. The net corrections are smaller there because for the fixed target experiments the S is quite different. Further, the muon mass sets the scale in the leading logarithm $\ln(S/m^2)$, while at a collider it is the electron mass.

From figure 35 and also from (4.9) it may be seen that for small y_l the photon energy is strongly bound and only soft photons occur. These corrections are negative. Without the soft photon exponentiation, they would even diverge when y_l vanishes and at the same time x_l approaches 1. This may be seen from (4.46) as well. At large y_l and small x_l the factorized correction seems to diverge also; see the squared logarithm in (4.45). This behaviour, however, is fictitious. It is compensated by corresponding terms from the hard non-factorizing corrections. The steep rise of the corrections at large y_l and small x_l is completely due to the Compton peak, which arises from the small Q_h^2 in the denominator of the photon propagator. This is explained in detail in section 8.4. From the Z-exchange diagrams, there

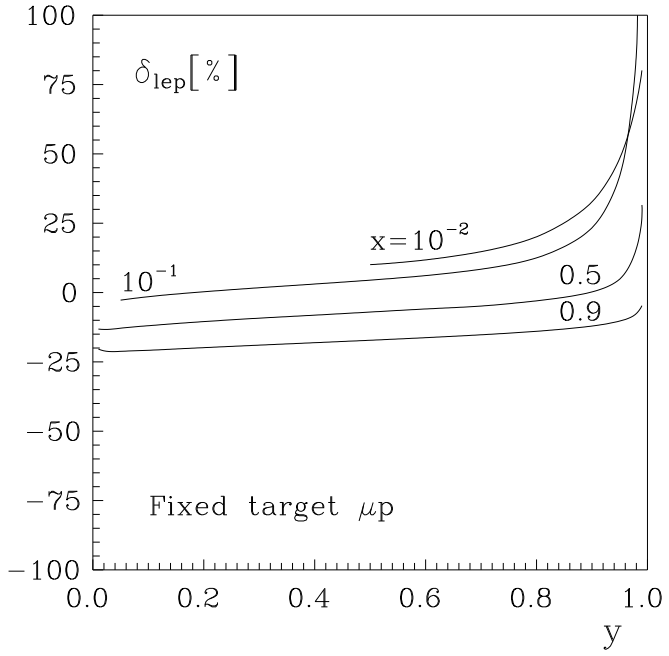

Figure 6: *Radiative correction $\delta_{\rm lep}$ in % for a cross-section measurement in terms of leptonic variables at a fixed target μp experiment.*

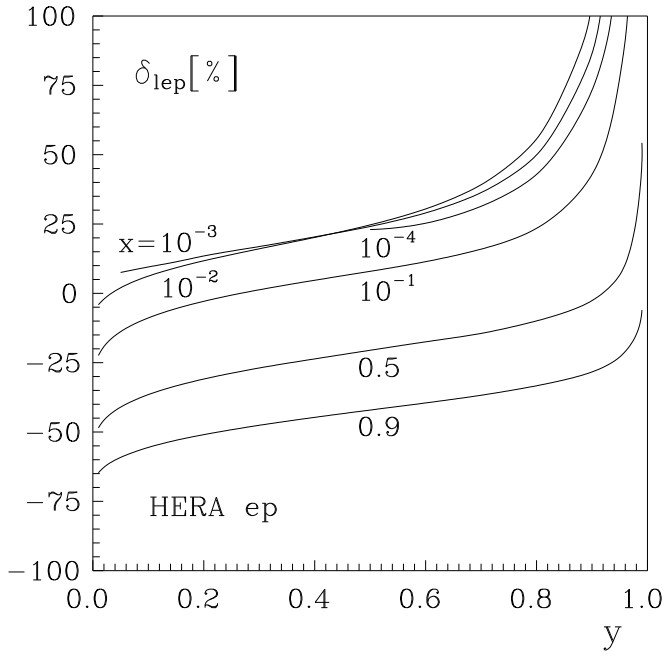

Figure 7: *Radiative correction $\delta_{\rm lep}$ in % for a cross-section measurement in terms of leptonic variables at HERA.*

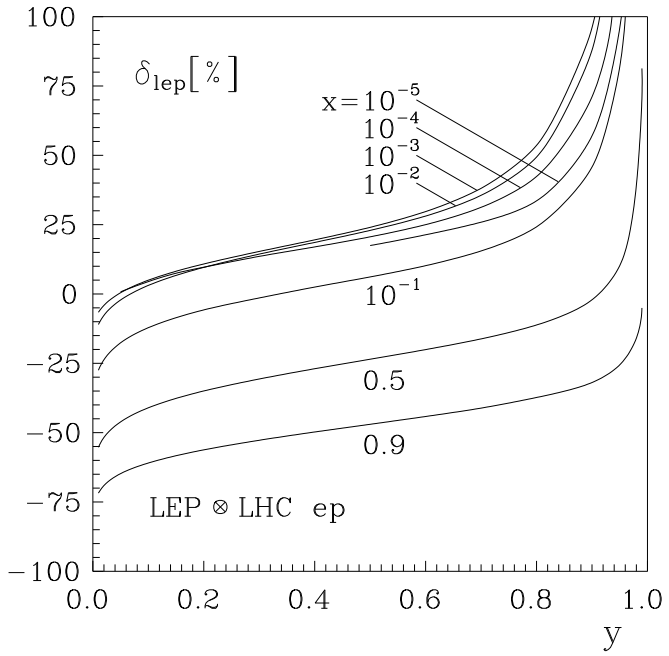

Figure 8: *Radiative correction $\delta_{\rm lep}$ in % for a cross-section measurement in terms of leptonic variables at LEP⊗LHC.*

is no contribution to the Compton peak and no steep rise of the corrections at large Q_l^2. This may be explicitly seen in figure 3 of [14].

At small values of x_l, the corrections are no longer monotonously dependent on x_l. In this region, the hard photon corrections are dominant. They are not proportional to the Born cross-section and an influence of the properties of the structure functions at smaller values of x may show up. We will come back to this point in section 8.

5.2 Mixed variables. A second analytical integration

For the case of mixed variables, it is $\mathcal{E}_m = (y_h, Q_l^2)$ and the integrations have to be performed over the variables $\mathcal{I}_m = (y_l, Q_h^2)$. The cross-section (5.2) becomes:

$$\begin{aligned}\frac{d^2\sigma_{\rm R}^{\rm F}}{dy_h dQ_l^2} &= \frac{2\alpha^3 S^2}{\lambda_S}\int dQ_h^2\, dy_l \sum_{i=1}^{3}\Bigg[\mathcal{A}_i(x_h,Q_h^2)\,\frac{1}{Q_h^4}\,\mathcal{S}_i(y_l,Q_l^2,y_h,Q_h^2)\\ &\quad - \mathcal{A}_i(x_m,Q_l^2)\frac{1}{Q_l^4}\,\mathcal{S}_i^{\rm B}(y_h,Q_l^2)\,\mathcal{L}^{\rm IR}(y_l,Q_l^2,y_h,Q_h^2)\Bigg]. \qquad (5.6)\end{aligned}$$

Here, the definition (3.12) of the variable x_m is used, $x_m = Q_l^2/(y_h S)$.

In contrast to the case of leptonic variables, in (5.6) one may perform an analytical integration over the variable y_l. As it is discussed in appendix B.3.3 and may be seen in figure 39, the integration region in (5.6) must be split into two regions I and II as long as the condition $Q_l^2 < y_h S$ is fulfilled, which corresponds to $x_m \leq 1$. If instead $x_m > 1$, there is only the region I, see figure 40. Some technical details about the analytical integration over y_l may be found in appendix D.4.

In the ultra-relativistic approximation, one gets the following expressions for $x_m < 1$:

$$\begin{aligned}
\mathcal{S}_1^{\rm I}(Q_l^2, y_h, Q_h^2) &\equiv \int_{y_l^{\rm min}}^{y_l^{\rm max}} dy_l\, \mathcal{S}_1(y_l, Q_l^2, y_h, Q_h^2) \\
&= \frac{1}{S}\Bigg[\frac{1}{2}\frac{Q_l^2}{Q_l^2 - Q_h^2}\left(1 + \frac{Q_h^4}{Q_l^4}\right)(\mathrm{L} + \mathrm{L}_1 - \mathrm{L}_2 - 1) \\
&\quad - \frac{1}{2}\frac{Q_l^2}{Q_h^2}\left(1 + \frac{Q_h^4}{Q_l^4}\right)(\mathrm{L}_t + \mathrm{L}_2) + \mathrm{L}_T - \mathrm{L}_t + \frac{1}{2}\left(1 - \frac{Q_h^2}{Q_l^2}\right)\Bigg], \qquad (5.7) \\
\mathcal{S}_2^{\rm I}(Q_l^2, y_h, Q_h^2) &\equiv \int_{y_l^{\rm min}}^{y_l^{\rm max}} dy_l\, \mathcal{S}_2(y_l, Q_l^2, y_h, Q_h^2) \\
&= S\Bigg\{\frac{1}{Q_l^2}\frac{Q_h^2 - y_h Q_l^2}{Q_l^2 - Q_h^2}\left(1 + \frac{Q_h^4}{Q_l^4}\right)(\mathrm{L} + \mathrm{L}_1 - \mathrm{L}_2 - 1) \\
&\quad + \frac{1}{Q_h^2}\left(1 + \frac{Q_h^4}{Q_l^4}\right)\left[y_h(1 + \frac{Q_l^2}{Q_h^2}) - \left(1 + \frac{Q_l^2}{Q_h^2} + \frac{Q_h^2}{Q_l^2}\right)\right](\mathrm{L}_t + \mathrm{L}_2) \\
&\quad + \frac{1}{Q_h^2}\left(1 + \frac{3}{2}\frac{Q_h^2}{Q_l^2} + 3\frac{Q_h^4}{Q_l^4} + 2\frac{Q_h^6}{Q_l^6}\right) \\
&\quad - \frac{y_h}{Q_h^2}\left(\frac{Q_l^2}{Q_h^2} + 2 + 4\frac{Q_h^2}{Q_l^2} + 3\frac{Q_h^4}{Q_l^4}\right) + \frac{1}{2}\frac{y_h^2}{Q_h^2}\left(2 + \frac{Q_l^2}{Q_h^2} + 2\frac{Q_h^2}{Q_l^2}\right)\Bigg\}, \qquad (5.8) \\
\mathcal{S}_3^{\rm I}(Q_l^2, y_h, Q_h^2) &\equiv \int_{y_l^{\rm min}}^{y_l^{\rm max}} dy_l\, \mathcal{S}_3(y_l, Q_l^2, y_h, Q_h^2) \\
&= \frac{Q_l^2}{Q_l^2 - Q_h^2}\left(1 + \frac{Q_h^4}{Q_l^4}\right)\left(2\frac{Q_h^2}{Q_l^2} - y_h\right)(\mathrm{L} + \mathrm{L}_1 - \mathrm{L}_2 - 1) \\
&\quad - \frac{Q_l^2}{Q_h^2}\left(1 + \frac{Q_h^4}{Q_l^4}\right)\left(2\frac{Q_h^2}{Q_l^2} - y_h + 2\right)(\mathrm{L}_t + \mathrm{L}_2) \\
&\quad + \frac{Q_l^2}{Q_h^2}\left(1 + \frac{Q_h^2}{Q_l^2}\right)^2\left(2\frac{Q_h^2}{Q_l^2} - y_h\right) - y_h\left(\frac{Q_l^2}{Q_h^2} + 1 + 2\frac{Q_h^2}{Q_l^2}\right), \qquad (5.9)
\end{aligned}$$

$$\begin{aligned}
\mathcal{S}_1^{\rm II}(Q_l^2, y_h, Q_h^2) &\equiv \int_{y_l^{\rm min}}^{y_l^{\rm max}} dy_l\, \mathcal{S}_1(y_l, Q_l^2, y_h, Q_h^2) \\
&= \frac{1}{S}\Bigg[-\frac{1}{2}\frac{Q_l^4}{Q_h^2(Q_l^2 - Q_h^2)}\left(1 + \frac{Q_h^4}{Q_l^4}\right)(\mathrm{L} - \mathrm{L}_1 + \mathrm{L}_2 - 1) \\
&\quad - \frac{1}{2}\frac{Q_l^2}{Q_h^2}\left(1 + \frac{Q_h^4}{Q_l^4}\right)\mathrm{L}_1 + \mathrm{L}_T + \frac{1}{2}\left(1 - \frac{Q_l^2}{Q_h^2}\right)\Bigg], \qquad (5.10) \\
\mathcal{S}_2^{\rm II}(Q_l^2, y_h, Q_h^2) &\equiv \int_{y_l^{\rm min}}^{y_l^{\rm max}} dy_l\, \mathcal{S}_2(y_l, Q_l^2, y_h, Q_h^2) \\
&= S\Bigg\{-\frac{Q_l^4}{Q_h^4}\frac{(1 - y_h)}{Q_l^2 - Q_h^2}\left(1 + \frac{Q_h^4}{Q_l^4}\right)(\mathrm{L} - \mathrm{L}_1 + \mathrm{L}_2 - 1) \\
&\quad + \frac{1}{Q_h^2}\left(1 + \frac{Q_h^4}{Q_l^4}\right)\left[y_h\left(1 + \frac{Q_l^2}{Q_h^2}\right) - \left(1 + \frac{Q_l^2}{Q_h^2} + \frac{Q_h^2}{Q_l^2}\right)\right]\mathrm{L}_1 \\
&\quad + \frac{1}{Q_l^2}\left(\frac{3}{2} + \frac{Q_h^2}{Q_l^2} + 3\frac{Q_l^2}{Q_h^2} + 2\frac{Q_l^4}{Q_h^4}\right)
\end{aligned}$$

$$
\begin{aligned}
&- \frac{y_h}{Q_h^2}\left(\frac{3Q_l^2}{Q_h^2} + 4 + 2\frac{Q_h^2}{Q_l^2} + \frac{Q_h^4}{Q_l^4}\right) \\
&+ \frac{1}{2}\frac{y_h^2}{Q_h^2}\left(2 + 2\frac{Q_l^2}{Q_h^2} + \frac{Q_h^2}{Q_l^2}\right)\Bigg\}, \qquad (5.11)
\end{aligned}
$$

$$
\begin{aligned}
\mathcal{S}_3^{\rm II}(Q_l^2, y_h, Q_h^2) &\equiv \int_{y_l^{\min}}^{y_l^{\max}} dy_l\, \mathcal{S}_3(y_l, Q_l^2, y_h, Q_h^2) \\
&= -\frac{(2-y_h)}{(Q_l^2 - Q_h^2)}\frac{Q_l^4}{Q_h^2}\left(1 + \frac{Q_h^4}{Q_l^4}\right)(\mathrm{L} - \mathrm{L}_1 + \mathrm{L}_2 - 1) \\
&+ \left(1 + \frac{Q_h^4}{Q_l^4}\right)\left[y_h\frac{Q_l^2}{Q_h^2} - 2\left(1 + \frac{Q_l^2}{Q_h^2}\right)\right]\mathrm{L}_1 \\
&+ 2(1-y_h)\frac{Q_l^2}{Q_h^2}\left(1 + \frac{Q_h^2}{Q_l^2}\right)^2 + y_h\left(1 - \frac{Q_l^2}{Q_h^2}\right). \qquad (5.12)
\end{aligned}
$$

The subtracted part of the cross-section also becomes integrated over y_l with the aid of appendix D.4:

$$
\begin{aligned}
\mathcal{L}_{\rm I}^{\rm IR}(Q_l^2, y_h, Q_h^2) &\equiv \int_{y_l^{\min}}^{y_l^{\max}} dy_l\, \mathcal{L}^{\rm IR}(y_l, Q_l^2, y_h, Q_h^2) \\
&= \frac{1}{S(Q_l^2 - Q_h^2)}\left[-1 - \frac{Q_l^2}{Q_h^2}(\mathrm{L}_t + \mathrm{L}_2) + (\mathrm{L} + \mathrm{L}_t + \mathrm{L}_1)\right], \qquad (5.13) \\
\mathcal{L}_{\rm II}^{\rm IR}(Q_l^2, y_h, Q_h^2) &\equiv \int_{y_l^{\min}}^{y_l^{\max}} dy_l \mathcal{L}^{\rm IR}(y_l, Q_l^2, y_h, Q_h^2) \\
&= \frac{1}{S(Q_l^2 - Q_h^2)}\left[\frac{Q_l^2}{Q_h^2} + \mathrm{L}_1 - \frac{Q_l^2}{Q_h^2}(\mathrm{L} + \mathrm{L}_2)\right]. \qquad (5.14)
\end{aligned}
$$

The following abbreviations are used:

$$
\mathrm{L} = \ln\frac{Q_l^2}{m^2}, \qquad \mathrm{L}_t = \ln\frac{Q_l^2}{Q_h^2}, \qquad \mathrm{L}_T = \ln\frac{1}{y_h}, \qquad (5.15)
$$

$$
\mathrm{L}_1 = \ln\frac{Q_h^2 - y_h Q_l^2}{|\,Q_l^2 - Q_h^2\,|}, \qquad \mathrm{L}_2 = \ln\frac{(1-y_h)Q_h^2}{|\,Q_l^2 - Q_h^2\,|}. \qquad (5.16)
$$

The final formula for $d^2\sigma_{\rm R}^{\rm F}/dy_h dQ_l^2$ can be written in the form:

$$
\begin{aligned}
\frac{d^2\sigma_{\rm R}^{\rm F}}{dy_h dQ_l^2} &= \frac{2\alpha^3 S^2}{\lambda_S}\Bigg\{\int_{Q_h^{2\min}}^{Q_l^2} dQ_h^2 \sum_{i=1}^{3}\Big[\mathcal{A}_i(x_h, Q_h^2)\frac{1}{Q_h^4}\mathcal{S}_i^{\rm I}(y_l, Q_l^2, y_h, Q_h^2) \\
&- \mathcal{A}_i(x_m, Q_l^2)\frac{1}{Q_l^4}\mathcal{S}_i^{\rm B}(y_h, Q_l^2)\mathcal{L}_{\rm I}^{\rm IR}(y_l, Q_l^2, Q_h^2)\Big] \\
&+ \int_{Q_l^2}^{y_h S} dQ_h^2 \sum_{i=1}^{3}\Big[\,\mathcal{A}_i(x_h, Q_h^2)\frac{1}{Q_h^4}\mathcal{S}_i^{\rm II}(Q_l^2, y_h, Q_h^2) \\
&- \mathcal{A}_i(x_m, Q_l^2)\frac{1}{Q_l^4}\mathcal{S}_i^{\rm B}(Q_l^2, y_h)\mathcal{L}_{\rm II}^{\rm IR}(Q_l^2, y_h, Q_h^2)\Big]\,\Bigg\}. \qquad (5.17)
\end{aligned}
$$

The above expressions again show remnants of the infrared singularity at $Q_l^2 = Q_h^2$. In contrast to the case of leptonic variables, one may easily see that the corresponding terms are multiplied by kinematical factors, which in the limit $Q_l^2 = Q_h^2$ become explicitly equal to the kinematical Born functions $\mathcal{S}_i^{\mathrm{B}}$, (2.14)–(2.16). This makes the finiteness of the $d^2\sigma_{\mathrm{R}}^{\mathrm{F}}$ obvious.

5.2.1 Discussion

The leptonic QED corrections in mixed variables are shown in figures 9–11 for three different kinematical situations. As in leptonic variables, at HERA and LEP⊗LHC they are similar, while in the fixed target case less pronounced.

The cross-section depends on Q_l^2 and y_h. From figure 39, and also from (4.9), it may be seen that for large y_h the photon energy is strongly bound; we have only soft photon corrections. These corrections are negative there. This is contrary to the case of leptonic variables, where this happened at small y_l. Without the soft photon exponentiation, they would even diverge when y_h approaches 1. This behaviour is enhanced, but less than for leptonic variables, if x_m approaches 1, too. This may be seen from (4.48). In principle, the Compton peak is present in mixed variables. It is considerably suppressed compared to the case of leptonic variables, see section 8.4. At small y_h, hard photon emission is possible and compensates for the negative soft photon corrections. The net correction is positive and remains moderate. If in addition x_m approaches 1, we observe that the corrections, if expressed in terms of the δ, rise steeply. This phenomenon is attributed to the following: the Born cross-section does not exist for $x_m > 1$, while hard photon emission does (see also figure 38). So, their ratio explodes and the δ becomes an inappropriate variable.

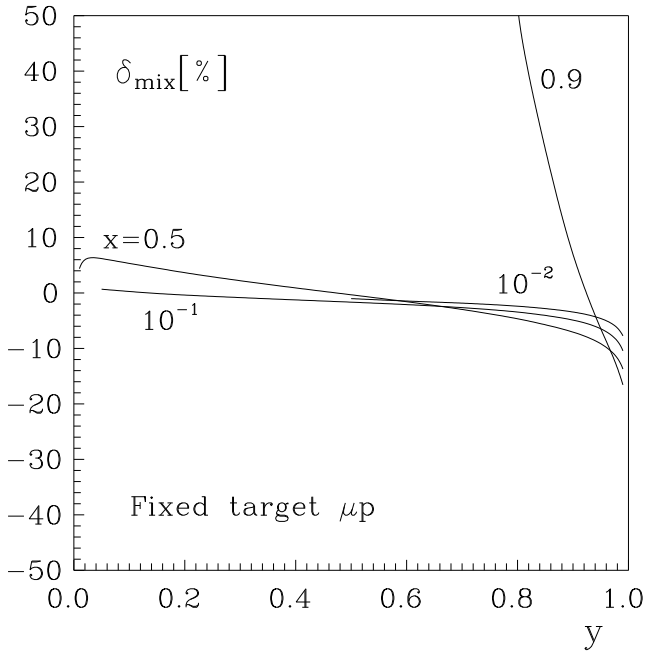

Figure 9: *Radiative correction δ_{mix} in % for a cross-section measurement in terms of mixed variables for fixed target μp scattering.*

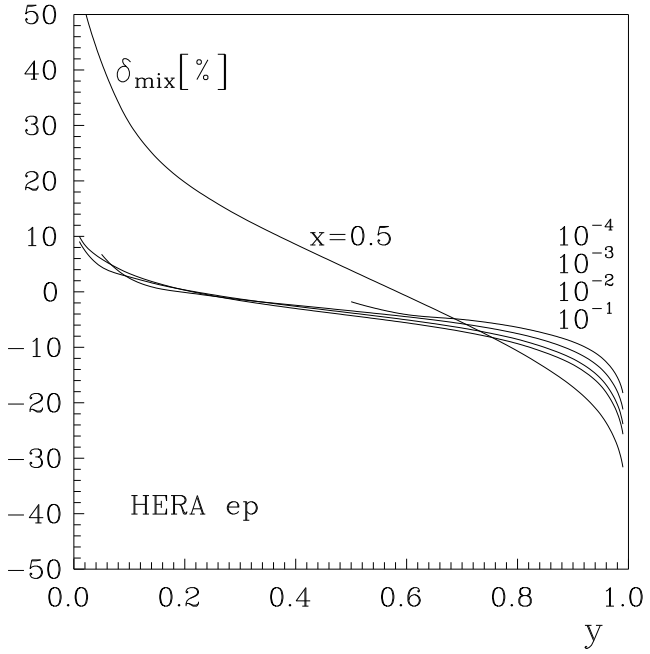

Figure 10: *Radiative correction $\delta_{\rm mix}$ in % for a cross-section measurement in terms of mixed variables at HERA.*

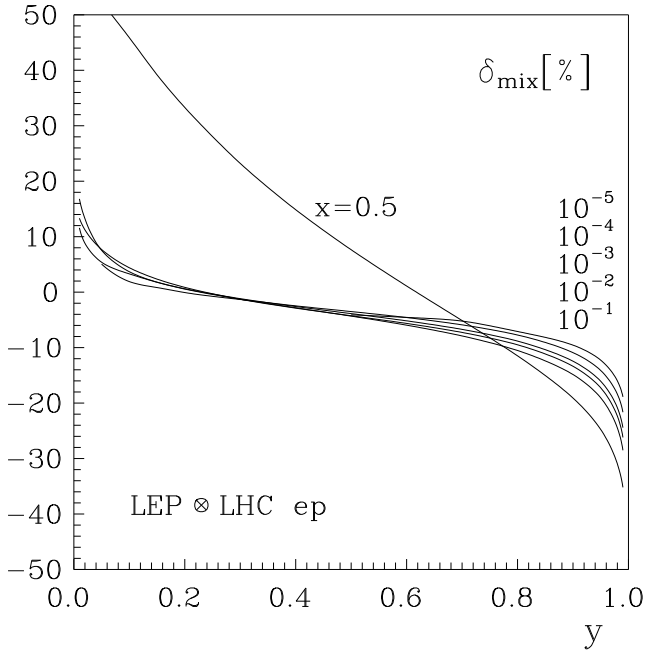

Figure 11: *Radiative correction $\delta_{\rm mix}$ in % for a cross-section measurement in terms of mixed variables at LEP⊗LHC.*

In sum, the features of the radiative corrections in terms of mixed variables are quite different from those in leptonic variables. This is an instructive illustration of the general statement that the radiative corrections depend substantial on the choice of variables, in which they are determined. In another context, namely for the neutrino-electron charged current scattering, a similar observation was made in [57].

5.3 Hadronic variables. A second analytical integration

For the cross-section in terms of hadronic variables $\mathcal{E}_h = (y_h, Q_h^2)$, the integrations have to be performed over $\mathcal{I}_h = (y_l, Q_l^2)$ and (5.2) becomes:

$$\begin{aligned}\frac{d^2\sigma_{\rm R}^{\rm F}}{dy_h dQ_h^2} &= \frac{2\alpha^3 S^2}{\lambda_S}\sum_{i=1}^{3}\frac{\mathcal{A}_i(x_h,Q_h^2)}{Q_h^4}\int dQ_l^2\, dy_l\Big[\mathcal{S}_i(y_l,Q_l^2,y_h,Q_h^2)\\ &\quad - \mathcal{S}_i^{\rm B}(y_h,Q_h^2)\mathcal{H}^{\rm IR}(y_l,Q_l^2,y_h,Q_h^2)\Big],\end{aligned} \tag{5.18}$$

where

$$\begin{aligned}\mathcal{H}^{\rm IR}(y_l,Q_l^2,y_h,Q_h^2) &\equiv \mathcal{F}^{\rm IR}(y_l,Q_l^2,y_h,Q_h^2)|_{Q^2=Q_h^2}\\ &= \frac{Q_h^2+2m^2}{Q_l^2-Q_h^2}\Big(\frac{1}{\sqrt{C_1}}-\frac{1}{\sqrt{C_2}}\Big) - m^2\Big(\frac{B_1}{C_1^{3/2}}+\frac{B_2}{C_2^{3/2}}\Big).\end{aligned} \tag{5.19}$$

In (5.18) we again can perform the analytical integration over y_l. As in the case of mixed variables, the region of integration in (5.18) must be split into two parts (see appendix B.4.2 and figure 41). The limits for y_l at given values of y_h, Q_h^2, Q_l^2 are naturally the same as for the mixed variables. The difference is with the Q^2, which interchange their roles.

After the integration over y_l, the following expression for $d^2\sigma_{\rm R}^{\rm F}/dy_h Q_h^2$ is obtained:

$$\begin{aligned}\frac{d^2\sigma_{\rm R}^{\rm F}}{dy_h dQ_h^2} &= \frac{2\alpha^3 S^2}{\lambda_S}\sum_{i=1}^{3}\frac{\mathcal{A}_i(x_h,Q_h^2)}{Q_h^4}\Bigg\{\int_{Q_l^{2\,\min}}^{Q_h^2} dQ_l^2\Big[\mathcal{S}_i^{\rm I}(Q_l^2,y_h,Q_h^2) - \mathcal{S}_i^{\rm B}(y_h,Q_h^2)\mathcal{H}_{\rm I}^{\rm IR}(Q_l^2,y_h,Q_h^2)\Big]\\ &\quad + \int_{Q_h^2}^{Q_l^{2\,\max}} dQ_l^2\Big[\mathcal{S}_i^{\rm II}(Q_l^2,y_h,Q_h^2) - \mathcal{S}_i^{\rm B}(y_h,Q_h^2)\mathcal{H}_{\rm II}^{\rm IR}(Q_l^2,y_h,Q_h^2)\Big]\Bigg\}.\end{aligned} \tag{5.20}$$

Here the functions $\mathcal{S}_i^{\rm I,II}(Q_l^2,y_h,Q_h^2)$ $(i=1,\ldots,3)$ are exactly the same as those for mixed variables [see (5.7)–(5.12)]. The definition of the $\mathcal{H}_{\rm I}^{\rm IR}(Q_l^2,y_h,Q_h^2)$ differs slightly from that of the $\mathcal{L}_{\rm I}^{\rm IR}(Q_l^2,y_h,Q_h^2)$. The integrals which are calculated with the aid of appendix D.4 differ also and the result in terms of hadronic variables is:

$$\begin{aligned}\mathcal{H}_{\rm I}^{\rm IR}(Q_l^2,y_h,Q_h^2) &\equiv \int_{y_l^{\min}{}_{\rm I}}^{y_l^{\max}} dy_l\,\mathcal{H}^{\rm IR}(y_l,Q_l^2,y_h,Q_h^2)\\ &= \frac{1}{S(Q_l^2-Q_h^2)}\left[-1+\frac{Q_h^2}{Q_l^2}(\mathrm{L}+\mathrm{L}_t+\mathrm{L}_1)-\mathrm{L}_t-\mathrm{L}_2\right],\end{aligned} \tag{5.21}$$

$$\begin{aligned}\mathcal{H}_{\rm II}^{\rm IR}(Q_l^2,y_h,Q_h^2) &\equiv \int_{y_l^{\min}{}_{\rm II}}^{y_l^{\max}} dy_l\,\mathcal{H}^{\rm IR}(y_l,Q_l^2,y_h,Q_h^2)\\ &= \frac{1}{S(Q_l^2-Q_h^2)}\left[\frac{Q_l^2}{Q_h^2}+\frac{Q_h^2}{Q_l^2}\mathrm{L}_1-\mathrm{L}-\mathrm{L}_2\right].\end{aligned} \tag{5.22}$$

The logarithms $\mathrm{L}, \mathrm{L}_a, a=1,2,t$ are defined in (5.15)–(5.16).

The remarks about the remnants of the infrared singularity and its numerical treatment may be simply taken over from the case of the mixed variables.

The reader may realize that there is one interesting difference between mixed and hadronic variables: in the latter case, one may perform also the last integration analytically, thus avoiding any numerical part of the calculation. In fact, we have done also this last step, but with a different parameterization of the phase space; see section 7.4.

5.3.1 Discussion

The leptonic QED corrections in hadronic variables are shown in figures 12-14. They are considerably smaller than those which are determined in terms of leptonic variables. From figure 41 and also from (4.9), it may be seen that for small y_h the photon energy is strongly bound; we have only soft photon corrections there. This is the origin of the similarity of the gross behaviour of the corrections in hadronic and mixed variables with each other. Without the soft photon exponentiation, the corrections would diverge when y_h approaches 1. This may be seen from (4.50). There is no explicit dependence of the dominant terms on x_h. Although, with the factor $\ln Q_h^2/m^2$, one may explain that at higher x_h the corrections are slightly more pronounced. Another singularity of the factorizing part of the corrections (4.49)–(4.50) is located at $y_h = 0$. As may be seen from the figures, it is compensated for in the net corrections. Again, as was mentioned in the case of leptonic variables, this singularity is cancelled by a corresponding behaviour of the hard non-factorizing bremsstrahlung. In fact, at $y_h = 0$ the corrections vanish even.

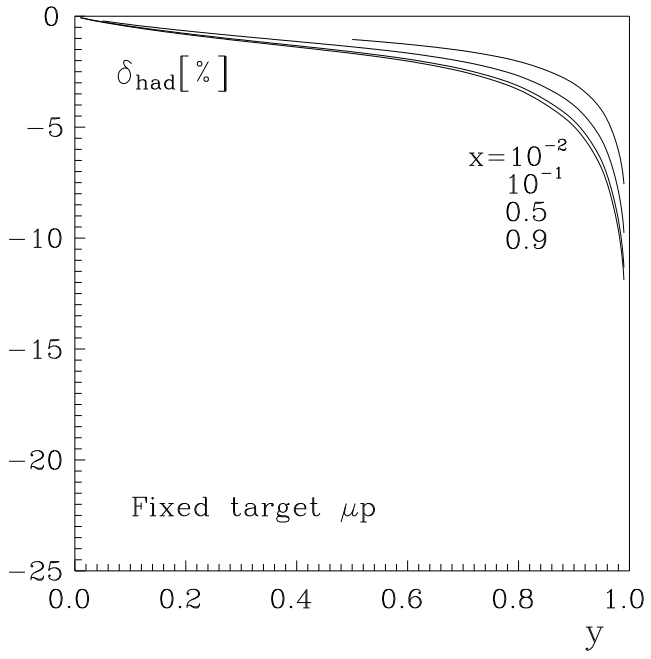

Figure 12: *Radiative correction $\delta_{\rm had}$ in % for a cross-section measurement in terms of hadronic variables for fixed target μp scattering.*

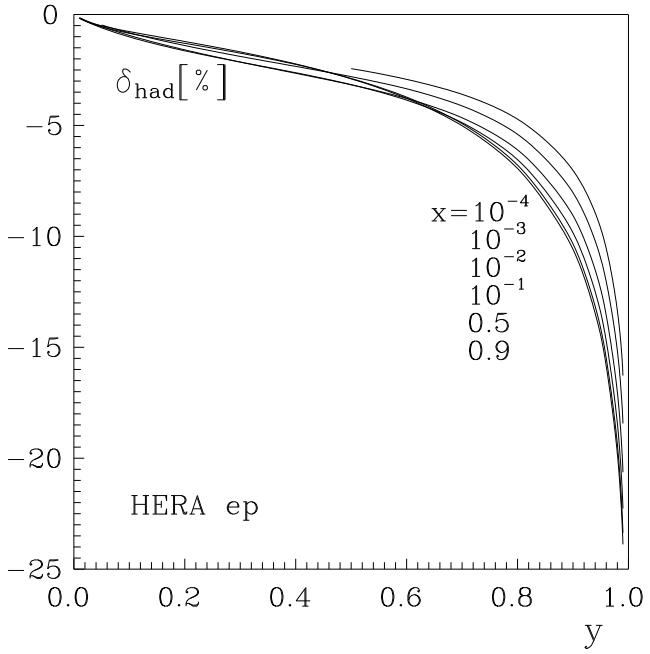

Figure 13: *Radiative correction $\delta_{\rm had}$ in % for a cross-section measurement in terms of hadronic variables at HERA.*

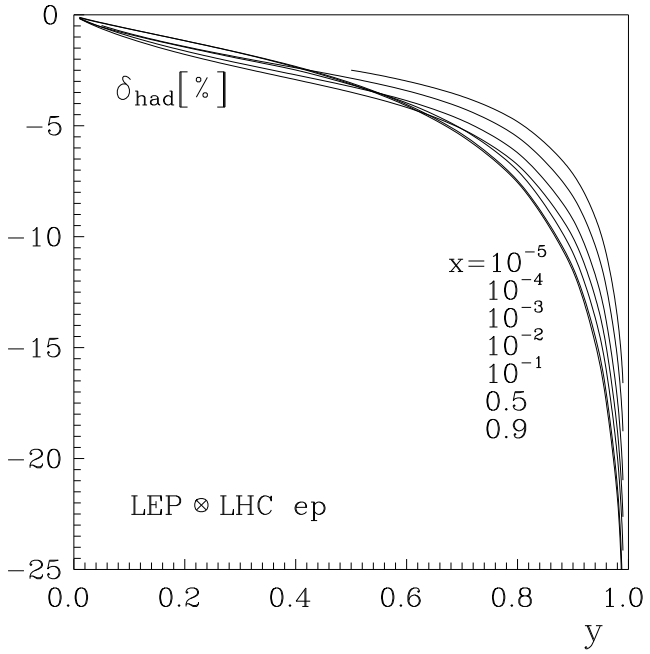

Figure 14: *Radiative correction $\delta_{\rm had}$ in % for a cross-section measurement in terms of hadronic variables at LEP⊗LHC.*

This may be explicitly seen from the formulae of section 7.4, where a completely integrated analytical expression for the corrections in hadronic variables is derived.

Finally, we should mention that a Compton peak may not be developed since Q_h^2 is fixed.

6 Photoproduction

The ep scattering process at vanishing photon momentum, $Q^2 \approx 0$, proceeds via the exchange of nearly real photons and is called photoproduction.

The process kinematics usually is described with the Q^2 as defined from the leptonic variables and the invariant mass W of the compound system consisting of the photon and the hadrons,

$$\begin{aligned} Q^2 = Q_l^2 &= (k_1 - k_2)^2, && (6.1)\\ W^2 &= -(Q_l + p_1)^2 \\ &= M^2 + (1 - x_l) y_l S = M^2 + y_l S - Q_l^2. && (6.2) \end{aligned}$$

For a fixed value of $W^2 << S$, the minimal value of Q^2 (B.25) may become extremely small. With (B.19), $W^2 \geq (M + m_\pi)^2$, it remains non-vanishing:

$$Q_l^{2\,\min}(W^2) \approx m^2 \frac{[W^2 - M^2]^2}{S^2} > 0. \tag{6.3}$$

The integrated deep inelastic cross-section is strictly finite.

For example, in the reaction $ep \to ep\rho$ at HERA energies the possible values of Q^2 extend from 10^{-15} to 10^5 GeV^2 [58]. In such a kinematical region, the description of the radiative corrections must be exact in both the proton mass M and the electron mass m. For this reason, we derive here formulae for the QED corrections in leptonic variables which remain valid at extremely small Q^2. The chosen integration variables differ slightly from those which we used so far:

$$\mathcal{E} = \mathcal{E}'_l = (W^2, Q_l^2), \qquad \mathcal{I} = \mathcal{I}'_l = (M_h^2, Q_h^2). \tag{6.4}$$

The invariant mass M_h^2 of the hadronic system is

$$M_h^2 = -(p_1 + Q_h)^2 = M^2 + y_h S - Q_h^2. \tag{6.5}$$

It will be convenient to treat the infrared singularity in a lorentz system where the above mentioned compound system is at rest: $\vec{p}_2 + \vec{k} = 0$. The necessary kinematical relations are derived in the appendices A.2 and B.2. In the following it will be described how the three different contributions to the corrections are treated: the infrared divergent correction $\delta^{\rm IR}_{\rm soft}$, the factorized hard part $\delta^{\rm IR}_{\rm hard}$, and the finite rest of the hard bremsstrahlung contribution.

The removal of the infrared divergence proceeds technically as it is described in section 4.2 but will be performed in the rest system introduced here. For the soft part of $\delta^{\rm IR}$ one gets again the expression (4.26). The velocities β_i, which are introduced in (4.20) are now to be expressed by (A.7) with the invariants (A.6). The result is:

$$\beta_1 = \sqrt{1 - \frac{4m^2M^2}{(S - Q_l^2)^2}}, \qquad \beta_2 = \sqrt{1 - \frac{4m^2M^2}{[S(1 - y_l) + Q_l^2]^2}}. \tag{6.6}$$

Further, for $\mathcal{S}_\Phi$ the exact definition (D.22) has to be used in terms of the momenta (A.7).

Integrating (4.13) threefold as it is explained in appendix D.3.2 one obtains the following expression:

$$\delta^{\rm IR}_{\rm hard}(y_l,Q_l^2,\epsilon) \;=\; 2\left[-\ln\frac{2\epsilon}{m}+\ln\frac{W^2-(M+m_\pi)^2}{m\sqrt{W^2}}\right]\left(\frac{1+\beta^2}{2\beta}\mathrm{L}_\beta-1\right), \tag{6.7}$$

where

$$\mathrm{L}_\beta = \ln\frac{\beta+1}{\beta-1}, \qquad \beta=\sqrt{1+\frac{4m^2}{Q_l^2}}. \tag{6.8}$$

Further, we need the exact QED vertex correction, which contains $\delta_{\rm vert}$ (see the second of references [5]):

$$\begin{aligned}\delta_{\rm vert}(\beta) \;&=\; -2\left(\mathcal{P}^{\rm IR}+\ln\frac{m}{\mu}\right)\left(\frac{1+\beta^2}{2\beta}\mathrm{L}_\beta-1\right)+\frac{3}{2}\beta\mathrm{L}_\beta-2\\ &\quad-\frac{1+\beta^2}{2\beta}\left[\mathrm{L}_\beta\ln\frac{4\beta^2}{\beta^2-1}+\mathrm{Li}_2\left(\frac{1+\beta}{1-\beta}\right)-\mathrm{Li}_2\left(\frac{1-\beta}{1+\beta}\right)\right].\end{aligned} \tag{6.9}$$

Finally one has to take into account also the contribution from the anomalous magnetic moment of the electron [59]. This vertex correction is needed only for the virtual photon exchange, i.e. one may neglect the axial vector part in the matrix element 2.1:

$$\gamma_\mu \;\to\; \delta_{\rm vert}(\beta)\gamma_\mu+im\mathcal{V}_{\rm anom}(\beta)\frac{(k_1+k_2)_\mu}{Q^2}, \tag{6.10}$$

$$\mathcal{V}_{\rm anom}(\beta) \;=\; -\frac{\mathrm{L}_\beta}{\beta}. \tag{6.11}$$

The cross-section contribution from the anomalous magnetic moment is[4]:

$$\frac{d^2\sigma_{\rm anom}}{dy_l dQ_l^2}=\frac{2\alpha^3 S}{\lambda_S Q_l^4}\frac{m^2}{x_l Q_l^2}\mathcal{V}_{\rm anom}(\beta)\left[2\beta^2y_l^2x_lF_1(x_l,Q_l^2)-(2-y_l)^2F_2(x_l,Q_l^2)\right]. \tag{6.12}$$

Combining the three factorizing corrections, one gets for the factorized part $\delta_{\rm VR}$ the following expression:

$$\begin{aligned}\delta_{\rm VR}(y_l,Q_l^2) \;&=\; \delta_{\rm vert}+\delta^{\rm IR}_{\rm hard}+\delta^{\rm IR}_{\rm soft}\\ &=\; \delta_{\rm inf}(y_l,Q_l^2)+\frac{1}{2\beta_1}\ln\frac{1+\beta_1}{1-\beta_1}+\frac{1}{2\beta_2}\ln\frac{1+\beta_2}{1-\beta_2}+\mathcal{S}_\Phi\\ &\quad+\frac{3}{2}\beta\mathrm{L}_\beta-2-\frac{1+\beta^2}{2\beta}\left[\mathrm{L}_\beta\ln\frac{4\beta^2}{\beta^2-1}+\mathrm{Li}_2\left(\frac{1+\beta}{1-\beta}\right)-\mathrm{Li}_2\left(\frac{1-\beta}{1+\beta}\right)\right],\end{aligned} \tag{6.13}$$

where

$$\delta_{\rm inf}(y_l,Q_l^2)=2\ln\frac{W^2-(M+m_\pi)^2}{m\sqrt{W^2}}\left(\frac{1+\beta^2}{2\beta}\mathrm{L}_\beta-1\right). \tag{6.14}$$

[4]The corresponding equation (47) in the second of [5] was not correct.

Finally, the infrared free part of the cross section (1.1) can be written as follows:

$$\frac{d^2\sigma_{\rm R}^{\rm F}}{dy_l dQ_l^2} = \frac{2\alpha^3 S}{\lambda_S}\int dM_h^2 dQ_h^2 \sum_{i=1}^{3}\Big[\mathcal{A}_i(x_h,Q_h^2)\frac{1}{Q_h^4}\mathcal{S}_i(y_l,Q_l^2,y_h,Q_h^2) - \mathcal{A}_i(x_l,Q_l^2)\frac{1}{Q_l^4}\,\mathcal{S}_i^B(y_l,Q_l^2)\,\mathcal{L}^{\rm IR}(y_l,Q_l^2,y_h,Q_h^2)\Big], \tag{6.15}$$

where $\mathcal{S}_i(y_l,Q_l^2,y_h,Q_h^2)$ $(i=1,2,3)$ are given by (3.14)–(3.16), and $\mathcal{L}^{\rm IR}(y_l,Q_l^2,y_h,Q_h^2)$ is defined by (5.4). We would like to remind that these expressions are exact in both masses m and M for the photon exchange contribution.

In sum, the cross-section is:

$$\frac{d^2\sigma_{\rm R}}{dy_l dQ_l^2} = \frac{d^2\sigma_{\rm anom}}{dy_l dQ_l^2} + \frac{d^2\sigma_{\rm R}^{\rm F}}{dy_l dQ_l^2} + \frac{d^2\sigma_{\rm B}}{dy_l dQ_l^2}\left\{\exp\left[\frac{\alpha}{\pi}\delta_{\rm inf}(\mathcal{E})\right] - 1 + \frac{\alpha}{\pi}\Big[\delta_{\rm VR}(\mathcal{E}) - \delta_{\rm inf}(\mathcal{E})\Big]\right\}. \tag{6.16}$$

Here, we should also mention that the structure functions must have a certain behaviour in the limit of small Q^2. From the relation between the total cross-section of photon-proton scattering and the structure function F_2 at small Q^2 [58],

$$\sigma_{\gamma p}^T(W) = \frac{4\pi\alpha}{Q^2}F_2(x,Q^2)|_{Q^2=0}, \tag{6.17}$$

one concludes that the structure functions should vanish with vanishing Q^2. One possibility is to multiply them by a global suppression factor [60]:

$$\mathcal{F}_{1,2}^{\rm NC}(x,Q^2) \to [1-\exp(-aQ^2)]\mathcal{F}_{1,2}^{\rm NC}(x,Q^2), \qquad a = 3.37\,{\rm GeV}^{-2}. \tag{6.18}$$

In our numerical results, we follow this prescription.

6.1 Discussion

The QED corrections in the case of photoproduction are shown in figure 15 for HERA energies. The structure functions [51, 61] are taken from [52] and [62].

As was already discussed in the section on leptonic variables, soft photon emission is located near $y_l = 0$. With rising y_l more and more hard photons may be emitted and the influence of the structure functions via the non-factorizing hard corrections becomes more pronounced. It is further interesting to observe that at the extreme small values of x_l as discussed here the radiative corrections vanish at $y_l = 0$. For the anomalous vertex correction (6.12) and the exponentiated soft photon correction (6.14) this follows immediately from the limits in (6.8): $\beta \to \infty$ and $\mathrm{L}_\beta \to 2/\beta$. Here, it is important to notice that the Q_l^2 becomes small even compared to the electron mass. In fact, with the aid of (6.2), (6.3) may be well approximated by $Q_l^{2\,\rm min} \sim m^2 y_l^2 << m^2$ for small y_l. Further, the $\delta_{\rm hard}^{\rm IR}$ of (6.7) vanishes explicitly. This reflects the general statement that for sufficiently small y_l energetic photons cannot be emitted. For the rest of the corrections, we see no trivial argument why they should vanish or compensate each other; but they do. A further interesting feature is of kinematical origin. At very small x_l, the Q_l^2 is also bound strongly. As may be seen in figure 35, then the allowed values of y_h are bound from above. In the ultra-relativistic approximation this property gets lost.

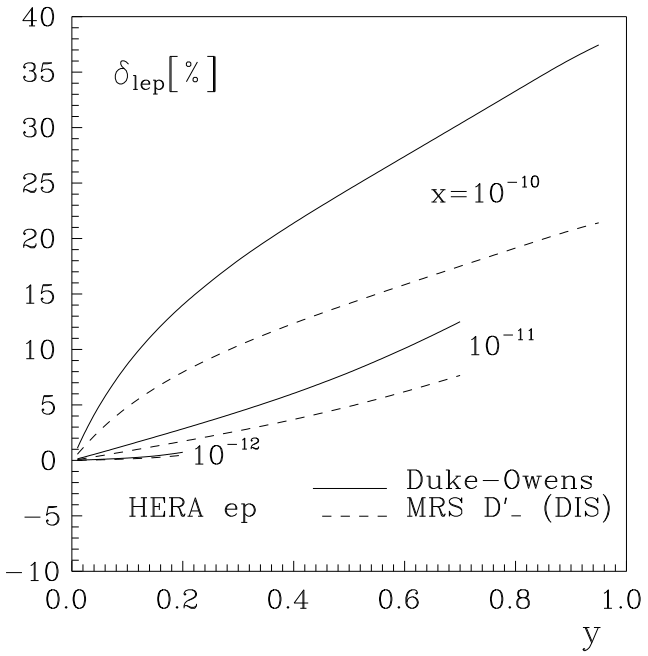

Figure 15: *Radiative correction for photoproduction at HERA with two different sets of structure functions.*

7 An alternative treatment of the phase space

So far, one unique phase space parameterization has been used for all three different sets of external variables. The infrared problem was treated in the proton rest system. Compared to this, for leptonic variables the rest system which was introduced for the treatment of the photoproduction process lead to considerable simplifications.

Here, we change to a completely different phase space parametrization, which is specially adapted to the case of hadronic and Jaquet-Blondel variables. The leptonic degrees of freedom will be integrated over at the very beginning of the calculation.

7.1 Hadronic variables. The phase space

Wherever possible, the ultra-relativistic kinematics will be used in this section. We start from the slightly rewritten expression (2.38):

$$\Gamma = \int \frac{d\vec{k_2}}{2k_2^0}\frac{d\vec{k}}{2k^0}\delta^4(k_1+p_1-k_2-p_2-k)d^4p_2\delta(p_2^2+M_h^2)dM_h^2. \tag{7.1}$$

Now, the integration variables we are interested in will be introduced. For that purpose, we consider the photon and the final state electron to be a compound system. The corresponding rest frame R is defined by the three-momentum relation $\vec{k}_2^R+\vec{k}^R=0$. The integration variables $\vec{k}_2, \vec{k}$ may be replaced by the following variables:

- the invariant mass of the (γe) compound system $\tau = -(k_2+k)^2$;

- the photonic angles ϑ_R, φ_R in the rest frame R of this compound system.

The phase space of the variables k_2, k may be parameterized as follows:

$$\int \frac{d\vec{k_2}}{2k_2^0}\frac{d\vec{k}}{2k^0}\delta^4(k_1+p_1-k_2-p_2-k) \;=\; \int d\tau\delta(\tau+\Lambda^2)d\Gamma_{\gamma e}. \tag{7.2}$$

Here, the phase space element of the (γe)-compound system is introduced:

$$d\Gamma_{\gamma e} = \frac{d\vec{k_2}}{2k_2^0}\frac{d\vec{k}}{2k^0}\delta^4(\Lambda-k_2-k). \tag{7.3}$$

In the rest frame R of the compound system, (7.3) may be rewritten as it is explained in appendix A.4.3:

$$\begin{aligned}\int d\Gamma_{\gamma e} &= \frac{\sqrt{\lambda(\tau,m^2,0)}}{8\tau}\int_{-1}^{1} d\cos\vartheta_R\int_0^{2\pi}d\varphi_R,\\ \sqrt{\lambda(\tau,m^2,0)} &= \tau-m^2.\end{aligned} \tag{7.4}$$

In a next step, the hadronic momentum transferred Q_h^2 is introduced into (7.1), and the corresponding δ-function under the p_2 integral is exploited. In appendix A.4.4, it is shown:

$$\int d^4p_2\delta(p_2^2+M_h^2)\delta\left[(k_1+p_1-p_2)^2+\tau\right]\delta\left[Q_h^2-(p_2-p_1)^2\right] = \frac{\pi}{2\sqrt{\lambda_S}}. \tag{7.5}$$

Then, with the relation $y_hS = Q_h^2+M_h^2-M^2$ from (6.5) one gets the identity $dQ_h^2dM_h^2 = SdQ_h^2dy_h$. This introduces the last of the hadronic variables into the integration measure:

$$\Gamma = \frac{\pi^2S}{4\sqrt{\lambda_S}}\int dy_h dQ_h^2\int d\tau\frac{1}{4\pi}\frac{\tau-m^2}{\tau}\int d\cos\vartheta_R d\varphi_R. \tag{7.6}$$

The physical region of (y_h, Q_h^2, τ) is derived in appendix B.4.4.

7.2 A twofold angular integration

In hadronic variables, the double differential cross-section of the process (1.2) becomes:

$$\frac{d^2\sigma_{\mathrm{R}}}{dy_hdQ_h^2} = \frac{2\alpha^3}{SQ_h^4}\int d\tau\sum_{i=1}^{3}A_i(x_h,Q_h^2)\mathcal{S}_i(y_h,Q_h^2,\tau), \tag{7.7}$$

where

$$\mathcal{S}_i(y_h,Q_h^2,\tau) = \frac{1}{4\pi}\frac{z_2}{\tau}\int d\cos\vartheta_R d\varphi_R\,\mathcal{S}_i(y_h,Q_h^2,\tau,\cos\vartheta_R,\varphi_R). \tag{7.8}$$

The functions $\mathcal{S}_i(y_h,Q_h^2,\tau,\cos\vartheta_R,\varphi_R)$ arise from the functions $\mathcal{S}_i(\mathcal{E},\mathcal{I},z_1,z_2)$ after the following substitutions for y_l, Q_l^2, and z_1 in (2.40)–(2.42) in accordance with appendix A.3 and with the definitions (2.34), (2.43):

$$Q_l^2 = Q_h^2+z_2-z_1, \tag{7.9}$$

$$z_1 = \frac{z_2}{2\tau}\left(Q_h^2+\tau+m^2-\sqrt{\lambda_1}\cos\vartheta_R\right), \tag{7.10}$$

$$1-y_l = \frac{1}{2}(1-y_h)\left(1+\frac{m^2}{\tau}\right)+\frac{z_2}{2\tau S}\sqrt{\lambda_\tau}\left(\cos\vartheta_p\cos\vartheta_R+\sin\vartheta_p\sin\vartheta_R\sin\varphi_R\right), \tag{7.11}$$

where

$$\cos\vartheta_p = \frac{S(Q_h^2 - z_2) - y_h S(Q_h^2 + \tau + m^2)}{\sqrt{\lambda_\tau}\sqrt{\lambda_1}}. \tag{7.12}$$

After performing the above insertions, the $\mathcal{S}_i$ may be integrated over the two photon angles with the aid of the tables of integrals of appendix E.1. In the ultra-relativistic approximation, the result is:

$$\begin{aligned}
\mathcal{S}_1(y_h, Q_h^2, \tau) &= Q_h^2\left[\frac{1}{z_2}(\mathrm{L}_\tau - 2) + \frac{1}{4}\frac{\tau - m^2}{\tau^2}\right] + \frac{1}{4} + \frac{1}{2}\left(1 - \frac{Q_h^2}{Q_\tau^2}\right)\mathrm{L}_\tau, && (7.13)\\
\mathcal{S}_2(y_h, Q_h^2, \tau) &= S^2\Bigg\{2(1-y_h)\left[\frac{1}{z_2}(\mathrm{L}_\tau - 2) + \frac{1}{4}\frac{\tau - m^2}{\tau^2}\right] - \frac{Q_\mathrm{h}^4}{Q_\tau^6}(\mathrm{L}_\tau - 3) && (7.14)\\
&\quad + \frac{Q_h^2}{Q_\tau^4}[1 - (1-y_h)(\mathrm{L}_\tau - 3)] - \frac{1}{Q_\tau^2}\left[(2-y_h)\mathrm{L}_\tau - \frac{1}{2}(1-y_h)(7-y_h)\right]\Bigg\},\\
\mathcal{S}_3(y_h, Q_h^2, \tau) &= S\Bigg\{2Q_h^2(2-y_h)\left[\frac{1}{z_2}(\mathrm{L}_\tau - 2) + \frac{1}{4}\frac{\tau - m^2}{\tau^2}\right] - y_h\left(\mathrm{L}_\tau - \frac{1}{2}\right)\\
&\quad + \frac{Q_h^2}{Q_\tau^2}\left[2 - (\mathrm{L}_\tau - 2)\left(2 - y_h + \frac{2Q_h^2}{Q_\tau^2}\right)\right]\Bigg\}, && (7.15)
\end{aligned}$$

where

$$\mathrm{L}_\tau = \ln\frac{Q_\tau^4}{m^2\tau}, \tag{7.16}$$

$$Q_\tau^2 = Q_h^2 + \tau - m^2. \tag{7.17}$$

The infrared singularity is located at $z_2 = 0$ and has to be treated appropriately.

7.3 The infrared divergence

As was done in section 4.1, the following ansatz will be used in order to separate the infrared divergent parts in (7.7):

$$\begin{aligned}
\frac{d^2\sigma_\mathrm{R}}{dy_h dQ_h^2} &= \frac{2\alpha^3}{SQ_h^4}\sum_{i=1}^{3} A_i(x_h, Q_h^2)\Bigg\{\mathcal{S}_i^\mathrm{B}(y_h, Q_h^2)\delta_\mathrm{R}^\mathrm{IR}(y_h, Q_h^2)\\
&\quad + \int d\tau\left[\mathcal{S}_i(y_h, Q_h^2, \tau) - \mathcal{S}_i^\mathrm{B}(y_h, Q_h^2)\mathcal{F}^\mathrm{IR}(y_h, Q_h^2, \tau)\right]\Bigg\}. && (7.18)
\end{aligned}$$

Here, we define the $\delta_\mathrm{R}^\mathrm{IR}(y_h, Q_h^2)$ in complete analogy with (4.14) as the sum of an infrared divergent soft and a finite hard contribution:

$$\begin{aligned}
\delta_\mathrm{soft}^\mathrm{IR}(y_h, Q_h^2, \epsilon) &= \frac{2}{\pi}\int\frac{d^3k}{2k^0}\mathcal{F}^\mathrm{IR}(Q_h^2, z_1, z_2)\theta(\epsilon - k^0), && (7.19)\\
\delta_\mathrm{hard}^\mathrm{IR}(y_h, Q_h^2, \epsilon) &= \frac{4}{\pi^2}\frac{\sqrt{\lambda_S}}{S}\int\frac{d\Gamma}{d\mathcal{E}}\mathcal{F}^\mathrm{IR}(Q^2, z_1, z_2)\theta(k^0 - \epsilon)\\
&= \int d\tau\frac{1}{4\pi}\frac{\tau - m^2}{\tau}\int d\cos\vartheta_R d\varphi_R\mathcal{F}^\mathrm{IR}(Q^2, z_1, z_2)\theta(k^0 - \epsilon). && (7.20)
\end{aligned}$$

The $\mathcal{F}^{\rm IR}(y_h, Q_h^2, \tau)$ will be determined below. The expression for $\delta^{\rm IR}_{\rm soft}(y_h, Q_h^2, \epsilon)$ is the equivalent of (4.10) and $\delta^{\rm IR}_{\rm hard}(y_h, Q_h^2, \epsilon)$ follows immediately from (4.14). Further,

$$\mathcal{F}^{\rm IR}(Q_h^2, z_1, z_2) \;=\; \frac{Q_h^2}{z_1 z_2} - m^2\left(\frac{1}{z_1^2}+\frac{1}{z_2^2}\right). \tag{7.21}$$

The hard part of the infrared divergent correction will be integrated first. The integrals over the photon angles in $\delta^{\rm IR}_{\rm hard}(y_h, Q_h^2, \epsilon)$ may be performed with the aid of (7.10) and of the table of integrals in appendix E.1:

$$\begin{aligned}
\delta^{\rm IR}_{\rm hard}(y_h, Q_h^2, \epsilon) &= \int d\tau \mathcal{F}^{\rm IR}(y_h, Q_h^2, \tau)\theta(k^0-\epsilon), &(7.22)\\
\mathcal{F}^{\rm IR}(y_h, Q_h^2, \tau) &= \frac{1}{4\pi}\frac{\tau-m^2}{\tau}\int d\cos\vartheta_R d\varphi_R \mathcal{F}^{\rm IR}(Q_h^2, z_1, z_2)\\
&= \frac{1}{z_2}\left(\mathrm{L}_\tau - 2\right) - \frac{1}{Q_\tau^2}\mathrm{L}_\tau + \frac{1}{\tau}, &(7.23)
\end{aligned}$$

and L_τ and Q_τ^2 are defined in (7.16) and (7.17).

The boundaries for the integration over τ may be found in (B.94). The potentially infrared divergent term in $\delta^{\rm IR}_{\rm hard}(y_h, Q_h^2, \epsilon)$ contains a dependence on $1/z_2$ and is integrated with the aid of the table of integrals E.2:

$$\begin{aligned}
\int_{\bar{z}_2}^{\tau^m}\frac{dz_2}{z_2}\left(\mathrm{L}_\tau - 2\right) &= 2\left(\mathrm{L_h}-1\right)\ln\left[\frac{Q_h^2}{2m\epsilon}\left(\frac{1}{y_h}-1\right)\right] - \frac{1}{2}\ln^2\left[\frac{Q_h^2}{m^2}\left(\frac{1}{y_h}-1\right)\right]\\
&\quad - 2\mathrm{Li}_2\left(1-\frac{1}{y_h}\right) - \mathrm{Li}_2(1). &(7.24)
\end{aligned}$$

With the aid of appendix E.3, the explicitly finite part of $\delta^{\rm IR}_{\rm hard}(y_h, Q_h^2, \epsilon)$ may finally also be integrated. We will not quote the result separately, but rather treat this contribution together with the finite hard cross-section in the next section.

Now, the infrared divergence in $\delta^{\rm IR}_{\rm soft}(y_h, Q_h^2, \epsilon)$ will be treated. For this purpose, the R system of the foregoing section is used. As derived in appendix A.3, the photon energy becomes:

$$k^{0,R} = |\vec{k}^R| = \frac{\tau-m^2}{2\sqrt{\tau}} = \frac{z_2}{2\sqrt{\tau}} < \epsilon. \tag{7.25}$$

Besides k^R, we will need the four momenta k_1^R, k_2^R in the limit $z_2 \to 0$, see A.9:

$$\begin{array}{lllllll}
k_2^{0,R} & \to & m, & |\vec{k}_2^R| = |\vec{k}^R| \sim z_2 & \to & 0, & \beta_2 \to 0,\\
k_1^{0,R} & \to & \dfrac{Q_h^2}{2m}, & |\vec{k}_1^R| & \to & \dfrac{Q_h^2}{2m}, & 1-\beta_1^2 \to \dfrac{4m^4}{(Q_h^2+2m^2)^2}.
\end{array} \tag{7.26}$$

Since the final state lepton is practically at rest there, the following isotropic relation holds:

$$-2kk_2 \to 2mk^{0,R}. \tag{7.27}$$

It is this property, which simplifies the angular integration. In (4.15), it is not necessary to introduce the Feynman parameter which finally lead to the complicated function S_Φ of (D.22).

Instead of (4.16), one gets:

$$\delta_{\rm soft}^{\rm IR}(\mathcal{E},\epsilon) \;\to\; \frac{2(2\pi)^2}{(2\sqrt{\pi})^n\Gamma\left(n/2-1\right)}\frac{1}{\mu^{n-4}}\int_0^{\epsilon}(k^{0,R})^{n-5}dk^{0,R}\int_0^{\pi}(\sin\vartheta)^{n-3}d\vartheta_1 \times\left[\frac{Q^2+2m^2}{mk_1^{0,R}(1-\beta_1\cos\vartheta_1)}-\frac{m^2}{(k_1^{0,R})^2(1-\beta_1\cos\vartheta_1)^2}-1\right], \tag{7.28}$$

where one has to use $Q^2\to Q_h^2$. Instead of (4.23) and (4.24), it is now

$$\delta_{\rm soft}^{\rm IR}(\mathcal{E},\epsilon) \;=\; \left[\mathcal{P}^{\rm IR}+\ln\frac{2\epsilon}{\mu}\right]\frac{1}{2}\int_{-1}^{1}d\xi\;\mathcal{F}(\xi)+\frac{1}{4}\int_{-1}^{1}d\xi\,\ln(1-\xi^2)\;\mathcal{F}(\xi), \tag{7.29}$$

with

$$\mathcal{F}(\xi)=\frac{2(Q_h^2+2m^2)}{Q_h^2}\frac{1}{1-\beta_1\xi}-\frac{4m^4}{Q_h^4}\frac{1}{(1-\beta_1\xi)^2}-1. \tag{7.30}$$

The integrations in (7.29) may be performed with the aid of appendix D.2:

$$\delta_{\rm soft}^{\rm IR}(y_h,Q_h^2,\epsilon)=2\left[\mathcal{P}^{\rm IR}+\ln\frac{2\epsilon}{\mu}\right](\mathrm{L_h}-1)-\mathrm{L_h^2}+\mathrm{L_h}-\mathrm{Li_2}(1)+1, \tag{7.31}$$

where $\mathcal{P}^{\rm IR}$ is introduced in (4.25), and

$$\mathrm{L_h}=\;\ln\frac{Q_h^2}{m^2}. \tag{7.32}$$

The cut-off parameter ϵ may be seen to be cancelled against the corresponding terms in (7.24).

In order to get an infrared finite and well-defined cross-section the photonic vertex correction $\delta_{\rm vert}$ has to be added to the radiative cross-section (7.18). It is given by (4.34), again with the replacement $Q^2\to Q_h^2$. In the sum, the infrared divergence cancels:

$$\delta_{\rm soft}^{\rm IR}(y_h,Q_h^2,\epsilon)+\delta_{\rm vert}(Q_h^2)=2\left(\mathrm{L_h}-1\right)\ln\frac{2\epsilon}{m}-\frac{3}{2}\mathrm{L_h^2}+\frac{5}{2}\mathrm{L_h}-1. \tag{7.33}$$

7.4 A third analytical integration

In (7.18), the last remaining integral is that over τ or, equivalently, over z_2. Since the structure functions depend on hadronic variables which are here at the same time the external variables the last integral may be performed analytically. For this purpose one has to integrate the functions $\mathcal{S}_i(y_h,Q_h^2,\tau)$ as given by (7.13)–(7.15). The cross-section may be reordered such that the infrared singular terms in the finite hard cross-section explicitly compensate each other:

$$\frac{d^2\sigma_{\rm R}}{dy_h dQ_h^2} \;=\; \frac{d^2\sigma_{\rm B}}{dy_h dQ_h^2}\frac{\alpha}{\pi}\left[\delta_{\rm soft}^{\rm IR}(y_h,Q_h^2,\epsilon)+\int_{\bar z_2}^{\tau^m}\frac{dz_2}{z_2}\left(\mathrm{L}_\tau-2\right)\right] +\frac{2\alpha^3}{SQ_h^4}\sum_{i=1}^{3}A_i(x_h,Q_h^2)\int_{m^2}^{\tau^m}d\tau\left[\mathcal{S}_i(y_h,Q_h^2,\tau)-\mathcal{S}_i^{\rm B}(y_h,Q_h^2)\frac{1}{z_2}\left(\mathrm{L}_\tau-2\right)\right]. \tag{7.34}$$

The resulting cross-section is rather compact and the last integrations over τ may be easily performed with the aid of appendix E.3.

The net cross-section is:

$$\frac{d^2\sigma}{dy_h dQ_h^2} = \frac{d^2\sigma_{\rm B}}{dy_h dQ_h^2} \exp\left[\frac{\alpha}{\pi}\delta_{\rm inf}(y_h, Q_h^2)\right] + \frac{2\alpha^3}{S}\sum_{i=1}^{3}\frac{1}{Q_h^4}\mathcal{A}_i(x_h, Q_h^2)\mathcal{S}_i(y_h, Q_h^2). \tag{7.35}$$

The $\delta_{\rm inf}(y_h, Q_h^2)$ and the $\mathcal{S}_i(y_h, Q_h^2)$ are defined in (1.9) and (1.10).

We would like to remark that these purely analytical formulae for the leptonic QED corrections in hadronic variables to neutral current deep inelastic scattering are an extremely esthetic result. They are published here for the first time. Numerically, the corrections agree completely with those derived within the approach of section 5.3.

As was mentioned above, the corrections vanish at $y \to 0$. That this is really the case may be seen by inspecting the analytical expressions.

7.5 Jaquet-Blondel variables

From hadronic variables, one may easily change to Jaquet-Blondel variables (1.8) in the phase space (7.6). The expression for $Q^2_{\rm JB}$ in terms of hadronic variables is derived in appendix B.5:

$$y_{\rm JB} = y_h, \tag{7.36}$$

$$Q^2_{\rm JB} = Q_h^2 - \frac{y_h}{1-y_h}(\tau - m^2). \tag{7.37}$$

The physical boundaries in the phase space integral (7.6),

$$\Gamma = \frac{\pi^2}{4}\int dy_{\rm JB}\, dQ^2_{\rm JB} \int d\tau \frac{1}{4\pi}\frac{\tau - m^2}{\tau}\int d\cos\vartheta_R\, d\varphi_R, \tag{7.38}$$

are also derived there. From the above relations, it may be seen that the Jaquet-Blondel variables and the hadronic variables are related in a one-to-one correspondence, with τ being a parameter.

In Jaquet-Blondel variables, the double differential cross-section of process (1.2) reads:

$$\frac{d^2\sigma_{\rm R}}{dy_{\rm JB} dQ^2_{\rm JB}} = \frac{2\alpha^3}{S}\int d\tau \sum_{i=1}^{3}\mathcal{A}_i(x_h, Q_h^2)\frac{1}{Q_h^4}\mathcal{S}_i(y_{\rm JB}, Q^2_{\rm JB}, \tau). \tag{7.39}$$

The $\mathcal{S}_i(y_{\rm JB}, Q^2_{\rm JB}, \tau)$ may be trivially obtained from (7.13)–(7.15) with the relations

$$y_h = y_{\rm JB}, \tag{7.40}$$

$$Q_h^2 = Q^2_{\rm JB} + \frac{y_{\rm JB}}{1-y_{\rm JB}}(\tau - m^2). \tag{7.41}$$

The explicit expressions are [43][5]:

$$\mathcal{S}_1(Q^2_{\rm JB}, y_{\rm JB}, \tau) = Q^2_{\rm JB}\left[\frac{1}{z_2}(\mathrm{L}_\tau - 2) + \frac{z_2}{4\tau^2}\right] + \frac{1-8y_{\rm JB}}{4(1-y_{\rm JB})} + \mathrm{L}_\tau\left(\frac{z_2}{2Q_\tau^2} + \frac{y_{\rm JB}}{1-y_{\rm JB}}\right), \tag{7.42}$$

[5]The equation (7.44) corrects the equation (17) in [43]. The error was created in the manuscript. Fortran program and numerical results were not influenced by this.

$$\begin{aligned}\mathcal{S}_2(Q^2_{\rm JB},y_{\rm JB},\tau) &= S^2\Bigg\{2(1-y_{\rm JB})\left[\frac{1}{z_2}\,(\mathrm{L}_\tau-2)+\frac{z_2}{4\tau^2}\right]-\frac{1}{Q^2_\tau}\left[2(\mathrm{L}_\tau-2)+\frac{1}{2}(1-{y_{\rm JB}}^2)\right]\\ &\quad+\frac{Q^2_{\rm JB}}{Q^4_\tau}(1-y_{\rm JB})\,[1-(1+y_{\rm JB})(\mathrm{L}_\tau-3)]-\frac{Q^4_{\rm JB}}{Q^6_\tau}(1-y_{\rm JB})^2(\mathrm{L}_\tau-3)\Bigg\},\end{aligned} \tag{7.43}$$

$$\begin{aligned}\mathcal{S}_3(Q^2_{\rm JB},y_{\rm JB},\tau) &= S\Bigg\{2Q^2_{\rm JB}(2-y_{\rm JB})\left[\frac{1}{z_2}(\mathrm{L}_\tau-2)+\frac{z_2}{4\tau^2}\right]+\frac{y_{\rm JB}(1+{y_{\rm JB}}^2)}{1-y_{\rm JB}}\mathrm{L}_\tau+5\\ &\quad-\frac{7y_{\rm JB}}{2(1-y_{\rm JB})}-(1-y_{\rm JB})(5+2y_{\rm JB})\\ &\quad+\frac{Q^2_{\rm JB}}{Q^2_\tau}(1-y_{\rm JB})\left[(1-y_{\rm JB})\left(3-\frac{2Q^2_{\rm JB}}{Q^2_\tau}\right)(\mathrm{L}_\tau-2)+12-5\mathrm{L}_\tau\right]\Bigg\}.\end{aligned} \tag{7.44}$$

The integral over τ has to be performed numerically as long as one cannot neglect the difference between $Q^2_{\rm JB}$ and Q^2_h – the structure functions are depending on Q^2_h and thus on τ.

The integrand in (7.39) is infrared singular at $\tau = m^2$, which corresponds to $z_2 = 0$. The treatment of the infrared singularity may be performed in full analogy with the foregoing section. In the infrared singular point, $z_2 \to 0$, the hadronic and the Jaquet-Blondel variables agree and the $\delta^{\rm IR}_{\rm soft}$ in these variables do so:

$$\begin{aligned}\delta^{\rm IR}_{\rm soft}(y_{\rm JB},Q^2_{\rm JB},\epsilon) &= \frac{1}{\pi}\int\frac{d^3k}{k^0}\mathcal{F}^{\rm IR}(Q^2_{\rm JB},z_1,z_2)\theta(\epsilon-k^0)\\ &= 2\left[\mathcal{P}^{\rm IR}+\ln\frac{2\epsilon}{\mu}\right](\mathrm{L}_{\rm JB}-1)-\mathrm{L}^2_{\rm JB}+\mathrm{L}_{\rm JB}-\mathrm{Li}_2(1)+1.\end{aligned} \tag{7.45}$$

The $\delta^{\rm IR}_{\rm hard}(y_{\rm JB},Q^2_{\rm JB},\epsilon)$ differs slightly from the hadronic correction:

$$\begin{aligned}\delta^{\rm IR}_{\rm hard}(y_{\rm JB},Q^2_{\rm JB},\epsilon) &= \frac{4}{\pi^2}\frac{\sqrt{\lambda_S}}{S}\int\frac{d\Gamma}{d\mathcal{E}}\mathcal{F}^{\rm IR}(Q^2_{\rm JB},z_1,z_2)\theta(k^0-\epsilon)\\ &= \int d\tau\frac{1}{4\pi}\frac{\tau-m^2}{\tau}\int d\cos\vartheta_R d\varphi_R\mathcal{F}^{\rm IR}(Q^2_{\rm JB},z_1,z_2)\theta(k^0-\epsilon).\end{aligned} \tag{7.46}$$

In fact, it is

$$\begin{aligned}\mathcal{F}^{\rm IR}(Q^2_{\rm JB},z_1,z_2) &= \frac{Q^2_{\rm JB}}{z_1z_2}-m^2\left(\frac{1}{z_1^2}+\frac{1}{z_2^2}\right)\\ &= \mathcal{F}^{\rm IR}(Q^2_h,z_1,z_2)-\frac{y_{\rm JB}}{1-y_{\rm JB}}\frac{1}{z_1}.\end{aligned} \tag{7.47}$$

Using the results of the calculation of the hadronic correction, it is sufficient to explicitly integrate the difference term in (7.47) over φ_R and $\cos\vartheta_R$ with the aid of appendix E.1. Then,

$$\delta^{\rm IR}_{\rm hard}(y_{\rm JB},Q^2_{\rm JB},\epsilon) = \int d\tau\mathcal{F}^{\rm IR}(y_{\rm JB},Q^2_{\rm JB},\tau)\theta(k^0-\epsilon), \tag{7.48}$$

where

$$\begin{aligned}\mathcal{F}^{\rm IR}(y_{\rm JB},Q^2_{\rm JB},\tau) &= \frac{1}{4\pi}\frac{\tau-m^2}{\tau}\int d\cos\vartheta_R d\varphi_R\mathcal{F}^{\rm IR}(Q^2_{\rm JB},z_1,z_2)\\ &= \frac{1}{z_2}(\mathrm{L}_\tau-2)-\frac{1}{(1-y_{\rm JB})}\frac{\mathrm{L}_\tau}{Q^2_\tau}+\frac{1}{\tau}.\end{aligned} \tag{7.49}$$

The L_τ and Q^2_τ are defined in (7.16) and (7.17), respectively; furthemore the substitutions (7.40) and (7.41) have to be used. The integral over τ may be performed with appendix E.2 for the potentially infrared singular terms and with appendix E.3 for the others; but now within the boundaries (B.106).

The result is:

$$\begin{aligned}\delta^{\rm IR}_{\rm hard}(y_{\rm JB},Q^2_{\rm JB},\epsilon) &= 2\,(\mathrm{L}_{\rm JB}-1)\ln\frac{\tau^{\max}}{2m\epsilon}-\frac{1}{2}\ln^2\frac{\tau^{\max}}{m^2}+\ln\frac{\tau^{\max}}{m^2}\\ &+\ \ln X_{\rm JB}\left[\ln(1-y_{\rm JB})-\ln X_{\rm JB}-\mathrm{L}_{\rm JB}\right]-\mathrm{Li}_2(X_{\rm JB})-2\mathrm{Li}_2(1-X_{\rm JB}),\end{aligned} \tag{7.50}$$

where

$$\mathrm{L}_{\rm JB} = \ln\frac{Q^2_{\rm JB}}{m^2}, \tag{7.51}$$

$$X_{\rm JB} = \frac{1}{x_{\rm JB}y_{\rm JB}}\left[1-x_{\rm JB}(1-y_{\rm JB})\right], \tag{7.52}$$

$$\tau^{\max} = (1-x_{\rm JB})(1-y_{\rm JB})S. \tag{7.53}$$

The photonic vertex correction $\delta_{\rm vert}$ is given by (4.34), but with the replacement $Q^2\to Q^2_{\rm JB}$.

The net factorized part is

$$\begin{aligned}\delta_{\rm VR}(y_{\rm JB},Q^2_{\rm JB}) &= \delta_{\rm vert}+\delta^{\rm IR}_{\rm soft}(y_{\rm JB},Q^2_{\rm JB},\epsilon)+\delta^{\rm IR}_{\rm hard}(y_{\rm JB},Q^2_{\rm JB},\epsilon)\\ &= \delta^{\rm inf}(Q^2_{\rm JB},y_{\rm JB})-\ln^2X_{\rm JB}+\ln X_{\rm JB}\left[\ln(1-y_{\rm JB})-1\right]\\ &\quad-\frac{1}{2}\ln^2\left[\frac{(1-x_{\rm JB})(1-y_{\rm JB})}{x_{\rm JB}y_{\rm JB}}\right]\\ &\quad+\frac{3}{2}\mathrm{L}_{\rm JB}-\mathrm{Li}_2(X_{\rm JB})-2\mathrm{Li}_2(1-X_{\rm JB})-1,\end{aligned} \tag{7.54}$$

where

$$\delta_{\rm inf}(y_{\rm JB},Q^2_{\rm JB}) = \ln\frac{(1-x_{\rm JB})(1-y_{\rm JB})}{1-x_{\rm JB}(1-y_{\rm JB})}\left(\ln\frac{Q^2_{\rm JB}}{m^2}-1\right). \tag{7.55}$$

The finite part of the radiative cross-section in Jaquet-Blondel variables is

$$\begin{aligned}\frac{d^2\sigma^{\rm F}_{\rm R}}{dy_{\rm JB}dQ^2_{\rm JB}} &= \frac{2\alpha^3}{S}\int d\tau\sum_{i=1}^{3}\Bigg[\mathcal{A}_i(x_h,Q^2_h)\frac{1}{Q^4_h}\mathcal{S}_i(y_{\rm JB},Q^2_{\rm JB},\tau)\\ &\quad-\mathcal{A}_i(x_{\rm JB},Q^2_{\rm JB})\frac{1}{Q^4_{\rm JB}}\,\mathcal{S}^B_i(y_{\rm JB},Q^2_{\rm JB})\,\mathcal{F}^{\rm IR}(y_{\rm JB},Q^2_{\rm JB},\tau)\Bigg].\end{aligned} \tag{7.56}$$

The net cross-section is:

$$\begin{aligned}\frac{d^2\sigma_{\rm R}}{dy_{\rm JB}dQ^2_{\rm JB}} &= \frac{d^2\sigma_{\rm B}}{dy_{\rm JB}dQ^2_{\rm JB}}\left\{\exp\left[\frac{\alpha}{\pi}\delta_{\rm inf}(y_{\rm JB},Q^2_{\rm JB})\right]-1+\frac{\alpha}{\pi}\left[\delta_{\rm VR}(y_{\rm JB},Q^2_{\rm JB})-\delta_{\rm inf}(y_{\rm JB},Q^2_{\rm JB})\right]\right\}\\ &\quad+\frac{d^2\sigma^{\rm F}_{\rm R}}{dy_{\rm JB}dQ^2_{\rm JB}}.\end{aligned} \tag{7.57}$$

7.5.1 Discussion

The leptonic QED corrections in Jaquet-Blondel variables are shown in figures 16–18. They behave quite similar to the corrections in hadronic variables. At small y, this follows from the fact that the variables become equal there. Thus, the vanishing of the corrections at $y_h \to 0$ is understood from the hadronic case. As was discussed with the mixed and hadronic variables, the soft photon corner is at $y_{\rm JB}$ approaching 1. From (7.55) one may see that the dominant soft photon corrections are negative and the more pronounced, the larger the $x_{\rm JB}$. This makes some difference to the hadronic variables. Again as in all the previous cases, the corrections for fixed target scattering are different from the collider cases due to the smaller value of S and to the difference of the muon and electron masses. The collider results are quite similar to each other.

8 Discussion

In the foregoing sections, we discussed some of the basic features of the leptonic QED corrections to the neutral current deep inelastic ep scattering in terms of different sets of kinematical variables.

Basic features of the magnitudes of the corrections and their behaviour as functions of the kinematics have been discussed there.

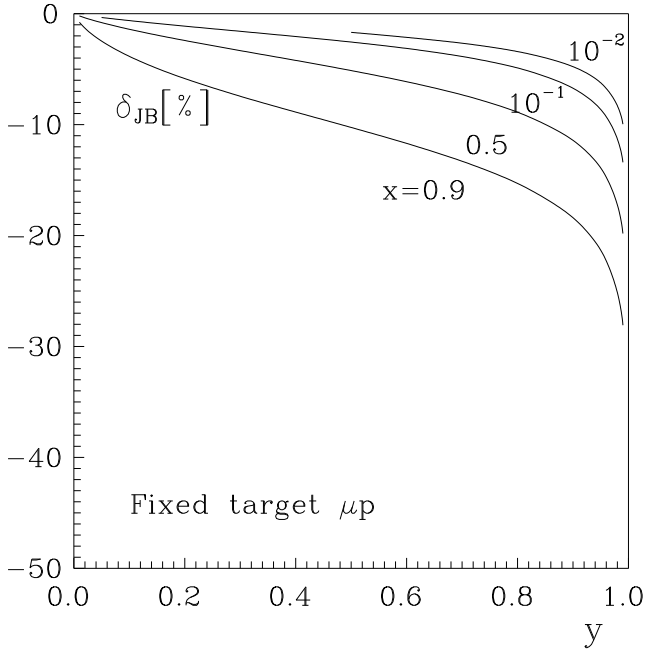

Figure 16: *Radiative cross-section for fixed target deep inelastic neutral current scattering in terms of Jaquet-Blondel variables.*

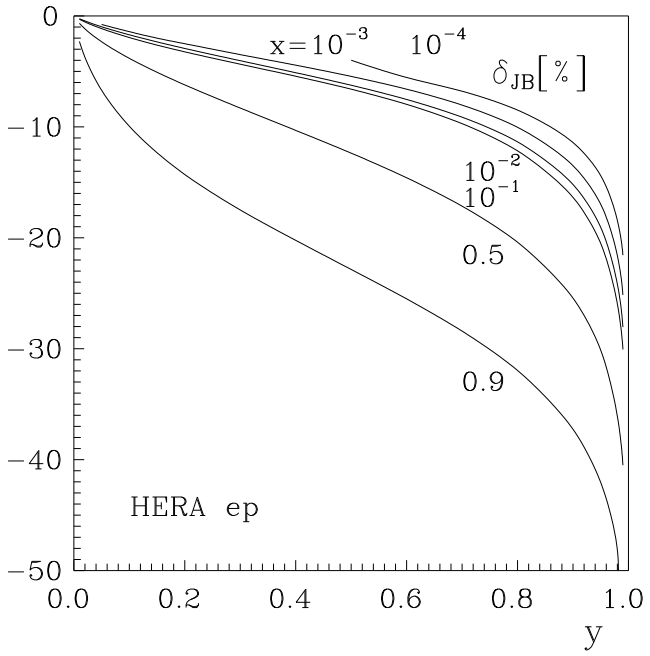

Figure 17: *Radiative cross-section for deep inelastic neutral current scattering at HERA in terms of Jaquet-Blondel variables.*

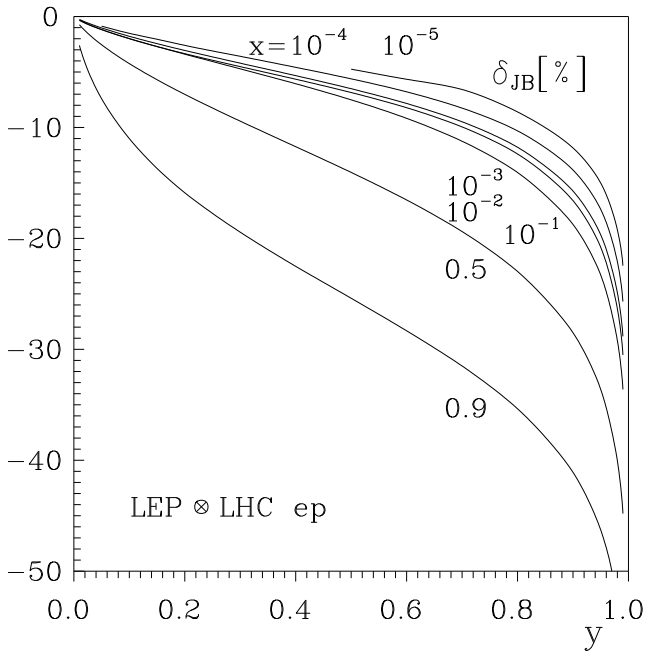

Figure 18: *Radiative cross-section for deep inelastic neutral current scattering at LEP⊗LHC in terms of Jaquet-Blondel variables.*

In this section, we discuss some additional features of the corrections:

- the dependence of the corrections on the structure functions;
- comparison with the leading logarithmic approximation;
- photonic cuts in leptonic variables;
- the Compton peak;
- other radiative corrections.

8.1 The influence of structure functions on the QED corrections

In figures 19 and 20, the radiative corrections in leptonic variables at HERA and LEP⊗LHC are parameterized with two different sets of structure functions [51, 52, 63, 64]. Both sets were derived before HERA started operation. If there are deviations between predictions with different structure functions, then they are due to the contribution from hard photon emission. For soft photons, the correction factorizes and the structure function dependence drops out in the corrections, when expressed in form of the ratios δ. In experimentally unexplored regions the predicted structure functions rely heavily on the predictive power of perturbative QCD. Especially for small values of x problems may arise. These are reflected in rising deviations of corrections with different structure functions when x becomes smaller. While, at intermediate and larger values of x, the dependence of the corrections on the choice of structure functions becomes minor. For this reason we changed the presentation of the corrections and chose the set of variables Q^2, x, thereby losing sensitivity to y.

Figures 21 and 22 show the same corrections as figures 19 and 20, respectively. But now with structure functions [65, 66, 63, 67] whose derivations took into account HERA data at low x. The disagreement of the predictions at small x remains but is much smaller.

A similar comparison for the other sets of variables is shown in figures 23–25. The structure functions [51, 52, 63, 64] which were not yet improved with the HERA data are used. The dependence of the corrections in mixed variables on the choice of structure functions is quite substantial but less pronounced than in the corresponding case in leptonic variables. For the hadronic and Jaquet-Blondel variables the influence is reasonably small. This follows from the smaller contribution of hard photon emission. The net corrections are negative. This proves the dominance of the factorizing soft and virtual photonic contributions. Their dependence on the structure functions cancels when δ is calculated.

The dependence of the QED corrections on the structure functions is not only influenced by different estimates of the QCD predictions for the parton distribution evolutions. The corrections show additional dependences on the low-Q^2 behaviour of the structure functions, the choice of Q^2 in the argument of the parton distributions, soft photon exponentiation, and the running of the QED coupling constant.

We use the corrections in mixed variables for an illustration of this. The Fortran program `TERAD91` [38] allows us to switch on and off the above indicated dependencies of the cross-sections with the following flags:

(i) For `IVAR`=0, the low-Q^2 behaviour of the structure functions remains untouched; for `IVAR`=2, the modification (6.18) is applied.

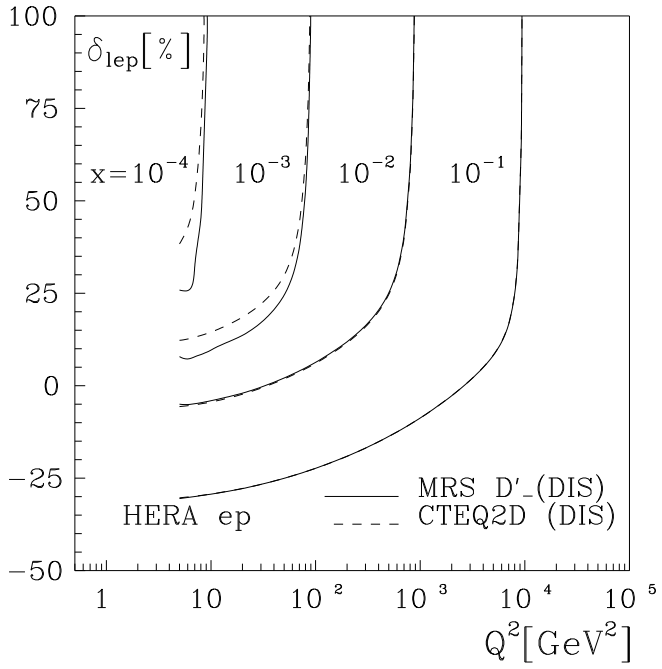

Figure 19: *Comparison of the radiative corrections $\delta_{\rm lep}(x,Q^2)$ at HERA in terms of two different sets of structure functions.*

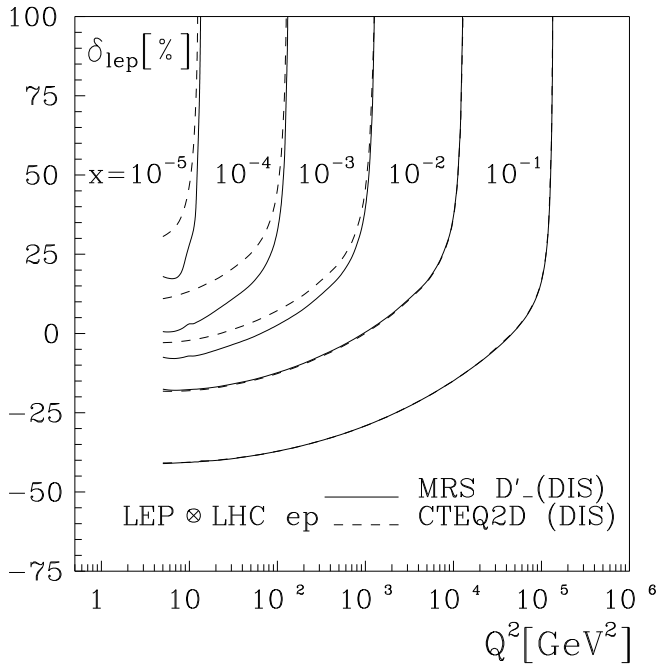

Figure 20: *Comparison of the radiative corrections $\delta_{\rm lep}(x,Q^2)$ at LEP⊗LHC in terms of two different sets of structure functions.*

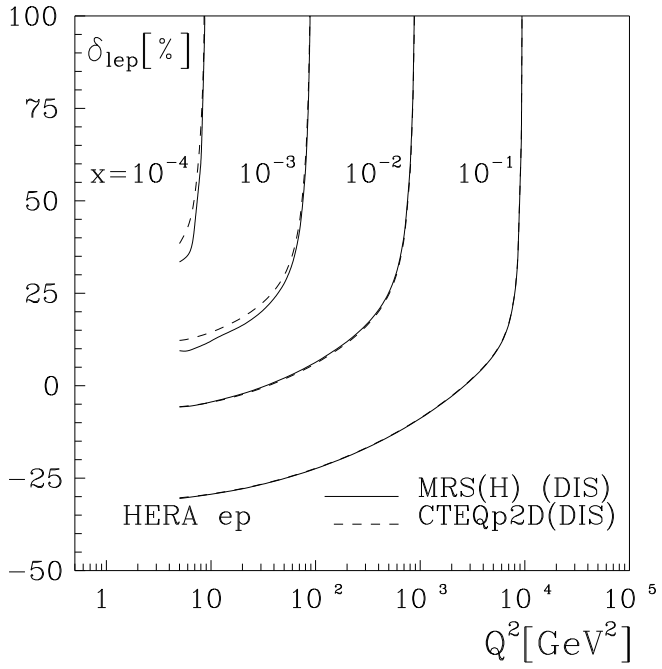

Figure 21: *Comparison of the radiative corrections $\delta_{\rm lep}(x,Q^2)$ at HERA in terms of two different sets of HERA-improved structure functions.*

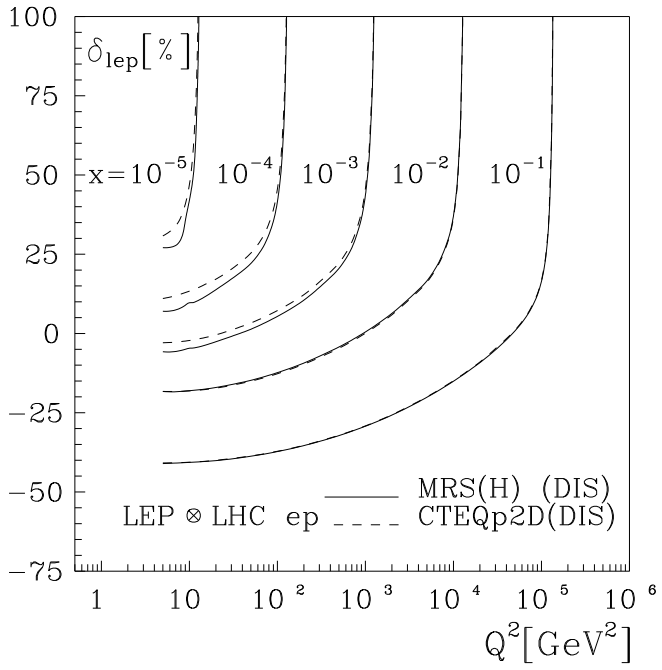

Figure 22: *Comparison of the radiative corrections $\delta_{\rm lep}(x,Q^2)$ at LEP⊗LHC in terms of two different sets of HERA-improved structure functions.*

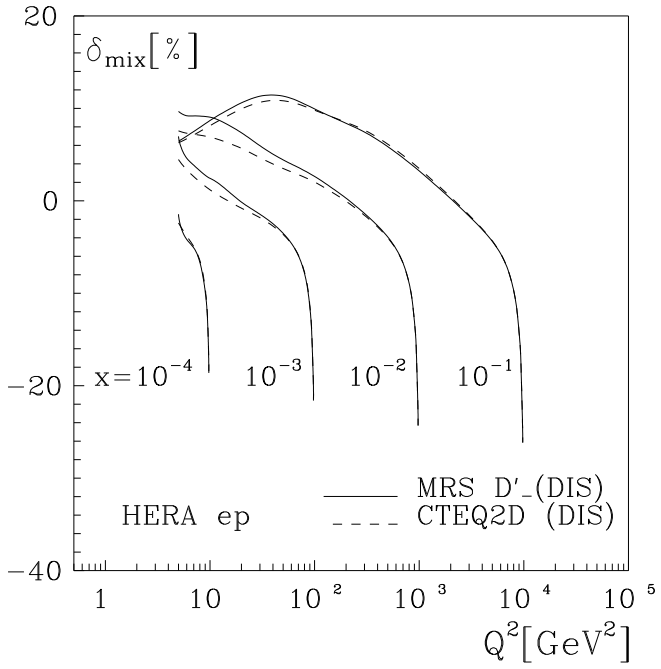

Figure 23: *Comparison of the radiative corrections $\delta_{\rm mix}(x,Q^2)$ at HERA in terms of two different sets of structure functions.*

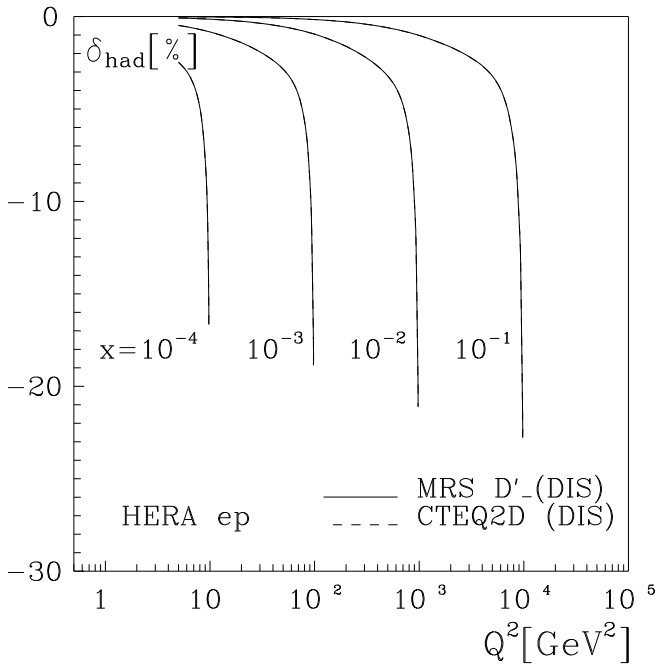

Figure 24: *Radiative corrections $\delta_{\rm had}(x,Q^2)$ at HERA in terms of two different sets of structure functions.*

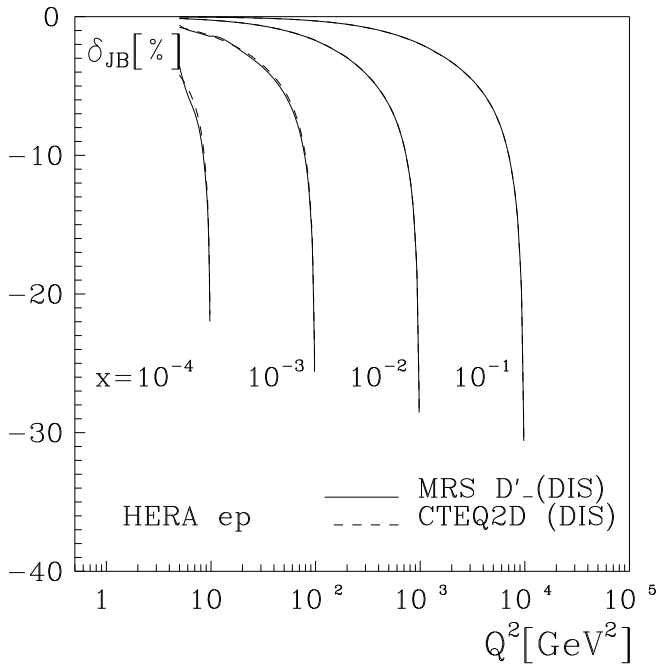

Figure 25: *Radiative corrections $\delta_{\rm JB}(x,Q^2)$ at HERA in terms of two different sets of structure functions.*

(ii) For `ITERAD`=0, the structure functions are assumed to depend on Q_l^2. A correct choice is `ITERAD`=1, which makes the structure functions dependent on Q_h^2.

(iii) With the settings `IEXP`=0,1 the soft photon exponentiation as it is introduced in (4.43) is switched off or on.

(iv) For `IVPOL`=0,1 the running of the QED coupling constant with the Q^2 of the t-channel momentum flow is switched off or on.

In the figures, the flag settings are quoted as follows: (`IVAR,ITERAD,IEXP,IVPOL`).

Figure 26 shows the dependence of the corrections on both the running of the QED coupling constant and the soft photon exponentiation. Both corrections are small and tend to compensate each other for large values of y. For $x_m = 0.5$ and the maximal value of Q^2, the values are: -34.4% for (0000), -29.8% for (0010), and -32.7% for (0011).

Figure 27 shows the dependence of the corrections on the choice of the Q^2 in the structure functions under the integral for the hard photon emission. There is a strong dependence when hard photon emission contributes substantially to the corrections. We see also a faking behaviour of the corrections at smaller values of Q^2, which is more pronounced at larger values of x. At $Q^2 = 5$ GeV^2, the parton distributions are artificially frozen since below this value the evolution may not be controlled. Thus, there is no room for a variation of Q^2 at all, and both flag settings become equal.

Finally, figure 28 shows the most realistic choice of the flags mentioned. As is evident from the above discussion and a comparison with the foregoing figures, the low-Q^2 modifications are extremely important for a correct description of the corrections at small Q^2 and large x.

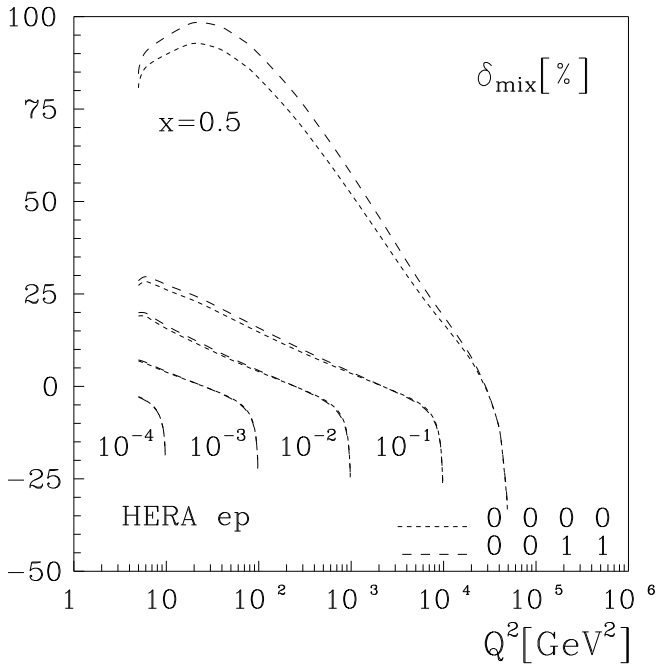

Figure 26: *Comparison of the radiative corrections $\delta_{\rm mix}(x,Q^2)$ at HERA with two parameterizations of structure functions. Flag settings (*`IVAR,ITERAD,IEXP,IVPOL`*) are explained in the text.*

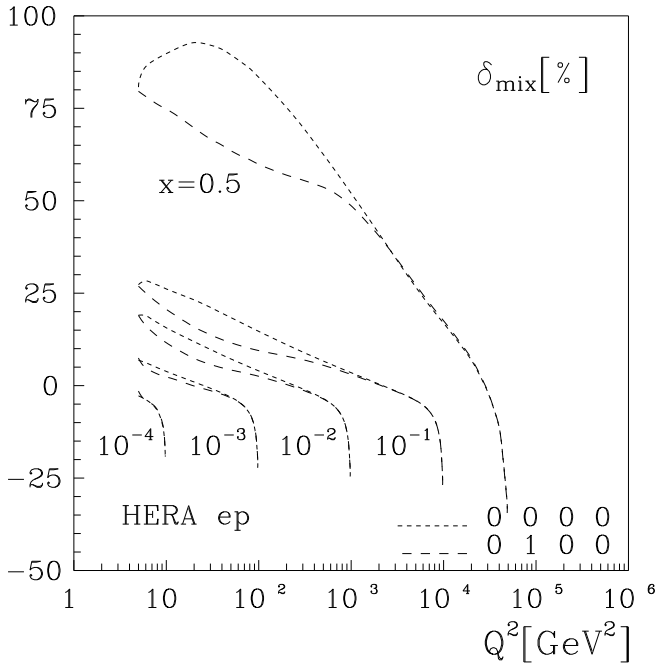

Figure 27: *Comparison of the radiative corrections $\delta_{\rm mix}(x,Q^2)$ at HERA with two parameterizations of structure functions; the flag settings are explained in the text.*

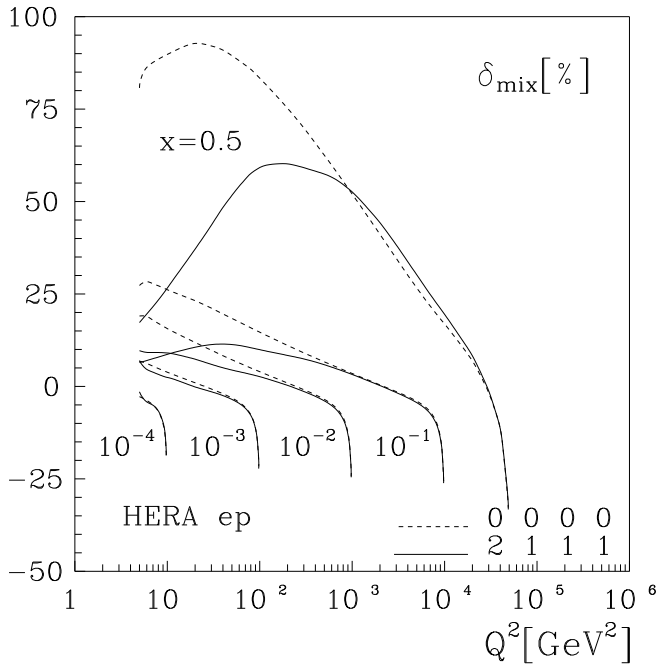

Figure 28: *Comparison of the radiative corrections $\delta_{\rm mix}(x,Q^2)$ at HERA with two parameterizations of structure functions. Flag settings are explained in the text.*

To summarize this part of the discussion, at least in certain regions of the phase space it is extremely important to ensure an iterative improvement of the various components of the description of deep inelastic scattering, including the interplay of structure functions and QED corrections.

8.2 A comparison with leading logarithmic approximations

An interesting and practically important question concerns the accuracy of the leading logarithmic approximations (LLA). For a comparison, we use the Fortran program `HELIOS` [33] with the same structure functions as in `TERAD`. For the special purpose here soft photon exponentiation, other higher order corrections, the low-Q^2 modifications etc. are excluded.

The comparison is performed for leptonic, mixed, and Jaquet-Blondel variables and shown in figures 29 – 31. For the comparison, the structure functions [63, 68] and the following flags in `TERAD` have been chosen: (`IVAR,ITERAD,IEXP,IVPOL`)=(0100).

Over a wide kinematical range, the leading logarithmic approximation works quite well and is completely sufficient for a description of the experimental data. For intermediate x in leptonic and small x in mixed and hadronic variables, the accuracy of the LLA is best.

One may also conclude from the figures that a complete $\mathcal{O}(\alpha)$ calculation will become necessary if the experimental accuracy reaches the level of one per cent or better.

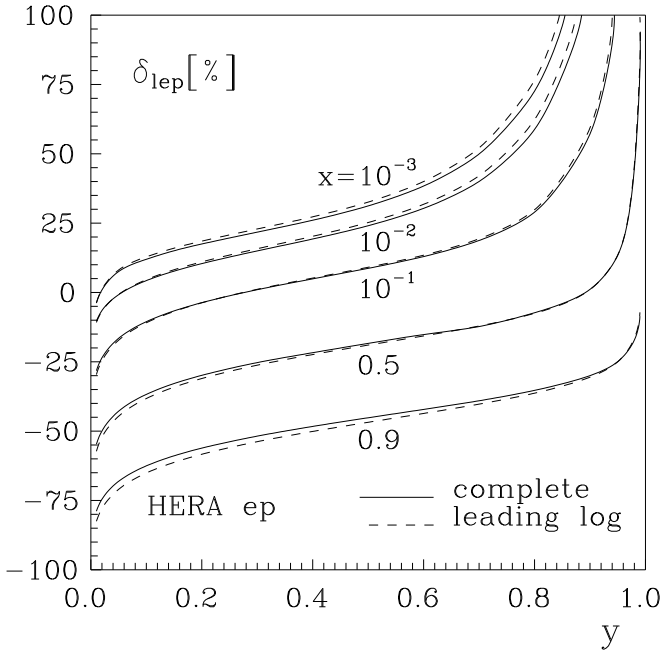

Figure 29: *Comparison of radiative corrections $\delta_{\rm lep}(x,Q^2)$ at HERA from a complete $\mathcal{O}(\alpha)$ and a LLA calculation.*

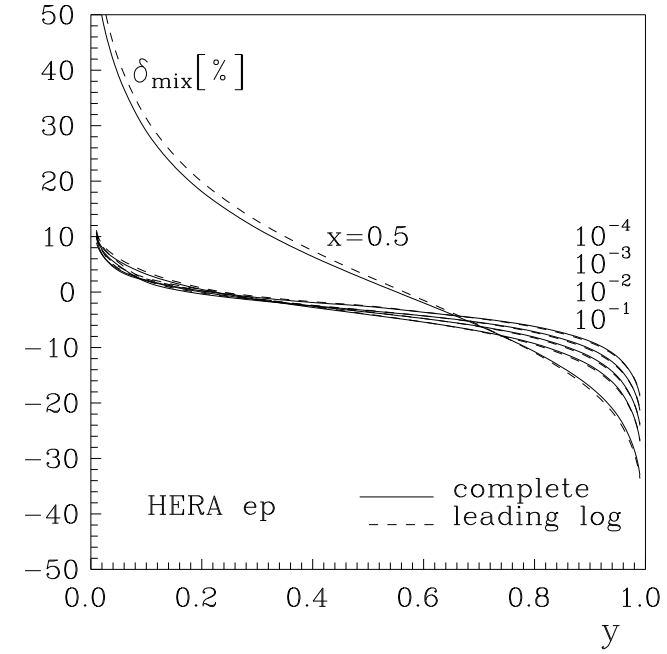

Figure 30: *Comparison of radiative corrections $\delta_{\rm mix}(x,Q^2)$ at HERA from a complete $\mathcal{O}(\alpha)$ and a LLA calculation.*

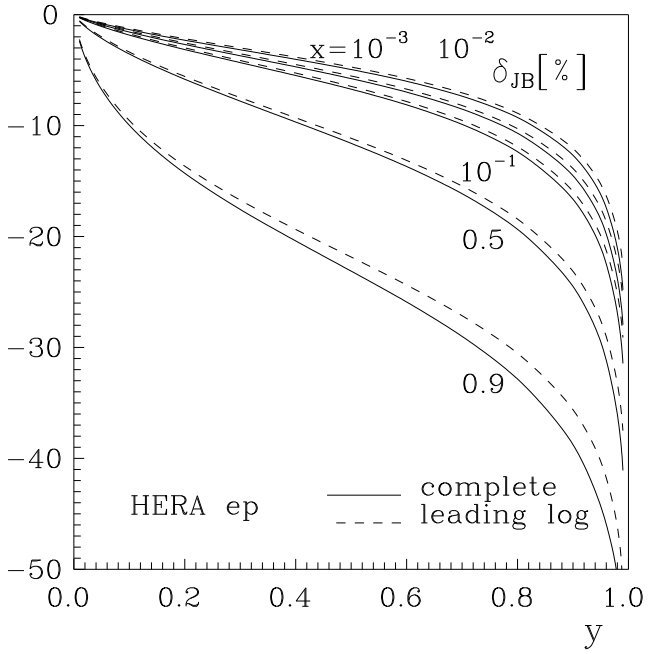

Figure 31: *Comparison of radiative corrections $\delta_{\rm JB}(x,Q^2)$ at HERA from a complete $\mathcal{O}(\alpha)$ and a LLA calculation.*

8.3 Photonic cuts

An instructive illustration of some basic features of the QED corrections is figure 32[6]. It shows the dependence of the correction $\delta_{\rm lep}$ on y_l in presence of cuts on the photon momentum which are introduced in appendix B.1.2.

To be definite, we chose $x = 0.001$ and HERA kinematics. The quark distributions are [61, 62]. It is assumed that photons may be observed if they have an energy larger than $E_m = 1$ GeV and are inside a cone with an opening angle of $\theta_\gamma^{\rm max} = 0.1$ rad. The cut conditions are inactive as long as the photon energy is smaller than E_m. The left-hand side of the second of (B.15) corresponds to this. As long as $z_E^{\rm min}$ is negative, the cut is fictitious. It starts to be influential if, in the ultra-relativistic limit,

$$y_l = y_h + \frac{E_m}{E_e}. \tag{8.1}$$

Since y_h is integrated over, this condition weakens to the following one:

$$y_l = \frac{E_m}{E_e} = 0.033. \tag{8.2}$$

At this value of y_l the rise of the cross-section is sharply interrupted. The collinear initial and final state photons may get an energy larger than E_m. If so they become cut when being

[6]The figure was made with data from `TERAD91`. Later, it was reproduced by the Monte-Carlo program `HERACLES` [29, 35]. We should like to thank H. Spiesberger for his careful analysis of the figure, which we used when preparing this section.

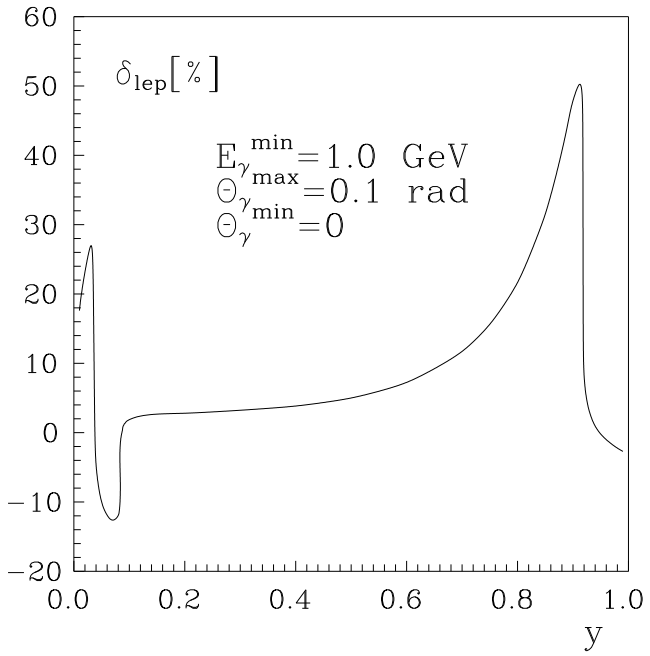

Figure 32: *Radiative cross-section for deep inelastic neutral current scattering at HERA in leptonic variables with photonic cuts; x=0.001.*

emitted inside the cut cone. The collinear final state photons escape from the cut cone and become non-observable if the electron scattering angle θ'_e,

$$\cos\theta'_e = \frac{1}{E'_e}\left[(1-y_l)E_e - x_l y_l E_p\right], \tag{8.3}$$

$$E'_e = \left[(1-y_l)E_e + x_l y_l E_p\right], \tag{8.4}$$

becomes larger than $\theta_\gamma^{\max}$. The value of y_l above which this is the case and the collinear final state photons become more and more unconstrained by our cuts is:

$$y_l = \frac{(1-\cos\theta'_e)\,E_e}{(1-\cos\theta'_e)\,E_e + (1+\cos\theta'_e)\,x_l E_p} = 0.084. \tag{8.5}$$

Above this value, the contribution from final state radiation to the cross-section rises.

Further, the emission of photons due to the Compton mechanism grows. This contribution peaks at large y_l and small x_l (see the next section). It is due to the t-channel exchange of photons with practically vanishing Q^2. Thus, it comes mainly from events with real photons whose transverse momenta are balanced with those of the scattered electrons and the longitudinal ones are opposite. If now y_l becomes larger than the value

$$y_l = 1 - \frac{(1-\cos\theta'_e)\,E_e}{(1-\cos\theta'_e)\,E_e + (1+\cos\theta'_e)\,x_l E_p} = 1 - 0.084 = 0.916, \tag{8.6}$$

these photons enter into the cut cone and will not contribute to the measured cross-section. The Compton peak starts to become cut.

8.4 The Compton peak

The Compton peak has been discussed first in [2]. The corresponding cross-section enhancement is due to energetic final state radiation from the lepton. It is related to large y_l and small x_l. As will be shown here, the origin of the Compton peak is deeply connected with the lower bound on the Q_h^2 which is reached when the integral over Q_h^2 is performed in order to get a cross-section in leptonic variables. The extremely small Q^2 of the virtual photon makes the kinematical situation resembling the scattering of light at matter.

As may be also seen from the figures, the Compton peak occurs in leptonic and mixed variables, while it is absent in hadronic and Jaquet-Blondel variables. The reason is that in the last two sets of variables, the Q_h^2 is an external variable and thus not free to vary down to the kinematical limit.

The Compton peak arises from the integration of the photon propagator dQ_h^2/Q_h^4 over Q_h^2 in the contribution from the γ exchange in formulae (5.3) and (5.6). We will indicate here the essential steps only. For the structure functions, Bjorken scaling will be assumed:

$$F_i(x_h, Q_h^2) \approx F_i(x_h). \tag{8.7}$$

Further, for an integration over Q_h^2 at fixed x_h the following change of integration variables is necessary:

$$dy_h dQ_h^2 = dx_h dQ_h^2 \frac{Q_h^2}{x_h^2 S}. \tag{8.8}$$

The variables x_h and Q_h^2 vary within limits which are derived in appendix B.2.5.

Using (8.7) and (8.8), the γ exchange part of the radiative cross-section may be rewritten as follows:

$$\frac{d^2\sigma_{\rm QED}(\gamma)}{dy_l dQ_l^2} = \frac{d^2\sigma_{\rm B}(\gamma)}{dy_l dQ_l^2}\frac{\alpha}{\pi}\hat{\delta}_{\rm VR} + \frac{d^2\sigma_{\rm R}^{\rm F}(\gamma)}{dy_l dQ_l^2}, \tag{8.9}$$

$$\begin{aligned}\frac{d^2\sigma_{\rm R}^{\rm F}(\gamma)}{dy_l dQ_l^2} &= \frac{2\alpha^3 S}{\lambda_S}\int dx_h dQ_h^2 \\ &\times \left\{\frac{2}{x_h^2 Q_h^4}F_1(x_h)S_1(y_l,Q_l^2;y_h,Q_h^2) + \frac{1}{x_h Q_h^4}F_2(x_h)S_2(y_l,Q_l^2;y_h,Q_h^2)\right. \\ &- \left.\left[\frac{2}{x_l^2 Q_l^4}F_1(x_l)S_1^B(y_l,Q_l^2) + \frac{1}{x_l Q_l^4}F_2(x_l)S_2^B(y_l,Q_l^2)\right]\mathcal{L}^{\rm IR}(y_l,Q_l^2;y_h,Q_h^2)\right\}.\end{aligned} \tag{8.10}$$

The correction $\hat{\delta}_{\rm VR}$ may be found in [5, 14]. For a discussion of the Compton peak, only the first two terms under the integral in (8.10) are relevant. Examining their variations as functions of Q_h^2 one may conclude that they are of two types. From the integrands $(1; 1/\sqrt{C_1}; 1/\sqrt{C_2})dQ_h^2/Q_h^2$, a $\ln(Q_h^{2\,\rm min}/Q_h^{2\,\rm max})$ emerges, while from the integrands $(1; 1/\sqrt{C_1}; 1/\sqrt{C_2})dQ_h^2/Q_h^4$ a $1/Q_h^{2\,\rm min}$. The latter, however, are screened by factors m^2 or M^2.

In [5, 14], the following formula has been derived after integration of (8.10) over Q_h^2 in the ultra-relativistic approximation:

$$\frac{d^2\sigma_{\rm QED}(\gamma)}{dy_l dQ_l^2} = \frac{2\alpha^3}{y_l Q_l^4}\left\{Y_+\left[\ln\frac{(1-x_l)^2 y_l^2}{x_l^2(1-y_l)}\left(\ln\frac{Q_l^2}{m_e^2}-1\right) + \frac{3}{2}\ln\frac{Q_l^2}{m_e^2} - \frac{1}{2}\ln^2(1-y_l) - 2\right]F_2(x_l)\right.$$

$$+\ 2Y_+\left(\ln\frac{Q_l^2}{m_e^2}-1\right)\int_1^{1/x_l}dz\frac{F_2(zx_l)-F_2(x_l)}{z-1}$$
$$+\ \int_1^{1/x_l}dz\frac{dz}{z^2}\left[U_e(\gamma;1,1-y_l)+U_e(\gamma;y_l-1,-1)\right]F_2(zx_l)\Bigg\}, \tag{8.11}$$

where

$$\begin{aligned}U_e(\gamma;a,b) &= -y_l^2\left(\ln\frac{Q_l^2}{m_e^2}-1\right)-\frac{y_l^2(a^2+b^2)(z-1)}{2ab}+\frac{y_l^2}{2z}\ln\frac{y_l(z-1)S}{x_lM^2}\\ &\quad-\frac{y_l^3}{2(1-z)}\left(\ln\frac{Q_l^2}{m_e^2}+\ln\frac{(za-b)^2}{(z-1)y_l^2}\right)-\frac{y_l}{b}\left[ay_l-\frac{y_l^2}{2z}-z(a^2+b^2)\right]\ln\frac{b^2S^2}{m^2M^2},\end{aligned} \tag{8.12}$$

and

$$z = \frac{x_h}{x_l}. \tag{8.13}$$

From the exact boundaries of appendix B.2.5 one gets the following relations:

$$Q_h^{2\,\max}(y_l,Q_l^2,x_h) \approx \frac{x_h}{x_l}Q_l^2, \tag{8.14}$$

$$Q_h^{2\,\min}(y_l,Q_l^2,x_h) \approx \frac{x_hx_lQ_l^2}{\left(\frac{x_h}{x_l}-1\right)Q_l^2+x_h^2M^2}M^2. \tag{8.15}$$

Therefore, one of the logarithmically peaking integrands in (8.10) is:

$$\int_{Q_h^{2\,\min}}^{Q_h^{2\,\max}}\frac{dQ_h^2}{Q_h^2}\approx\ln\frac{(x_h-x_l)y_lS+(x_hM)^2}{(x_lM)^2}\approx\ln\frac{(z-1)y_lS}{x_lM^2}. \tag{8.16}$$

This contribution is explicitly seen in (8.12). Two additional logarithmically enhanced contributions may be found in the last term in (8.12). The above mentioned screening of the other potential sources of kinematical peaks in the variable Q_h^2 may also be seen in (8.11) – the inverse powers of M^2 are absent.

The argument of the logarithm at the right hand side of (8.16) may become very large at $x_l\approx 0, y_l\approx 1$ $(x_h > x_l)$. This is the origin of the Compton peak. We would like to stress that the cross-section depends on the proton mass M on purely kinematical grounds. It has nothing to do with assumptions in the quark parton model. In the above considerations we used one implicit assumption. Namely, for the argument to hold, the parton distribution must be a slowly varying, non-vanishing function at smallest Q_h^2. This is exactly, what they aren't. We remember here about the discussion of (6.3). Thus, the Compton peak is at least partly regularized by this damping of the quark distributions. In view of lack of a reliable model for the parton distributions in the region of smallest Q_h^2 it is not evident which theoretical prediction of the radiative corrections is best. Maybe one should look inversely onto the problem: a clean measurement of the Coulomb peak could teach us something about the parton distributions which give rise to it [69]. We do not think that there are strong arguments to favor $\Lambda_{\rm QCD}$ as a scale of damping of the parton distributions at small Q_h^2 as was proposed in [70].

So far, we discussed the case of leptonic variables. In section 5.2.1, it was mentioned that the Compton peak in mixed variables is much less pronounced but present. The cross-section

in mixed variables has been integrated once, over y_l, in (5.7)–(5.17). Only in one of the two regions, in region I, the Q_h^2 may become small. There, again the integration starts from $Q_h^{2\,\mathrm{min}}$. The minimal value of Q_h^2 has been determined in (B.62). With the aid of (B.22), in the ultra-relativistic limit in m_e it is $y_l^{\mathrm{max}}(Q_l^2) = 1 - M^2 Q_l^2/S^2$ and

$$\begin{aligned} Q_h^{2\,\mathrm{min}} &= Q_l^2\,(1 - y_l^{\mathrm{max}} + y_h) \\ &= x_m y_h^2 (1 + r x_m) S \approx x_m y_h^2 S. \end{aligned} \tag{8.17}$$

The corresponding kinematical singularity is located at $x_m \to 0, y_h \to 0$. The extreme value of Q_h^2 for mixed variables is scaled by a factor of the order of S/M^2 compared to the case of leptonic variables and the peak is much less pronounced in the experimentally accessible kinematical ranges.

8.5 Summary and outlook

In this article, we gave a comprehensive presentation of the $\mathcal{O}(\alpha)$ leptonic QED corrections to deep inelastic ep scattering. The detailed analysis of the kinematics of deep inelastic scattering is of a general interest. It has been performed exactly in both the electron and proton masses in order to scope both with extreme kinematical situations and the characteristic singularities of the totally differential cross-section. Then, for several sets of kinematical variables semi-analytical integrations have been performed. The remaining two integrals for leptonic variables have to be taken numerically while for mixed and Jaquet-Blondel variables one integral remains. The hadronic case has been solved completely analytically. Most of the results of this article have not been published before.

It was not the intention to cover all relevant radiative corrections.

Here we would like to mention which corrections have been left out of the presentation:

- Electroweak one loop corrections [14]. These have to be treated in the quark parton model.
- The QED corrections which are not related to the lepton legs – the lepton-quark interference and the quarkonic radiation. Their calculation rests also on the quark parton model. In leptonic variables, they are published in [14] and in mixed variables known [71]. In other variables they are under study.
- Within the LLA approach, there exist predictions for QED corrections also in other variables: calorimetric and double angle [72]. A semi-analytical, complete $\mathcal{O}(\alpha)$ calculation in these variables seems to be nontrivial.
- The Monte-Carlo approach has been left out completely. The kinematics to be used is evidently the same. But the rest of the calculation is a totally different subject.
- Further, there is the wide field of higher order corrections. These have certainly to be included in certain regions of the phase space if an accuracy of one per cent or better is aimed at. The soft photon exponentiation is part of this and the hard photon contributions beyond $\mathcal{O}(\alpha)$ are certainly needed in LLA. Partial solutions are obtained in [34, 72, 73].

- Aiming at an accuracy of 1% or better, one has to concern about QCD corrections to the parton distributions. This and the inclusion of higher order corrections is being done within the project `HECTOR` [74].

- Finally, one should mention that for many physical applications charged current scattering has to be described with the same accuracy as the neutral current one. A lot of theoretical work remains to be done here. So far we may refer only to [16, 29].

To summarize, in this article we treated the numerically largest QED radiative corrections semi-analytically in several of the most important kinematical variables. This gives an important tool for a satisfactory description of fixed target and HERA data and the possibility to estimate the corrections at much higher beam energies. The most important next (or alternative) steps have been indicated.

Acknowledgements

We would like to acknowledge the participation of N.M. Shumeiko in the long first period of work on the project, when many of the basic techniques had been developed in the context of corrections in leptonic variables. We would like to thank A. Arbuzov, B. Badelek, J. Blümlein, P. Christova, J. Feltesse, W. Hollik, M. Klein, G. Kramer, K. Kurek, D. Lehner, H. Spiesberger for numerous, valuable discussions. It is a great pleasure to thank DESY–IfH Zeuthen and DESY–Hamburg for the opportunity to work at DESY on this project. We also thank the Heisenberg-Landau fund for financial support. A. A. thanks the ICTP for the hospitality and financial support.

A Kinematics and phase space

A.1 Kinematics and phase space for section 3

Throughout this section, all definitions and relations are understood to be exact in the electron and proton masses.

Let us introduce the following kinematical λ-functions:

$$\begin{aligned}
\lambda_k &\equiv \lambda[-(p_1+k)^2,-p_1^2,-k^2] &&= (y_l-y_h)^2S^2,\\
\lambda_S &\equiv \lambda[-(p_1+k_1)^2,-p_1^2,-k_1^2] &&= S^2-4m^2M^2,\\
\lambda_l &\equiv \lambda[-(p_1+k_2)^2,-p_1^2,-k_2^2] &&= (1-y_l)^2S^2-4m^2M^2,\\
\lambda_q &\equiv \lambda[-(p_1+Q_l)^2,-p_1^2,-Q_l^2] &&= y_l^2S^2+4M^2Q_l^2,\\
\lambda_h &\equiv \lambda[-(p_1+p_2)^2,-p_1^2,-p_2^2] &&= y_h^2S^2+4M^2Q_h^2,\\
\lambda_\tau &\equiv \lambda[-(p_1+\Lambda)^2,-p_1^2,-\Lambda^2] &&= (1-y_h)^2S^2-4M^2\tau,
\end{aligned} \tag{A.1}$$

where

$$-\Lambda^2=\tau=-(k_2+k)^2=z_2+m^2 \tag{A.2}$$

and

$$\begin{aligned}
\lambda(x,y,z) &= x^2+y^2+z^2-2xy-2xz-2yz\\
&= (x-y-z)^2-4yz\\
&= [x-(\sqrt{y}+\sqrt{z})^2][x-(\sqrt{y}-\sqrt{z})^2].
\end{aligned} \tag{A.3}$$

In the proton rest system, $\vec{p}_1=0$, the following relations hold:

$$\begin{aligned}
|\vec{k}| &= \frac{1}{2M}\sqrt{\lambda_k}, & k^0 &= \frac{S}{2M}(y_l-y_h),\\
|\vec{k}_1| &= \frac{1}{2M}\sqrt{\lambda_S}, & k_1^0 &= \frac{S}{2M},\\
|\vec{k}_2| &= \frac{1}{2M}\sqrt{\lambda_l}, & k_2^0 &= \frac{S}{2M}(1-y_l),\\
|\vec{Q}_l| &= \frac{1}{2M}\sqrt{\lambda_q}, & Q_l^0 &= \frac{S}{2M}y_l,\\
|\vec{p}_2| &= |\vec{Q}_h| = \frac{1}{2M}\sqrt{\lambda_h}, & p_2^0 &= M+\frac{S}{2M}y_h,\\
|\vec{\Lambda}| &= \frac{1}{2M}\sqrt{\lambda_\tau}, & \Lambda^0 &= \frac{S}{2M}(1-y_h).
\end{aligned} \tag{A.4}$$

They may be derived with the aid of the relation [75]

$$4M_A^2|\vec{p}_{\rm B}|^2=\lambda[-(p_{\rm A}+p_{\rm B})^2,-p_{\rm A}^2,-p_{\rm B}^2]|_{\vec{p}_{\rm A}=0}. \tag{A.5}$$

Thus, to any of the momenta in the rest system of the proton corresponds one of the relativistic invariant λ-functions. From (A.1) and (A.4) it follows that the invariants (3.1) totally fix the spatial configuration of momenta of reaction (1.2) which in the proton rest system can be drawn as a momentum tetrahedron; see figure 3.

A.2 Kinematics for section 6

For the calculation of QED corrections to the photoproduction process sets of external and integration variables are used which differ from the set y_l, Q_l^2, y_h, Q_h^2. Further, the infrared singularity is treated in a different rest frame. For these reasons, some additional kinematical relations are needed here.

Let us introduce the following λ-functions:

$$\begin{aligned}
\lambda'_k &\equiv \lambda[-p_2^2, -(p_2+k)^2, -k^2] &&= (W^2 - M_h^2)^2, \\
\lambda'_1 &\equiv \lambda[-(p_1-k_2)^2, -(p_2+k)^2, -k_1^2] &&= (S - Q_l^2)^2 - 4m^2W^2, \\
\lambda'_2 &\equiv \lambda[-(p_1+k_1)^2, -(p_2+k)^2, -k_2^2] &&= [(1-y_l)S + Q_l^2]^2 - 4m^2W^2 \\
&&&= (S - W^2 + M^2)^2 - 4m^2W^2.
\end{aligned} \tag{A.6}$$

With the aid of them and of (A.5), the following relations may be found in the rest frame of the compound system, which is defined by the condition $\vec{k}^R + \vec{p}_2^R = 0$:

$$\begin{aligned}
|\vec{k}^R| &= \frac{\sqrt{\lambda'_k}}{2\sqrt{W^2}}, & k^{0,R} &= \frac{W^2 - M_h^2}{2\sqrt{W^2}}, \\
|\vec{k}_1^R| &= \frac{\sqrt{\lambda'_1}}{2\sqrt{W^2}}, & k_1^{0,R} &= \frac{S - Q_l^2}{2\sqrt{W^2}}, \\
|\vec{k}_2^R| &= \frac{\sqrt{\lambda'_2}}{2\sqrt{W^2}}, & k_2^{0,R} &= \frac{(1-y_l)S + Q_l^2}{2\sqrt{W^2}}.
\end{aligned} \tag{A.7}$$

The invariant mass of the compound system at rest is $W^2 = -(k+p_2)^2$.

A.3 Kinematics for section 7

In the approach of section 7 to the phase space, the first two integrations will be performed over the photonic angles in the rest frame R of the (γe) compound system: $\vec{\Lambda}^R = \vec{k}^R + \vec{k}_2^R = 0$. For that purpose, the expressions for some four momenta and invariants are needed in that system in order to finally express y_l, Q_l^2, z_1 in (2.40)–(2.42). The velocities which are used in the infrared divergent part of the cross-section are also calculated in the R frame.

The necessary λ-functions are:

$$\begin{aligned}
\lambda''_k &\equiv \lambda[-(\Lambda-k)^2, -\Lambda^2, -k^2] &&= (\tau - m^2)^2, \\
\lambda_1 &\equiv \lambda[-(\Lambda-k_1)^2, -\Lambda^2, -k_1^2] &&= (Q_h^2 + z_2)^2 + 4m^2Q_h^2, \\
\lambda_2 &\equiv \lambda[-(\Lambda-k_2)^2, -\Lambda^2, -k_2^2] &&= (\tau - m^2)^2,
\end{aligned} \tag{A.8}$$

and the λ_τ has been introduced in (A.1).

The four-momenta are:

$$\begin{aligned}
|\vec{k}^R| &= \frac{\sqrt{\lambda''_k}}{2\sqrt{\tau}}, & k^{0,R} &= \frac{\tau - m^2}{2\sqrt{\tau}} = \frac{z_2}{2\sqrt{\tau}}, \\
|\vec{k}_1^R| &= \frac{\sqrt{\lambda_1}}{2\sqrt{\tau}}, & k_1^{0,R} &= \frac{Q_h^2 + \tau + m^2}{2\sqrt{\tau}}, \\
|\vec{k}_2^R| &= \frac{\sqrt{\lambda_2}}{2\sqrt{\tau}}, & k_2^{0,R} &= \frac{\tau + m^2}{2\sqrt{\tau}}, \\
|\vec{p}_1^R| &= \frac{\sqrt{\lambda_\tau}}{2\sqrt{\tau}}, & p_1^{0,R} &= \frac{(1-y_h)S}{2\sqrt{\tau}}.
\end{aligned} \tag{A.9}$$

In the R system the following cartesian coordinates are chosen: the z-axis be parallel to $\vec{k}_1^R$ and the yz-plane spanned by the vectors $\vec{k}_1^R, \vec{p}_1^R$; the angle between the z-axis and $\vec{p}_1^R$ be ϑ_p.

Then it is:

$$k = \left\{k^{0,R}\sin\vartheta_R\cos\varphi_R,\ k^{0,R}\sin\vartheta_R\sin\varphi_R,\ k^{0,R}\cos\vartheta_R,\ k^{0,R}\right\}, \tag{A.10}$$

$$k_1 = \left\{0,\ 0,\ |\vec{k}_1^R|,\ k_1^{0,R}\right\}, \tag{A.11}$$

$$k_2 = \left\{-k^{0,R}\sin\vartheta_R\cos\varphi_R,\ -k^{0,R}\sin\vartheta_R\sin\varphi_R,\ -k^{0,R}\cos\vartheta_R,\ k_2^{0,R}\right\}, \tag{A.12}$$

$$p_1 = \left\{0,\ |\vec{p}_1^R|\sin\vartheta_p,\ |\vec{p}_1^R|\cos\vartheta_p,\ p_1^{0,R}\right\}. \tag{A.13}$$

From these expressions, one may easily derive (7.9)–(7.12).

A.4 Some phase space parameterizations

A.4.1 The integral $d^3k_2/2k_2^0$

The following phase space integral has to be calculated in section 3.1:

$$I = \int \frac{d^3k_2}{2k_2^0} = \int \frac{|\vec{k}_2|}{2} dk_2^0 d\cos\vartheta d\varphi. \tag{A.14}$$

It is:

$$Q_l^2 = -2m^2 + 2k_1^0 k_2^0 \left(1 - \beta_1\beta_2\cos\vartheta_{12}\right). \tag{A.15}$$

One has the freedom to identify $\vartheta_{12} = \vartheta$. In the rest system of the proton the formulae of appendix A.1 may be used. It follows:

$$y_l = 1 - \frac{2M}{S}k_2^0, \qquad S = 2Mk_1^0. \tag{A.16}$$

These two relations allow to replace the energies introduced above by the invariants y_l and Q_l^2. The corresponding two three-momenta may also be expressed with the aid of A.4:

$$|\vec{k}_1| = \frac{\sqrt{\lambda_S}}{2M}, \qquad |\vec{k}_2| = \frac{\sqrt{\lambda_l}}{2M}. \tag{A.17}$$

Inserting these relations into (A.14), one gets:

$$I = \frac{\pi S}{2\sqrt{\lambda_S}} \int dy_l dQ_l^2. \tag{A.18}$$

A.4.2 The integral $d\Gamma_k$

In section 3.1, the following expression has to be simplified:

$$d\Gamma_k = \frac{d\vec{k}}{2k^0}\,\delta\left[(p_1+Q_h)^2+M_h^2\right]\delta\left[Q_h^2-(p_2-p_1)^2\right]. \tag{A.19}$$

With $Q_l = Q_h + k$ it is in the proton rest system:

$$\begin{aligned} d\Gamma_k &= \frac{1}{2}k_0 dk_0\, d\cos\vartheta_\gamma\, d\varphi\,\delta\left[(p_1+Q_l-k)^2+M_h^2\right]\delta\left[Q_h^2-(Q_l-k)^2\right] \\ &= \frac{1}{2}k_0 dk_0\, d\cos\vartheta_\gamma\, d\varphi\,\delta\left[(-M^2+2p_1(Q_l-k)+(Q_l-k)^2+M_h^2\right]\delta\left[Q_h^2-(Q_l-k)^2\right] \\ &= \frac{1}{2}k_0 dk_0\, d\cos\vartheta_\gamma\, d\varphi\,\delta\left[(-M^2+2p_1(Q_l-k)+Q_h^2+M_h^2\right]\delta\left[Q_h^2-Q_l^2+2Q_lk\right] \\ &= \frac{1}{2}k_0\frac{1}{2M}\frac{d\varphi}{2|Q_l|k_0} = \frac{d\varphi}{8M|\vec{Q}_l|}. \end{aligned} \tag{A.20}$$

Here φ is the angle between the planes defined by the three-momenta $(\vec{k}_1,\vec{k}_2)$ and $(\vec{k},\vec{p}_2)$, see figure 3.

Now the integration over dz_2 may be introduced with the aid of an auxiliary δ-function $\delta(z_2+2k_2k)$:

$$d\Gamma_k = \frac{dz_2}{8M|\vec{Q}_l|}d\varphi\,\delta(z_2+2k_2Q_l-2k_2Q_h). \tag{A.21}$$

The following coordinate system will be chosen. The z axis is parallel to $\vec{Q}_l$. The vector $\vec{k}_2$ stays within the xz planeand has an angle ϑ_p with respect to the z axis. The projection of the vector $\vec{Q}_h = \vec{p}_2$ into the xy plane has angle φ to the x axis, and the vector itself has the angle ϑ with respect to the z axis. Then, it will be

$$\vec{k}_2\cdot\vec{Q}_h = \vec{k}_2\cdot\vec{p}_2 = |\vec{k}_2||\vec{p}_2|(\sin\vartheta_p\sin\vartheta\cos\varphi+\cos\vartheta_p\cos\vartheta), \tag{A.22}$$

and

$$\begin{aligned} d\Gamma_k &= \frac{dz_2}{16M|\vec{Q}_l||\vec{k}_2||\vec{p}_2||\sin\vartheta_p\sin\vartheta\cos\varphi|} \\ &\equiv \frac{dz_2}{16M|\vec{Q}_l\cdot(\vec{k}_2\times\vec{p}_2)|}. \end{aligned} \tag{A.23}$$

The three-momenta used here and in the following may be calculated with the aid of the λ-functions (A.1). The $d\Gamma_k$ is related to the volume V_T of the tetrahedron of momenta as shown in figure 3:

$$V_T \equiv \frac{1}{6}\left|\vec{Q}_l\cdot(\vec{k}_2\times\vec{p}_2)\right| = \frac{1}{24M}\sqrt{R_z}. \tag{A.24}$$

Explicitly,

$$V_T = \frac{1}{6}\left\{\vec{Q}_l^2\vec{k}_2^2\vec{p}_2^2-\vec{Q}_l^2(\vec{k}_2\vec{p}_2)^2-\vec{k}_2^2(\vec{p}_2\vec{Q}_l)^2-\vec{p}_2^2(\vec{Q}_l\vec{k}_2)^2+2(\vec{Q}_l\vec{k}_2)(\vec{k}_2\vec{p}_2)(\vec{p}_2\vec{Q}_l)\right\}^{1/2}. \tag{A.25}$$

The positive-definite function R_z in (A.24) is the Gram determinant of 4-vectors k_1, p_1, k_2, p_2,

$$R_z \equiv -\Delta_4(k_1,p_1,k_2,p_2) = -\begin{vmatrix} k_1^2 & (k_1p_1) & (k_1k_2) & (k_1p_2) \\ (p_1k_1) & p_1^2 & (p_1k_2) & (p_1p_2) \\ (k_2k_1) & (k_2p_1) & k_2^2 & (k_2p_2) \\ (p_2k_1) & (p_2p_1) & (p_2k_2) & p_2^2 \end{vmatrix}. \tag{A.26}$$

It may be expressed by the G-function introduced in [75]:

$$R_z = -\frac{1}{16M^4} G(\lambda_l,\lambda_h,\lambda_\tau,\lambda_q,\lambda_S,\lambda_k). \tag{A.27}$$

For further use, it is convenient to write R_z in a form which exhibits its explicit dependence on z_1 or z_2:

$$\begin{aligned} R_z &= -A_1z_1^2 + 2B_1z_1 - C_1 \equiv -A_2z_2^2 + 2B_2z_2 - C_2, && \text{(A.28)} \\ A_2 &= \lambda_q \equiv A_1, && \text{(A.29)} \\ B_2 &= \Big\{2M^2Q_l^2(Q_l^2-Q_h^2) + (1-y_l)(y_lQ_h^2 - y_hQ_l^2)S^2 + S^2(1)Q_l^2(y_l-y_h)\Big\} \\ &\equiv -B_1\Big\{(1)\leftrightarrow -(1-y_l)\Big\}, && \text{(A.30)} \\ C_2 &= \Big\{(1-y_l)Q_h^2 - Q_l^2\,[(1)-y_h]\Big\}^2 S^2 + 4m^2\Big[(y_l-y_h)(y_lQ_h^2-y_hQ_l^2)S^2 - M^2(Q_h^2-Q_l^2)^2\Big\} \\ &\equiv C_1\Big\{(1)\leftrightarrow -(1-y_l)\Big\}, && \text{(A.31)} \end{aligned}$$

with the discriminant

$$D_z = B_{1,2}^2 - A_{1,2}C_{1,2} = \frac{1}{64M^4}\lambda(\lambda_S,\lambda_l,\lambda_q)\lambda(\lambda_q,\lambda_h,\lambda_k). \tag{A.32}$$

With (A.24), the phase space takes the form

$$d\Gamma_k = 2\times\frac{dz_2}{4\sqrt{R_z}} = \frac{dz_2}{2\sqrt{R_z}}, \tag{A.33}$$

where the overall factor of 2 at the right hand side corresponds to $\varphi\in[0,\pi]\leftrightarrow z_{1(2)}\in[z_{1(2)}^{\min},z_{1(2)}^{\max}]$. The latter boundaries for the integration over $z_{1(2)}$ are derived in appendix B.1.

A.4.3 The compound phase space volume $d\Gamma_{\gamma e}$

The following phase space integral has to be calculated in section 7.1:

$$\begin{aligned} I &= \int d\Gamma_{\gamma e} = \int \frac{d\vec{k}_2}{2k_2^0}\frac{d\vec{k}}{2k^0}\delta^4(\Lambda-k_2-k) \\ &= \int \frac{d\vec{k}_2}{2k_2^0}\delta[(\Lambda-k_2)^2] = \int \frac{|\vec{k}_2|}{2}dk_2^0 d\cos\vartheta d\varphi\,\delta[(\Lambda-k_2)^2]. && \text{(A.34)} \end{aligned}$$

In the rest system of the (γe) compound one may use the expressions for the energies and momenta (A.9). In this system, it is

$$\int dk_2^0\delta[(\Lambda-k_2)^2] = \int dk_2^0\delta(-\tau-m^2+2\sqrt{\tau}k_2^0) = \frac{1}{2\sqrt{\tau}}. \tag{A.35}$$

With $|\vec{k}_2| = \sqrt{\lambda_2}/2\sqrt{\tau}$ and $\lambda_2 = \lambda(\tau,m^2,0) = (\tau-m^2)^2$, see appendix A.3, one gets:

$$I = \frac{\tau-m^2}{8\tau}\int d\cos\vartheta d\varphi. \tag{A.36}$$

A.4.4 The integral $d^3p_2/2p_2^0$

In section 7.1, the following integral has to be calculated:

$$\begin{aligned} I &= \int d^4p_2 \delta\left(p_2^2+M_h^2\right)\delta\left[(p_2-p_1)^2-Q_h^2\right]\delta\left[(p_2-p_1-k_1)^2+\tau\right] \\ &= 2\pi\int\frac{|\vec{p}_2|}{2}dp_2^0 d\cos\vartheta\,\delta\left[(p_2-p_1)^2-Q_h^2\right]\delta\left[(p_2-p_1-k_1)^2+\tau\right]. \end{aligned} \tag{A.37}$$

In the rest system of the proton it is $\tau = -(p_2-p_1-k_1)^2 = M_h^2+S-2Mp_2^0+2p_2k_1$. In appendix A.1, the expressions for the four-momenta p_2 and k_1 in this frame in terms of invariants have been derived. It is $-2p_2k_1 = -(\sqrt{\lambda_h\lambda_S}/2M^2)\cos\vartheta+\ldots$ This relation allows to use the second of the δ-functions for the calculation of the integral over $\cos\vartheta$:

$$\int d\cos\vartheta\,\delta\left[-(p_2-p_1-k_1)^2+\tau\right] = \frac{2M^2}{\sqrt{\lambda_h\lambda_S}}. \tag{A.38}$$

With $|\vec{p}_2| = \sqrt{\lambda_h}/2M$ and $-(p_2-p_1)^2+Q_h^2 = -2Mp_2^0+M^2+M_h^2+Q_h^2$, the last δ-function allows to perform the integration over dp_2^0 and one gets:

$$I = \frac{\pi}{2\sqrt{\lambda_S}}. \tag{A.39}$$

A.4.5 Notations

Here, we confront some old and new notations. This may prove useful if someone tries to read the preprints [4], [5]:

$$\begin{array}{rclcrclcrcl} S_l &=& y_lS, & & T &=& y_hS, & & t &=& Q_h^2, \\ Q^2 &=& Q_l^2, & & X &=& (1-y_l)S, & & Y &=& Q_l^2, \\ S_X = S-X &=& y_lS. & & & & & & & & \end{array} \tag{A.40}$$

B Kinematic boundaries

We now come to the derivation of the many different kinematical boundaries which are connected with the different choices of the integration variables and their sequential order. By $v^{\max(\min)}(V_1,V_2,\ldots)$, the maximum (minimum) value of v will be denoted which may be taken at fixed values of $V_1,V_2,\ldots$ Further, the extreme value of variable v is $\bar{v}$; it depends only on S and possibly on M,m.

The physical regions of invariants (3.1) may be found from the conditions of existence of the momentum tetrahedron depicted in figure 3. This tetrahedron is defined by the triangles $\Delta(\vec{k}_1,-\vec{k}_2,-\vec{Q}_l)$, $\Delta(\vec{Q}_l,-\vec{p}_2,-\vec{k})$, and $\Delta(\vec{k}_1,-\vec{\Lambda},-\vec{p}_2)$ in the proton rest system. The areas of these triangles are equal to

$$\frac{1}{4}\sqrt{-\lambda(\vec{k}_1^2,\vec{k}_2^2,\vec{Q}_l^2)}, \qquad \frac{1}{4}\sqrt{-\lambda(\vec{Q}_l^2,\vec{p}_2{}^2,\vec{k}^2)}, \qquad \frac{1}{4}\sqrt{-\lambda(\vec{k}_1^2,\vec{\Lambda}^2,\vec{p}_2{}^2)},$$

correspondingly; they exist if

$$\lambda(\vec{k}_1^2,\vec{k}_2^2,\vec{Q}_l^2)\le 0, \qquad \lambda(\vec{Q}_l^2,\vec{p}_2{}^2,\vec{k}^2)\le 0, \qquad \lambda(\vec{k}_1^2,\vec{\Lambda}^2,\vec{p}_2{}^2)\le 0. \tag{B.1}$$

With the expressions (A.1) for the squared three-momenta in terms of λ-functions, the following boundary conditions are derived:

$$\lambda(\lambda_S, \lambda_l, \lambda_q) \leq 0, \qquad \lambda(\lambda_q, \lambda_h, \lambda_k) \leq 0, \qquad \lambda(\lambda_S, \lambda_\tau, \lambda_h) \leq 0. \tag{B.2}$$

The boundary equation for the first condition is:

$$M^2 Q_l^4 + Q_l^2 y_l S^2 + m^2 y_l^2 S^2 - \lambda_S Q_l^2 = 0. \tag{B.3}$$

The boundary equation for the second condition is:

$$y_l^2 S^2 Q_h^2 + y_h^2 S^2 Q_l^2 - M^2 (Q_l^2 - Q_h^2)^2 - y_l y_h (Q_l^2 + Q_h^2) S^2 = 0. \tag{B.4}$$

It is symmetric with respect to the interchanges $(y_l \leftrightarrow y_h)$ and $(Q_l^2 \leftrightarrow Q_h^2)$.

The third boundary condition may be rewritten:

$$(2M^2 z_2 + y_h S^2 + 2M^2 Q_h^2)^2 - \lambda_S \lambda_h \leq 0. \tag{B.5}$$

The z_2 is known to be positive definite (see appendix B.1.1). The maximal value $z_2^{\max}(y_h, Q_h^2)$ of z_2 at given values of (y_h, Q_h^2) is one of the roots $z_2^{\pm}(y_h, Q_h^2)$ of (B.5),

$$z_2^{\pm}(y_h, Q_h^2) = \frac{1}{2M^2} \left[-(y_h S^2 + 2M^2 Q_h^2) \pm \sqrt{\lambda_S \lambda_h} \right], \tag{B.6}$$

namely z_2^+. It is positive definite if

$$M^2 Q_h^4 + Q_h^2 y_h S^2 + m^2 y_h^2 S^2 - \lambda_S Q_h^2 \leq 0. \tag{B.7}$$

From the zero of (B.7) the third boundary equation results. By the replacements $Q_h^2 \leftrightarrow Q_l^2$ and $y_l \leftrightarrow y_h$ it transforms into the boundary equation of the first condition.

B.1 Boundaries for z_1, z_2

B.1.1 Boundaries for $z_{1(2)}(y_l, Q_l^2, y_h, Q_h^2)$

From (A.32) and (B.2) one may conclude $D_z \geq 0$. The invariants z_1 and z_2 are positive definite. This may be understood easiest from the general statement that an invariant of the form $I = -2pk$ is positive definite when the momenta p, k are on the mass shell. One may also use an argument based on the photon energy in (A.9), which is proportional to z_2. For z_1 the same property may be derived by a replacement of k_2 in favour of k_1 in the arguments which lead to the lower boundary of z_2 (i.e. in section A.3).

From (A.1) and (A.29) it follows $A_{1,2} > 0$. The R_z which is introduced in (A.24) and rewritten in (A.28) is proportional to the volume of the tetrahedron in figure 3, i.e. it is also positive definite. This volumee vanishes at the boundary values of the physical regions of the invariants. Rewriting R_z,

$$R_z = \lambda_q \left[z_{1(2)}^{\max} - z_{1(2)} \right] \left[z_{1(2)} - z_{1(2)}^{\min} \right], \tag{B.8}$$

one may derive an expression for the boundary values of z_1 and z_2 at fixed values of y_l, Q_l^2, y_h, Q_h^2:

$$z_{1,2}^{\max,\min}(y_l, Q_l^2; y_h, Q_h^2) = \frac{B_{1,2} \pm \sqrt{D_z}}{A_z} = \frac{C_{1,2}}{B_{1,2} \mp \sqrt{D_z}}. \tag{B.9}$$

The D_z in the above relation must be positive. Since the $z_{1(2)}$ are positive definite, the $B_{1(2)}$ must be positive, too. Finally, from the second equality in the above chain, the $C_{1(2)}$ are also seen to be positive. In the ultra-relativistic approximation, the latter is also evident from (A.31).

We mention here that the integration limits for z_2 at fixed values of y_h, Q_h^2 will be derived in appendix B.4 and at fixed $y_{\rm JB}$, $Q^2_{\rm JB}$ in appendix B.5. They are also influenced by the photonic cuts, which are introduced for leptonic variables in section 6; see appendix B.1.2.

B.1.2 Boundaries for $z_{1(2)}(y_l, Q_l^2, y_h, Q_h^2)$ with photonic cuts

In section 5 we argued that cuts may be applied on the momentum of the bremsstrahlung photon. This is of some interest in the case of leptonic variables in the region of small x and large y. In this appendix, the necessary formulae will be derived.

We define the photonic cuts by the following conditions:

$$\begin{array}{rcccl} E_\gamma & \geq & E_m & = & E_\gamma^{\rm min}, \\ \cos(\theta_\gamma^{\rm min}) = c_{\rm min} \geq \cos\theta_\gamma & \geq & c_{\rm max} & = & \cos(\theta_\gamma^{\rm max}). \end{array} \tag{B.10}$$

With these cuts, photons with an energy larger than $E_\gamma^{\rm min}$ and within a cone defined by $\cos(\theta_\gamma^{\rm max,min})$ are *excluded* from the observed cross-section.

Both experiments at HERA have a γ counter which may register photons with an energy $E_\gamma \geq 1$ GeV and an emission angle $0 \leq \theta_\gamma \leq 0.5$ mrad in the HERA laboratory system.

In order to incorporate the cuts (B.10) into the cross-section calculations one needs two invariants which depend exclusively on E_γ and θ_γ and, possibly, on E_e and E_p, the energies of the electron and proton beams in the laboratory system.

One candidate is z_1:

$$z_1 = -2k_1k = 2E_eE_\gamma(1-\beta_e\cos\theta_\gamma), \tag{B.11}$$

$$\beta_e = \sqrt{1-\frac{m^2}{E_e^2}}. \tag{B.12}$$

Another one may be found to be

$$I_\gamma = -2p_1k = (y_l-y_h)S = 2E_pE_\gamma(1+\beta_p\cos\theta_\gamma), \tag{B.13}$$

$$\beta_p = \sqrt{1-\frac{M^2}{E_p^2}}. \tag{B.14}$$

Dividing (B.11) by (B.13) one gets a first condition which is formulated completely in terms of integration variables and measurable parameters. A second one may be obtained by eliminating the $\cos\theta_\gamma$ from (B.11) with the aid of (B.13):

$$\begin{array}{rcccl} z_c^{\rm min} \equiv \dfrac{E_e(1-\beta_e c_{\rm min})}{E_p(1+\beta_p c_{\rm min})}S(y_l-y_h) & \leq & z_1 & \leq & \dfrac{E_e(1-\beta_e c_{\rm max})}{E_p(1+\beta_p c_{\rm max})}S(y_l-y_h) \equiv z_c^{\rm max}, \\ z_E^{\rm min} \equiv 2E_eE_m(1+\dfrac{\beta_e}{\beta_p}) - \dfrac{E_e\beta_e}{E_p\beta_p}S(y_l-y_h) & \leq & z_1. & & \end{array} \tag{B.15}$$

Taking into account $z_2 = z_1 + Q_l^2 - Q_h^2$ one may realize that (B.15) represents cut conditions on the first integration variable.

The actual modifications of the analytical integrations over $z_{1(2)}$ due to the cuts may be found in D.1. After this first integration, the *finite hard* cross-section part undergoes two numerical integrations, which are not essentially affected by the cuts. Concerning the treatment of the infrared singularity, nothing changes compared to the presentation in section 4. The reason is simple. We subtracted from and added to the complete bremsstrahlung correction a simplified expression, well adapted to the infrared problem. Now, in the presence of cuts, we have the freedom to subtract and add the *same* expressions. Here, it is of importance that the applied cuts do not influence the infrared behaviour since the contribution of hard photons is manipulated.

Concluding,

$$\begin{aligned}
\hat{z}_1^{\max} &= \min\left\{z_1^{\max}(y_l, Q_l^2, y_h, Q_h^2), z_c^{\max}(E_e, E_p, c_{\max}, y_l, y_h)\right\}, \\
\hat{z}_1^{\min} &= \max\left\{z_1^{\min}(y_l, Q_l^2, y_h, Q_h^2), z_c^{\min}(E_e, E_p, c_{\min}, y_l, y_h), z_E^{\min}(E_e, E_p, y_l, y_h)\right\}, \\
\hat{z}_2^{\min(\max)} &= z_1^{\min(\max)} + Q_l^2 - Q_h^2. \qquad \text{(B.16)}
\end{aligned}$$

B.1.3 Boundaries for $z_2(y_h, Q_h^2)$

The following boundaries are used for the calculation of cross sections in hadronic and Jaquet-Blondel variables where the integration over τ is the third one. After two integrations over photonic angles the ultra-relativistic approximations are justified and will be applied. For given values of y_h and Q_h^2, the upper limit of z_2 is given in (B.6) while the lower one is zero; compare the expression for $k^{0,R}$ in (A.9):

$$0 \le z_2 \le x_h(1 - y_h)S. \qquad \text{(B.17)}$$

The boundary values of z_2 define also those for the variable τ when the latter is used as the argument of the last integration at given values of either y_h, Q_h^2 or y_{JB}, Q_{JB}^2.

B.2 Boundaries for leptonic variables

From now on, we will use the following notations for external variables: if a variable is maximal or minimal as a function of the other one (and of S and the masses), the superscripts min or max will be used to indicate this. Absolute extremes which depend only on S and the masses get a bar.

The maxima and minima of an internal variable at fixed values of the other internal variable and of the external variables get the subscripts I, III, and II, IV, respectively. In the figures these functions are boundaries. If the integration order is changed the corresponding curves in the figures get a different analytical meaning. This will become clear in the following discussions of integration regions.

B.2.1 External variables $\mathcal{E}_l = (y_l, Q_l^2)$

We start with the derivation of absolute bounds for W^2.

For the invariant hadronic mass M_h^2 the lower limit is defined by the kinematical threshold of hadron production, i.e. the mass of the lightest strongly interacting particle, the pion. The upper limit of M_h^2, for a given W^2, may be derived from the expression for k_0 in the rest system (A.7). It is reached for $k_0 = 0$:

$$(M + m_\pi)^2 \leq M_h^2 \leq W^2. \tag{B.18}$$

The above inequality may also be interpreted as the absolute lower limit of W^2.

The upper bound for $W^2 = -(p_1 + k_1 - k_2)^2$ follows from a consideration of the defining four momentum squared in the centre-of-mass system:

$$(M + m_\pi)^2 \leq W^2 \leq \bar{W}^2 = (\sqrt{s} - m)^2 \equiv (\sqrt{S + M^2 + m^2} - m)^2. \tag{B.19}$$

One may eliminate W^2 from (B.19) with the aid of (6.2)[7]:

$$0 \leq y_l S - Q_l^2 \leq \left(\sqrt{S + M^2 + m^2} - m\right)^2 - M^2. \tag{B.20}$$

The boundary equation (B.3) originally depends on the variables we are interested in: y_l and Q_l^2. It may be pursued once more. The boundaries for y_l at a given value of Q_l^2 shall be determined. The lower bound of y_l results from (B.20); the upper limit is the solution of (B.3):

$$y_l^{\min}(Q_l^2) = \frac{Q_l^2}{S} \leq y_l \leq y_l^{\max}(Q_l^2), \tag{B.21}$$

where

$$y_l^{\max}(Q_l^2) = \frac{1}{2m^2}\left[\frac{1}{S}\sqrt{\lambda_S \lambda_m} - Q_l^2\right] \leq \bar{y}_l. \tag{B.22}$$

Here the $\bar{y}_l$ is the maximum of y_l and may be determined by differentiation of (B.22) with respect to Q_l^2:

$$\bar{y}_l = \frac{S - 2mM}{S}. \tag{B.23}$$

The absolute minimum of Q_l^2 is zero. The condition $y_l^{\min}(Q_l^2) = y_l^{\max}(Q_l^2)$ is fulfilled at $Q_l^2 = 0$ and also at the absolute maximum of Q_l^2. It may be used for a determination of the limits of the latter variable:

$$0 \leq Q_l^2 \leq \frac{\lambda_S}{S + M^2 + m^2} \equiv \bar{Q}_l^2. \tag{B.24}$$

The physical region $\mathcal{E}_l = (Q_l^2, y_l)$ is shown in figure 33.

B.2.2 External variables $\mathcal{E}'_l = (W^2, Q_l^2)$

The bounds for W^2, (B.19), have been derived in the foregoing appendix.

Those for Q_l^2 at a given value of W^2 may be obtained from (B.3) by replacing the y_l by W^2 with the aid of (6.2):

$$Q_l^{2\,\max(\min)}(W^2) = \frac{S\,(S - W^2 + M^2) - 2m^2\,(W^2 + M^2) \pm \sqrt{\lambda_S \lambda'_2}}{2\,(S + M^2 + m^2)}. \tag{B.25}$$

From the lower limit in (B.25) the estimation of the lowest accessible Q^2 (6.3) in the photoproduction region was derived.

The physical region $\mathcal{E}'_l = (W^2, Q_l^2)$ is shown in figure 34.

[7] If not stated differently, the pion mass is neglected here and in the following.

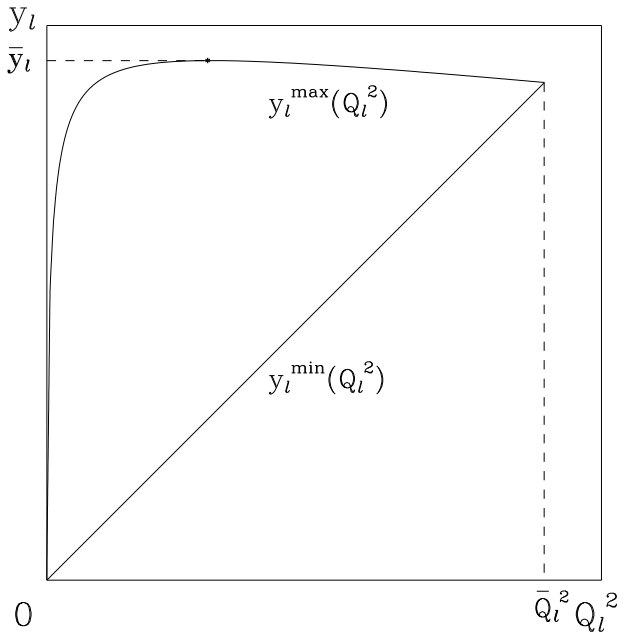

Figure 33: *Physical region (Q_l^2, y_l) for the cross-section in leptonic variables.*

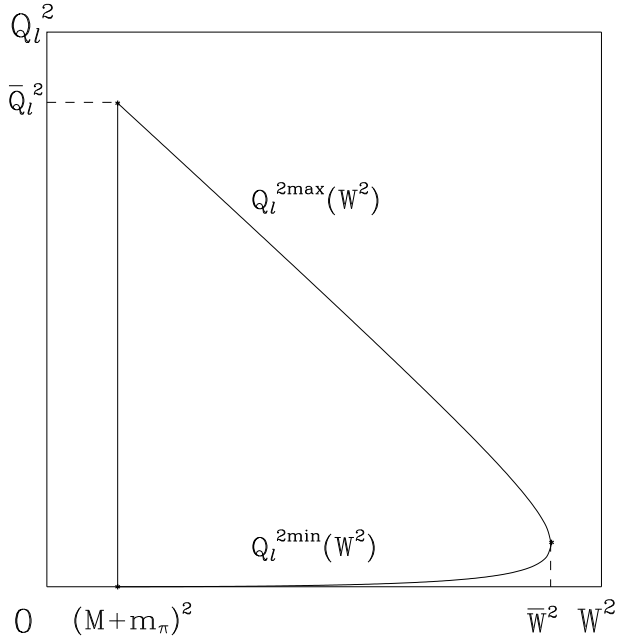

Figure 34: *Physical region (W^2, Q_l^2) for the photoproduction process.*

B.2.3 Integration variables $\mathcal{I}_l = (y_h, Q_h^2)$

For the hard photon corrections in leptonic variables, the last two integrations are numerically performed over $\mathcal{I}_l = (y_h, Q_h^2)$. The hard part of the infrared divergent contribution is integrated analytically; thereby the last integration is that over y_h.

Inserting (6.5) into (B.18), one gets a first condition the left hand side of which is equivalent to $x_h = 1$:

$$0 \leq y_h S - Q_h^2 \leq W^2 - M^2. \tag{B.26}$$

The (B.4) defines a pair of intersecting straight lines :

$$Q^2_{h\mathrm{I,II}} = Q_l^2 + \frac{S}{2M^2}(y_l - y_h)(y_l S \pm \sqrt{\lambda_q}). \tag{B.27}$$

From the second relation, the lower bound of Q_h^2 is obtained:

$$Q_h^{2\,\min}(y_h, y_l, Q_l^2) = Q^2_{h\mathrm{II}}. \tag{B.28}$$

The upper bound of Q_h^2 depends on the actual value of y_h. The two curves $Q_h^2 = y_h S$ and $Q_h^2 = Q^2_{h\mathrm{I}}$ meet at the maximum value of Q_h^2 which is reached at the following value of y_h:

$$y_{hd}(y_l, Q_l^2) = \frac{y_l(y_l S + \sqrt{\lambda}_q) + 2Q_l^2 r}{y_l S + \sqrt{\lambda}_q + 2M^2}, \tag{B.29}$$

$$r = M^2/S. \tag{B.30}$$

At $y_h > y_{hd}$ it is $Q_h^{2\,\max}(y_h, y_l, Q_l^2) = Q^2_{h\mathrm{I}}$.

The minimum of y_h may be obtained from the equality $Q^2_{h\mathrm{II}} = y_h S$; see figure 35:

$$y_h^{\min}(y_l, Q_l^2) = \frac{y_l(y_l S - \sqrt{\lambda_q}) + 2Q_l^2 r}{y_l S - \sqrt{\lambda_q} + 2M^2}. \tag{B.31}$$

The maximum of y_h at a fixed value of y_l is equal to y_l and independent of Q_l^2; this may be seen from the expression for k^0 in (A.4). The infrared singularity is located at $\mathcal{F}(y_l, Q_l^2)$. When calculating the hard part (4.13) of the infrared divergent cross-section contribution, one has to take into account an additional condition:

$$k^0 \geq \epsilon > 0. \tag{B.32}$$

In the approach to the phase space where the boundaries of this appendix are used the infrared problem is treated in the proton rest frame. From the expression for k^0 in (A.4) the following modification of the integration boundary results:

$$y_h^{\max} = y_l \to y_h^{\max}(\epsilon) = y_l - \frac{2\epsilon M}{S}. \tag{B.33}$$

The net physical region for $\mathcal{I}_l = (y_h, Q_h^2)$ is:

$$\begin{aligned}
Q^2_{h\mathrm{II}} \leq\ & Q_h^2 \leq y_h S && \text{if } y_h \leq y_{h_d},\\
Q^2_{h\mathrm{II}} \leq\ & Q_h^2 \leq Q^2_{h\mathrm{I}} && \text{if } y_h \geq y_{h_d},\\
y_h^{\min}(y_l, Q_l^2) \leq\ & y_h \leq y_h^{\max}(\epsilon).
\end{aligned} \tag{B.34}$$

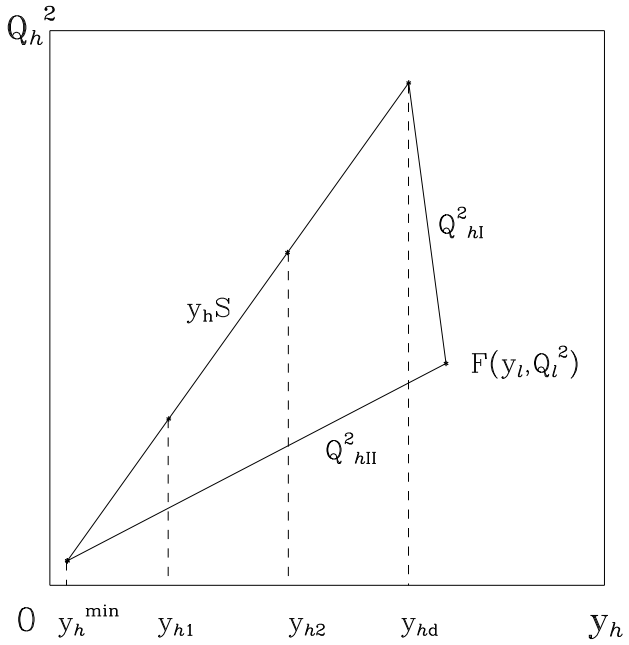

Figure 35: *Integration region (y_h, Q_h^2) for the cross-section in leptonic variables.*

When calculating the twofold integrals in (4.13) over the kinematical domain, which is derived here, one will need the substitutions of $\sqrt{C_1}$ and $\sqrt{C_2}$ at the kinematical boundaries. The square roots at $(Q_h^2)_{\rm I,II}$ can be taken exactly:

$$\sqrt{C_1(Q^2_{h\rm I})} = (y_l - y_h)S\left[S\frac{\sqrt{\lambda_q} + y_l S}{2M^2} + Q_l^2\right], \tag{B.35}$$

$$\sqrt{C_2(Q^2_{h\rm I})} = (y_l - y_h)S\left[(1-y_l)S\frac{\sqrt{\lambda_q} + y_l S}{2M^2} - Q_l^2\right], \tag{B.36}$$

$$\sqrt{C_1(Q^2_{h\rm II})} = (y_l - y_h)S\left[S\frac{\sqrt{\lambda_q} - y_l S}{2M^2} - Q_l^2\right], \tag{B.37}$$

$$\sqrt{C_2(Q^2_{h\rm II})} = (y_l - y_h)S\left[(1-y_l)S\frac{\sqrt{\lambda_q} - y_l S}{2M^2} + Q_l^2\right]. \tag{B.38}$$

The corresponding roots at $Q_h^2 = y_h S$ may be taken in the ultra-relativistic approximation in the electron mass; see the expressions (A.31). One arrives at the following absolute values:

$$\sqrt{C_1} \simeq S^2|y_h - x_l y_l(1 + y_h - y_l)|, \tag{B.39}$$

$$\sqrt{C_2} \simeq S^2|y_h(1-y_l) - x_l y_l(1 - y_h)|, \tag{B.40}$$

which vanish inside the region of integration over y_h, (B.34), at

$$y_{h_1} = \frac{x_l y_l(1-y_l)}{1 - y_l x_l}, \tag{B.41}$$

$$y_{h_2} = \frac{x_l y_l}{1 - y_l(1 - x_l)}, \tag{B.42}$$

correspondingly. Within the kinematical limits of figure 35, the following inequalities hold:

$$y_h^{\min} < y_{h1} < y_{h2} < y_{hd} < y_h^{\max}(\epsilon). \tag{B.43}$$

The integration region $\mathcal{I}_l = (y_h, Q_h^2)$ is shown in figure 35.

B.2.4 Integration variables $\mathcal{I}_l' = (M_h^2, Q_h^2)$

The boundaries for M_h^2 have been derived in (B.18):

$$(M + m_\pi)^2 \leq M_h^2 \leq W^2.$$

The infrared singularity is located at $\mathcal{F}(W^2, Q_l^2)$. When calculating the hard part (4.13) of the infrared divergent cross-section contribution, one has to take into account the additional condition for the photon energy (A.7):

$$k^{0,R} = \frac{W^2 - M_h^2}{2\sqrt{W^2}} \geq \epsilon > 0. \tag{B.44}$$

This condition may be transformed into the following modification of the upper bound of M_h^2:

$$(M + m_\pi)^2 \leq M_h^2 \leq W^2 - 2\epsilon\sqrt{W^2}. \tag{B.45}$$

The limits of the variable Q_h^2 for given values of W^2, M_h^2, Q_l^2 will be derived now. For that purpose, one has to replace in (B.4) the y_l with (6.2) by W^2 and Q_l^2 and the y_h with (6.5) by M_h^2 and Q_h^2 and solve the resulting inequality for Q_h^2 in terms of M_h^2, Q_l^2, W^2:

$$Q_{h\,\mathrm{I,II}}^2 = Q_h^{2\,\max(\min)}(W^2, M_h^2, Q_l^2) = \frac{1}{2W^2}\left[\left(W^2 - M_h^2\right)\left(y_l S \pm \sqrt{\lambda_q}\right) + 2M_h^2 Q_l^2\right]. \tag{B.46}$$

The two straight lines meet in the infrared point while the two extreme values of Q_h^2 at given external variables are reached for $M_h^2 = (M + m_\pi)^2$.

The physical region $\mathcal{I}_l' = (M_h^2, Q_h^2)$ is shown in figure 36.

B.2.5 Integration variables $\mathcal{I}_l'' = (x_h, Q_h^2)$

For the discussion of the Compton peak we need the integration boundaries for the variables x_h and Q_h^2 where the latter has to be integrated over first.

Using in (B.4) the relation $y_h = Q_h^2/(x_h S)$, one immediately arrives at the boundaries for Q_h^2 at given values of x_h, y_l, Q_l^2:

$$Q_{h\,\mathrm{I,II}}^2 = Q_h^{2\,\max(\min)}(y_l, Q_l^2, x_h) = \frac{x_h(x_h y_l S - Q_l^2)(y_l S \pm \sqrt{\lambda_q}) + 2Q_l^2(x_h M)^2}{2[x_h y_l S - Q_l^2 + (x_h M)^2]}. \tag{B.47}$$

At the lower limit of x_h the two curves $Q_{h\,\mathrm{I,II}}^2$ meet; see figure 37. From (B.47) one derives that this is realized if $x_h = x_l$, which is at the same time the infrared point. The upper limit for x_h may be got by rewriting (6.5) and inserting (B.18):

$$Q_h^2/x_h - Q_h^2 = M_h^2 - M^2 \geq m_\pi(2M + m_\pi). \tag{B.48}$$

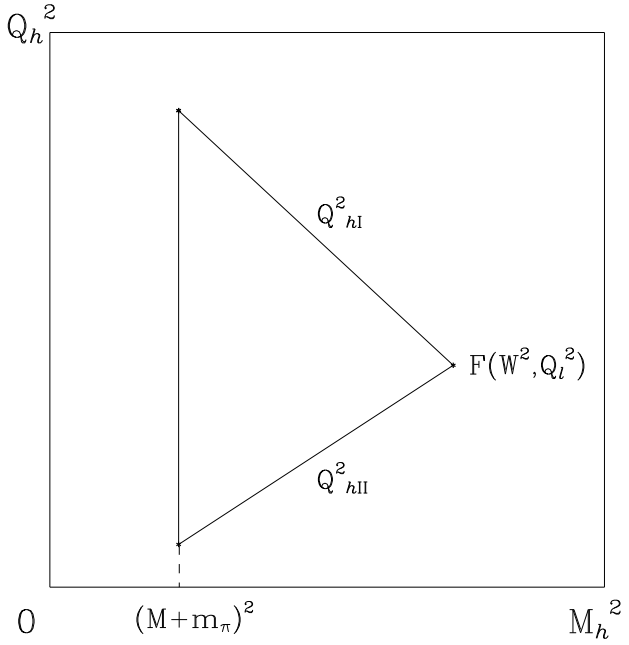

Figure 36: *Integration region (M_h^2, Q_h^2) for the cross-section in leptonic variables.*

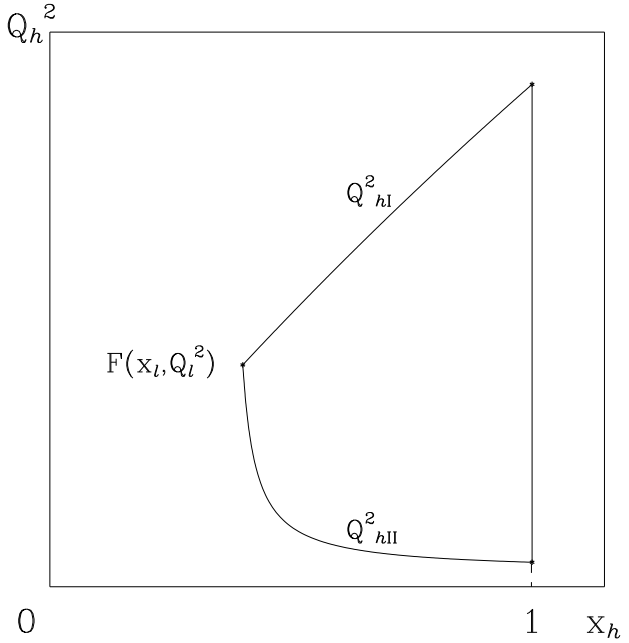

Figure 37: *Integration region (x_h, Q_h^2) for the cross-section in leptonic variables.*

Neglecting here the pion mass, the absolute maximum of x_h is evidently equal to one:

$$x_l \leq x_h \leq 1, \tag{B.49}$$

Taking the pion mass into account, the value $x_h = 1$ is forbidden; in fact $x_h = 1$ corresponds to the kinematics of the elastic channel.

The integration region $\mathcal{I}_l = (y_h, Q_h^2)$ is shown in figure 37.

B.3 Boundaries for mixed variables

B.3.1 External variables $\mathcal{E}_m = (y_h, Q_l^2)$

The boundaries for Q_l^2 are the same as in the case of leptonic variables; see (B.24):

$$0 \leq Q_l^2 \leq \frac{\lambda_S}{S + M^2 + m^2} \equiv \bar{Q_l^2}.$$

The maximum of y_h in the two-dimensional distribution $[y_h(Q_l^2); y_l(y_h, Q_h^2, Q_l^2)]$ is, independent of the value of Q_l^2, equal to y_l. Thus, its absolute maximum is given by the value for $y_l^{\max}(Q_l^2)$ of (B.22). The minimal value of $y_h(Q_l^2)$ may be obtained by studying the functional dependence of $y_h^{\min}(y_l, Q_l^2)$ in (B.34) on y_l. The extremum is reached at $y_l = y_l^{\max}(Q_l^2)$. The explicit expressions are:

$$y_h^{\min}(Q_l^2) \;\leq\; y_h \;\leq\; y_h^{\max}(Q_l^2), \tag{B.50}$$

where

$$\begin{aligned} y_h^{\min}(Q_l^2) &= \frac{Q_l^2 \left(\sqrt{(y_l^{\max} S)^2 + 4M^2 Q_l^2} - y_l^{\max} S \right)}{S \left[\sqrt{(y_l^{\max} S)^2 + 4M^2 Q_l^2} + y_l^{\max} S - 2Q_l^2 \right]} \\ &= \frac{Q_l^2 \left(\sqrt{\lambda_m} + Q_l^2 \right) \left(S - \sqrt{\lambda_S} \right)}{S \left(\sqrt{\lambda_m} - Q_l^2 \right) \left(S + \sqrt{\lambda_S} - Q_l^2 - \sqrt{\lambda_m} \right)} \leq \frac{Q_l^2}{S}, \qquad \text{(B.51)} \\ y_h^{\max}(Q_l^2) &= \frac{1}{2m^2} \left[\frac{1}{S} \sqrt{\lambda_S \lambda_m} - Q_l^2 \right] \leq \bar{y_l}. \qquad \text{(B.52)} \end{aligned}$$

At the right hand side of (B.51), the $y_l^{\max}$ stands for $y_l^{\max}(Q_l^2)$ [see (B.22)] and

$$\lambda_m = Q_l^2 \left(Q_l^2 + 4m^2 \right). \tag{B.53}$$

The second part of (B.51) has been obtained from the identity

$$\sqrt{(y_l^{\max} S)^2 + 4M^2 Q_l^2} = \frac{1}{2m^2} \left(S \sqrt{\lambda_m} - Q_l^2 \sqrt{\lambda_S} \right).$$

The two curves $y_h^{\max}(Q_l^2)$ and $y_h^{\min}(Q_l^2)$ meet each other at $Q_l^2 = \bar{Q_l^2}$ as defined in (B.24).

With the variables $\mathcal{E}_m$ one may define a corresponding set of scaling variables:

$$Q_m^2 = Q_l^2, \qquad y_m \equiv y_h, \qquad x_m = \frac{Q_l^2}{-2p_1 Q_h} = \frac{Q_l^2}{y_h S}. \tag{B.54}$$

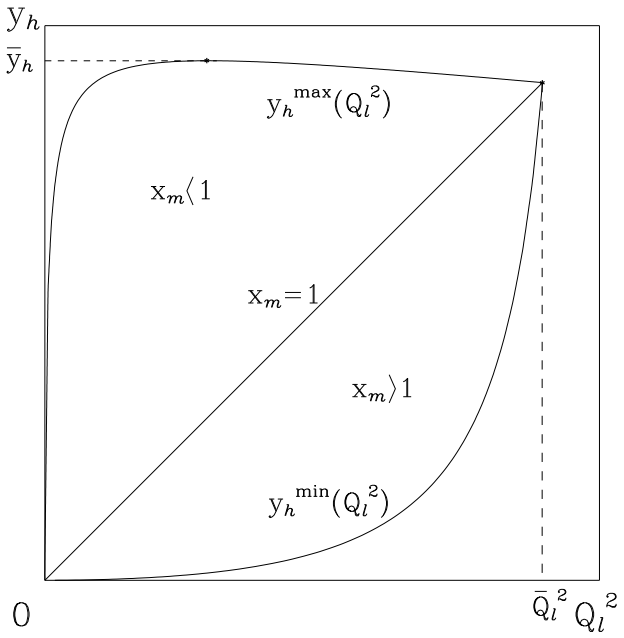

Figure 38: *Physical region (y_h, Q_l^2) for the cross-section in mixed variables; lower part for $x_m > 1$, upper part for $x_m < 1$.*

Here the mixed variable x_m is defined from both leptonic and hadronic variables, while y_m is defined exclusively by the hadronic kinematics. For $y_h S \geq Q_l^2$, the scaling variable x_m fulfills $0 \leq x_m \leq 1$, while at $y_h S \leq Q_l^2$ it is $x_m \geq 1$.

Values of x which are larger than 1 seem to be exceptional. Nevertheless they are physical in the case of x_m. This statement may be checked e.g. by reproducing the phase space volume (C.7) in mixed variables.

The physical region $\mathcal{E}_m = (Q_l^2, y_h)$ is shown in figure 38.

In the kinematical region with $x_m > 1$ it is ensured that $Q_l^2 - Q_h^2 > 0$ since $y_h S = Q_h^2 + M_h^2 - M^2 < Q_l^2$. Thus, the infrared point may not be reached and only the radiative process is possible. The equality in (B.51) is realized for $y_l^{\max} S = Q_l^2$; then it is $y_h^{\min} S = Q_l^2$.

B.3.2 Integration variables $\mathcal{I}_m = (y_l, Q_h^2)$

The *complete* analytical integration of the hard part of the infrared divergent cross section will be performed first over Q_h^2 and then over y_l. We consider only the case $x_m \leq 1$ explicitly.

As in the case of leptonic variables, the bounds for Q_h^2 at given values of y_l, y_h, Q_l^2 may be derived from (B.26) and (B.27), and figure 39. The $Q_h^{2\,\max}(y_l, y_h, Q_l^2)$ is either equal to $Q_{h\mathrm{I}}^2$ or to $y_h S$; both curves meet at the value y_{ld}:

$$y_{ld} \;=\; \frac{1}{2} y_h \left[1 + x_m + (1 - x_m) \sqrt{1 + \frac{4r}{y_h}} \right], \tag{B.55}$$

with $r = M^2/S$.

The lower bound $Q_h^{2\,\min}(y_l, y_h, Q_l^2)$ is equal to $Q_{h\,\mathrm{II}}^2$:

$$Q_{h\,\mathrm{I,II}}^2 = Q_l^2 + \frac{S}{2M^2}(y_l - y_h)(y_l S \pm \sqrt{\lambda_q}).$$

The upper bound for y_l is dependent only on Q_l^2; see (B.22):

$$y_l^{\max}(Q_l^2) = \frac{1}{2m^2}\left[\frac{1}{S}\sqrt{\lambda_S \lambda_m} - Q_l^2\right].$$

The lower bound for y_l is reached at the infrared singularity $\mathcal{F}(y_h, Q_l^2)$. In the calculation of the hard part (4.13) of the infrared divergent cross-section contribution one has to take into account an additional condition:

$$k^0 \geq \epsilon > 0. \tag{B.56}$$

The infrared problem is treated in the proton rest frame. Corresponding to (A.4), this condition may be transformed into the following modification of the integration boundaries (B.34):

$$y_l^{\min} = y_h \to y_l^{\min}(\epsilon) = y_h + \frac{2\epsilon M}{S}. \tag{B.57}$$

The integration boundaries are:

$$\begin{aligned}
Q_{h\,\mathrm{II}}^2 \leq\ & Q_h^2 \leq y_h S && \text{if } y_l \geq y_{l_d},\\
Q_{h\,\mathrm{II}}^2 \leq\ & Q_h^2 \leq Q_{h\,\mathrm{I}}^2 && \text{if } y_l \leq y_{l_d},\\
y_l^{\min}(\epsilon) \leq\ & y_l \leq y_l^{\max}(Q_l^2).
\end{aligned} \tag{B.58}$$

The integration region $\mathcal{I}_m = (y_l, Q_h^2)$ is shown in figures 39 and 40.

In appendix D.3.3, the square roots of the functions C_1 and C_2 will be needed. In appendix B.2.3, we discussed these roots at the integration boundaries for the case of leptonic variables. Here, exactly the same discussion applies with inclusion of the relations (B.35)–(B.40). Although, there is one modification which concerns the location of the zeros of C_1 and C_2 at the boundary $Q_h^2 = y_h S$. Differing from the leptonic case here they are at some values of y_l for fixed external values of y_h and Q_l^2:

$$\begin{aligned}
y_{l_1} &= 1 + y_h - \frac{1}{x_m},\\
y_{l_2} &= 1 - x_m(1 - y_h).
\end{aligned} \tag{B.59}$$

They satisfy the inequalities

$$y_{l_1} < y_h < y_{l_d} < y_{l_2} < y_l^{\max}, \tag{B.60}$$

if additionally the condition $y_h < 1/(1+r)$ is fulfilled. In this case, the y_{l_1} does not belong to the physical interval $(y_h,\ y_l{}^{max})$ of variation of y_l, see figure 39.

We only mention that one needn't know the values of the roots of C_1 and C_2 on the fourth boundary since the integration is performed along its direction in the phase space.

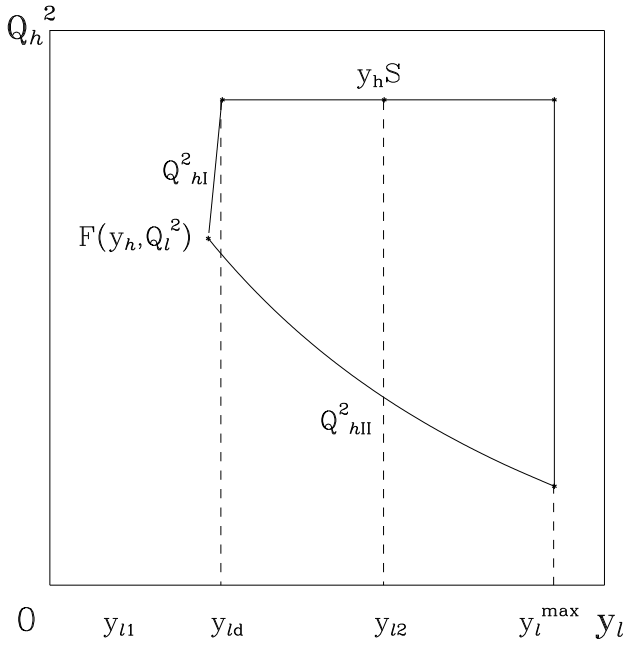

Figure 39: *Integration region (y_l, Q_h^2) for the cross-section in mixed variables, $x_m \leq 1$.*

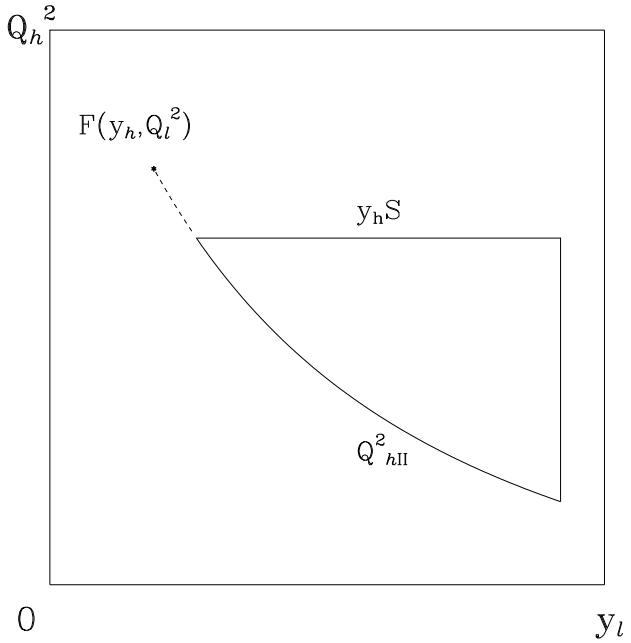

Figure 40: *Integration region (y_l, Q_h^2) for the cross-section in mixed variables, $x_m > 1$.*

B.3.3 Integration variables $\mathcal{I}'_m = (Q_h^2, y_l)$

Here the boundaries for the integration of the hard, infrared finite part of the bremsstrahlung cross-section are derived. In this case, the integrals over y_l are performed analytically in appendix D.4. The last one over Q_h^2 has to be done numerically.

The lower limit of y_l at fixed values of Q_l^2, y_h, and Q_h^2 may be found from (B.4):

$$y_l^{\min}(y_h, Q_h^2, Q_l^2) = \frac{1}{2Q_h^2}\left[y_h(Q_l^2+Q_h^2) + \frac{1}{S}|Q_l^2 - Q_h^2|\sqrt{\lambda_h}\right]. \tag{B.61}$$

There is only one solution if $x_m > 1$ since then it is definitely $Q_l^2 > Q_h^2$. For the more common case $x_m < 1$ the solution has two branches. Geometrically, they coincide with the curves $Q_{h\,\mathrm{I,II}}^2$ in figure 39. The two curves (B.61) meet at the infrared point $\mathcal{F}(y_l, Q_h^2)$. This point marks the lowest allowed value for y_l since $y_l \geq y_h$; see (A.4). There is no need to exclude the infrared singularity from the integration boundary, since the integrand has been regulated there. The upper limit $y_l^{\max}(y_h, Q_h^2; Q_l^2)$ of y_l does not depend on y_h or Q_h^2 and is as derived earlier [see (B.22)]:

$$y_l^{\max}(Q_l^2) \;=\; \frac{1}{2m^2}\left[\frac{1}{S}\sqrt{\lambda_S\lambda_m} - Q_l^2\right] \leq \bar{y}_l.$$

The upper limit of Q_h^2 derives from the inequality $M_h^2 \geq M^2$ together with (6.5). It is independent of the actual value of Q_l^2: $Q_h^{2\,\max}(y_h, Q_l^2) = y_h S$. The curves $y_l^{\min}(y_h, Q_h^2, Q_l^2)$ and $y_l^{\max}(Q_l^2)$ meet at $Q_h^2 = Q_h^{2\,\min}$; this condition may be used for the calculation of $Q_h^{2\,\min}(y_h, Q_l^2)$:

$$\begin{aligned} Q_h^{2\,\min}(y_h, Q_l^2) &= Q_l^2 + \frac{S}{2M^2}\left(y_l^{\max} - y_h\right)\left[y_l^{\max}S - \sqrt{(y_l^{\max}S)^2 + 4M^2Q_l^2}\right] \\ &= Q_l^2 - \frac{S\left(y_l^{\max} - y_h\right)\left(Q_l^2 + \sqrt{\lambda_m}\right)}{S + \sqrt{\lambda_S}}. \end{aligned} \tag{B.62}$$

Taking all the above conditions together, the physical region for the integration variables is found:

$$\begin{aligned} Q_h^{2\,\min}(y_h, Q_l^2) \;\leq\; Q_h^2 \;\leq\; y_h S, \\ y_l^{\min}(y_h, Q_l^2, Q_h^2) \;\leq\; y_l \;\leq\; y_l^{\max}(y_h, Q_l^2, Q_h^2). \end{aligned} \tag{B.63}$$

For the analytical integration over y_l in appendix D.4, we need the expressions for the roots of C_1 and C_2 at the integration boundaries.

At $y_l^{\max}$, they are:

$$\sqrt{C_1(y_l^{\max})} = \frac{\sqrt{\lambda_S}[Q_l^4 + 2m^2(Q_l^2+Q_h^2)] - \sqrt{\lambda_m}S(Q_l^2 + 2m^2y_h)}{2m^2}, \tag{B.64}$$

$$\sqrt{C_2(y_l^{\max})} = \frac{\sqrt{\lambda_S}[Q_l^2Q_h^2 + 2m^2(Q_l^2+Q_h^2)] - \sqrt{\lambda_m}S(Q_h^2 + 2m^2y_h)}{2m^2}, \tag{B.65}$$

$$\sqrt{\lambda_q(y_l^{\max})} = \frac{S\sqrt{\lambda_m} - \sqrt{\lambda_S}Q_l^2}{2m^2}. \tag{B.66}$$

Since the lower boundary of y_l has two branches, the roots have different analytical expressions there and the integration region has to be divided into two subregions:

- Region I: $Q_l^2 \geq Q_h^2$
- Region II: $Q_l^2 \leq Q_h^2$

The following relations hold:

$$\sqrt{C_1(y_l^{\min})}^{\mathrm{I}} = \frac{(Q_l^2 - Q_h^2)\left[2SQ_h^2 - Q_l^2(y_h S + \sqrt{\lambda_h})\right]}{2Q_h^2}, \tag{B.67}$$

$$\sqrt{C_2(y_l^{\min})}^{\mathrm{I}} = \frac{(Q_l^2 - Q_h^2)\left[2SQ_h^2 - Q_h^2(y_h S - \sqrt{\lambda_h})\right]}{2Q_h^2}, \tag{B.68}$$

$$\sqrt{\lambda_q(y_l^{\min})}^{\mathrm{I}} = \frac{y_h S(Q_l^2 - Q_h^2) + (Q_l^2 + Q_h^2)\sqrt{\lambda_h}}{2Q_h^2}, \tag{B.69}$$

$$\sqrt{C_1(y_l^{\min})}^{\mathrm{II}} = \frac{(Q_h^2 - Q_l^2)\left[2SQ_h^2 - Q_l^2(y_h S - \sqrt{\lambda_h})\right]}{2Q_h^2}, \tag{B.70}$$

$$\sqrt{C_1(y_l^{\min})}^{\mathrm{II}} = \frac{(Q_h^2 - Q_l^2)\left[2SQ_h^2 - Q_h^2(y_h S + \sqrt{\lambda_h})\right]}{2Q_h^2}, \tag{B.71}$$

$$\sqrt{\lambda_q(y_l^{\min})}^{\mathrm{II}} = \frac{y_h S(Q_h^2 - Q_l^2) + (Q_l^2 + Q_h^2)\sqrt{\lambda_h}}{2Q_h^2}. \tag{B.72}$$

All these roots are positive definite. Again, the values of the roots at the fourth boundary are not needed since the integration is performed along its direction.

B.4 Boundaries for hadronic variables

B.4.1 External variables $\mathcal{E}_h = (y_h, Q_h^2)$

The physical region of $\mathcal{E}_h = (y_h, Q_h^2)$ may be derived from the boundary condition (B.7) and from the inequality

$$0 \leq y_h S - Q_h^2 = W^2 - M^2 \leq \bar{W}^2 - M^2, \tag{B.73}$$

where $\bar{W}^2$ may be taken from (B.19). This proceeds exactly as in the case of the leptonic variables, by a replacement of (y_l, Q_l^2) by (y_h, Q_h^2) everywhere in the argumentations.

One gets for $\mathcal{E}_h$ the following physical region:

$$\begin{aligned} 0 \;\leq\; Q_h^2 \;&\leq\; \frac{\lambda_S}{S + M^2 + m^2} \equiv \bar{Q}_h^2, \\ y_h^{\min}(Q_h^2) = \frac{Q_h^2}{S} \;&\leq\; y_h \;\leq\; y_h^{\max}(Q_h^2), \end{aligned} \tag{B.74}$$

where

$$y_h^{\max}(Q_h^2) = \frac{1}{2m^2}\left[\frac{1}{S}\sqrt{\lambda_S Q_h^2(Q_h^2 + 2m^2)} - Q_h^2\right] \leq \bar{y}_h. \tag{B.75}$$

Here, the $\bar{y}_h$ is the maximal possible value of y_h:

$$\bar{y}_h = \frac{S - 2mM}{S}. \tag{B.76}$$

The physical region $\mathcal{E}_h = (Q_h^2, y_h)$ coincides with that for the case of leptonic variables, which is shown in figure 33.

B.4.2 Integration variables $\mathcal{I}_h = (y_l, Q_l^2)$

Similar to the case of the mixed variables, for the determination of the hard part of the infrared divergent contribution we first integrate over Q_l^2 and afterwards over y_l. This will be done in appendix D.3.4.

Two bounds for Q_l^2 at given values of y_l, y_h, Q_h^2 may be derived from (B.27) by interchanging y_l with y_h and Q_l^2 with Q_h^2 as was indicated in connection with (B.4),

$$Q^2_{l\,\mathrm{I,II}} = Q_h^2 + \frac{S}{2M^2}(y_l - y_h)\left(\pm\sqrt{\lambda_h} - y_h S\right), \tag{B.77}$$

and two others from (B.3),

$$Q^2_{l\,\mathrm{III,IV}} = \frac{1}{2M^2}\left[(1-y_l)S^2 - 4m^2M^2 \pm \sqrt{\lambda_S\lambda_l}\right]. \tag{B.78}$$

As may be seen in figure 41, the absolute maximum $\bar{y}_l$ of y_l divides the curved boundary into two parts. The $\bar{y}_l$ is defined in (B.23). It is the root of λ_l: $\lambda_l(\bar{y}_l) = 0$. Thus, the two curves $Q^2_{l\,\mathrm{III,IV}}$ meet there. Further, the minimum of y_l at given y_h is equal to y_h and independent of Q_h^2.

When calculating the hard part (4.13) of the infrared divergent cross-section contribution, one has to take into account an additional condition:

$$k^0 \geq \epsilon > 0. \tag{B.79}$$

The infrared problem is treated in the proton rest frame. With the expression for k^0 in (A.4), this condition may be transformed into the following modification of the lower bound for y_l:

$$y_l^{\min} = y_h \to y_l^{\min}(\epsilon) = y_h + \frac{2\epsilon M}{S}. \tag{B.80}$$

For a complete definition of the integration region one needs yet the points where each of the two straight boundaries meets one of the two curved. The points y_{l3} and y_{l2} are determined from the conditions $Q^2_{l\,\mathrm{II}} = Q^2_{l\,\mathrm{IV}}$ and $Q^2_{l\,\mathrm{I}} = Q^2_{l\,\mathrm{III}}$, respectively:

$$\begin{aligned} y_{l2(3)} &= \frac{[(1-y_h)(S \pm \sqrt{\lambda_S} + 2y_hS)S - 2M^2(Q_h^2 + 2m^2)](\sqrt{\lambda_h} \mp y_hS)}{2S[(1-y_h)(\sqrt{\lambda_h} \mp y_hS)S \pm 2M^2(Q_h^2 + m^2)]} \\ &\quad \mp \frac{2M^2Q_h^2[(1-2y_h)S \mp \sqrt{\lambda_S}]}{2S[(1-y_h)(\sqrt{\lambda_h} \mp y_hS)S \pm 2M^2(Q_h^2 + m^2)]}. \end{aligned} \tag{B.81}$$

In the ultra-relativistic approximation,

$$y_{l2} \approx \frac{2S + y_h(\sqrt{\lambda_h} - y_hS) - 2rQ_h^2}{2S + \sqrt{\lambda_h} - y_hS}, \tag{B.82}$$

$$y_{l3} \approx y_h + \frac{2rQ_h^2}{y_hS + \sqrt{\lambda_h}}. \tag{B.83}$$

The integration limits may be summarized as follows:

$$\begin{array}{lcll} Q_l^{2\min}(y_l, y_h, Q_h^2) &=& Q^2_{l\,\mathrm{II}} & \text{if } y_l^{\min}(\epsilon) \leq y_l \leq y_{l3}, \\ Q_l^{2\min}(y_l, y_h, Q_h^2) &=& Q^2_{l\,\mathrm{IV}} & \text{if } y_{l3} \leq y_l \leq \bar{y}_l, \\ Q_l^{2\max}(y_l, y_h, Q_h^2) &=& Q^2_{l\,\mathrm{I}} & \text{if } y_l^{\min}(\epsilon) \leq y_l \leq y_{l2}, \\ Q_l^{2\max}(y_l, y_h, Q_h^2) &=& Q^2_{l\,\mathrm{III}} & \text{if } y_{l2} \leq y_l \leq \bar{y}_l. \end{array} \tag{B.84}$$

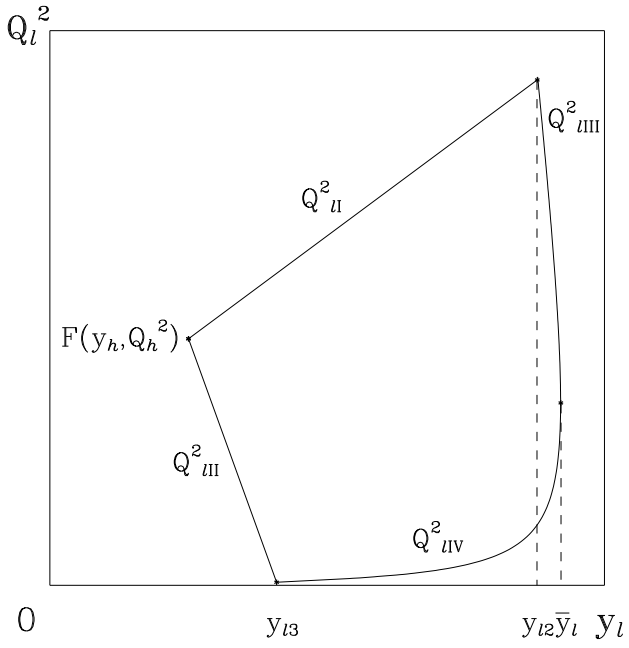

Figure 41: *Integration region (y_l, Q_l^2) for the cross-section in hadronic variables.*

The integration region $\mathcal{I}_h = (y_l, Q_l^2)$ is shown in figure 41. The infrared divergence is located at $\mathcal{F}(y_h, Q_h^2)$.

In the course of the integrations, the values of the roots of C_1 and C_2 are needed at the boundaries. They may be determined exactly:

$$\sqrt{C_1(Q^2_{l\,\mathrm{I,II}})} = (y_l - y_h)S\left[(1-y_l+y_h)S\frac{\sqrt{\lambda_l} \mp y_h S}{2M^2} \mp Q_h^2\right], \tag{B.85}$$

$$\sqrt{C_2(Q^2_{l\,\mathrm{I,II}})} = (y_l - y_h)S\left[(1-y_h)S\frac{\sqrt{\lambda_l} \mp y_h S}{2M^2} \pm Q_h^2\right], \tag{B.86}$$

$$\begin{aligned}\sqrt{C_1(Q^2_{l\,\mathrm{III,IV}})} = &-\frac{1}{2M^2}\Bigg\{\sqrt{\lambda_S}\left[(1-y_l+y_h)(1-y_l)S^2 - 2M^2(Q_h^2+2m^2)\right]\\ &\pm\sqrt{\lambda_l}\left[(1-y_l+y_h)S^2 - 4m^2M^2\right]\Bigg\},\end{aligned} \tag{B.87}$$

$$\begin{aligned}\sqrt{C_2(Q^2_{l\,\mathrm{III,IV}})} = &\frac{1}{2M^2}\Bigg\{\sqrt{\lambda_S}\left[(1-y_l)(1-y_h)S^2 - 4m^2M^2\right]\\ &\pm\sqrt{\lambda_l}\left[(1-y_h)S^2 - 2M^2(Q_h^2+2m^2)\right]\Bigg\}.\end{aligned} \tag{B.88}$$

B.4.3 Integration variables $\mathcal{I}'_h = (Q_l^2, y_l)$

Here, the boundaries for the integration over leptonic variables will be derived for the case where the integration over y_l is performed before that over Q_l^2. This is needed in appendix D.4 and will be used for the calculation of the finite hard part of the cross-section. We remind that

in this case the boundaries for y_l are the same as in the case of the mixed variables. Thus, the minimal value of y_l for given values of Q_l^2, y_h, and Q_h^2 is given by (B.61),

$$y_l^{\min}(y_h, Q_h^2, Q_l^2) = \frac{1}{2Q_h^2}\left[y_h(Q_l^2 + Q_h^2) + \frac{1}{S}|Q_l^2 - Q_h^2|\sqrt{\lambda_h}\right],$$

and the maximal value by (B.22):

$$y_l^{\max}(y_h, Q_h^2, Q_l^2) = \frac{1}{2m^2}\left[\frac{1}{S}\sqrt{\lambda_S\lambda_m} - Q_l^2\right] \leq \bar{y}_l.$$

For fixed y_h, Q_h^2, one may see in figure 41 that $y_l^{\max}$ and $y_l^{\min}$ are equal for the extreme values of Q_l^2. Solving the resulting equation, one gets:

$$Q_l^{2\,\min(\max)}(y_h, Q_h^2) = \frac{Q_h^4\left(S \mp \sqrt{\lambda_S}\right)\left(S \mp \sqrt{\lambda_S} - y_h S \mp \sqrt{\lambda_h}\right)}{2S\left(y_h S \mp \sqrt{\lambda_h}\right)(Q_h^2 + m^2 y_h) + 4M^2 Q_h^2(Q_h^2 + m^2)}. \tag{B.89}$$

Concluding, the physical region of $\mathcal{I}_h' = (Q_l^2, y_l)$ is:

$$\begin{aligned} Q_l^{2\,\min}(y_h, Q_h^2) &\leq Q_l^2 \leq Q_l^{2\,\max}(y_h, Q_h^2), \\ y_l^{\min}(Q_l^2; y_h, Q_h^2) &\leq y_l \leq y_l^{\max}(Q_l^2; y_h, Q_h^2). \end{aligned} \tag{B.90}$$

B.4.4 Variables in section 7: $\mathcal{E}_h = (y_h, Q_h^2)$, $\mathcal{I}_h = (\tau)$

In this section, we restrict ourselves to the ultra-relativistic approximation.

The physical region for the external variables is as derived in section B.4.1:

$$\begin{aligned} 0 &\leq y_h \leq 1, \\ 0 &\leq Q_h^2 \leq y_h S. \end{aligned} \tag{B.91}$$

The limits for $\tau = z_2 + m^2$ at given values of y_h and Q_h^2 follow from those for z_2 which are derived in appendix B.1.3. For the case of the hard photon contribution to the infrared singular cross-section part one has also to take into account the condition

$$k^0 \geq \epsilon > 0. \tag{B.92}$$

The infrared problem is treated in the rest frame of the (γe) compound system. There, this condition may be fulfilled by the demand

$$z_2 \geq \bar{z}_2 = 2m\epsilon. \tag{B.93}$$

The boundaries are then:

$$m^2 + 2m\epsilon \leq \tau \leq m^2 + x_h(1 - y_h)S \approx x_h(1 - y_h)S. \tag{B.94}$$

At the lower boundary, one has to retain the influence of the electron mass in order to ensure the positive definiteness of the phase space measure and to prevent unphysical singularities during the integrations.

B.5 Boundaries for Jaquet-Blondel variables: $\mathcal{E}_{\mathrm{JB}} = (y_{\mathrm{JB}}, Q^2_{\mathrm{JB}})$, $\mathcal{I}_{\mathrm{JB}} = (\tau)$

In this section, we restrict ourselves to the ultra-relativistic approximation. The definitions of the Jaquet-Blondel variables are:

$$y_{\mathrm{JB}} = y_h, \tag{B.95}$$
$$Q^2_{\mathrm{JB}} = \mathcal{N}(\vec{p}_{2\perp})^2. \tag{B.96}$$

The normalization $\mathcal{N}$ has to be adjusted such that in the limiting case of the Born kinematics it will hold $Q^2_{\mathrm{JB}} = Q^2_h$. We will immediately see that

$$\mathcal{N} = \frac{1}{1 - y_h + \ldots}, \tag{B.97}$$

where the dots stand for some terms proportional to m^2 and M^2. An exact expression for Q^2_{JB} in terms of y_h, Q^2_h, τ may be obtained in the rest frame of the proton. In the momentum tetrahedron of figure 3 it is $\vec{k}_1 - \vec{p}_2 = \vec{\Lambda}$. In this system, these three three-vectors span a triangle whose area may be expressed in two ways:

$$\frac{1}{2}|\vec{k_1}||\vec{p}_{2\perp}| = \sqrt{-\frac{1}{4}\lambda(\vec{k_1}^2, \vec{p_2}^2, \vec{\Lambda}^2)}. \tag{B.98}$$

The three three-vectors squared are expressed by invariants in (A.4):

$$(\vec{p}_{2\perp})^2 = -\frac{1}{4M^2\lambda_S}\lambda(\lambda_S, \lambda_h, \lambda_\tau). \tag{B.99}$$

With this expression, the Q^2_{JB} is determined after the normalization has been adjusted such that for $z_2 = 0$ the Q^2_{JB} becomes Q^2_h:

$$Q^2_{\mathrm{JB}} = Q^2_h \frac{[Q^2_h - y_h(Q^2_h + z_2)]S^2 - M^2(Q^2_h + z_2)^2 - m^2\lambda_h}{(1 - y_h)Q^2_h S^2 - M^2 Q^4_h - m^2\lambda_h}. \tag{B.100}$$

If the electron mass is neglected the Q^2_{JB} becomes

$$Q^2_{\mathrm{JB}} = \frac{(1 - y_h)Q^2_h - y_h z_2 - (Q^2_h + z_2)^2 r/S}{(1 - y_h) - Q^2_h r/S}, \tag{B.101}$$

where it is $r = M^2/S$. Neglecting also the proton mass, one finally obtains

$$Q^2_{\mathrm{JB}} = Q^2_h - \frac{y_h}{1 - y_h} z_2. \tag{B.102}$$

The hadronic and Jaquet-Blondel–transferred momentum squares are related by $y_h = y_{\mathrm{JB}}$ and the additional variable z_2. This property may be used for a derivation of the kinematical boundaries. We start from the hadronic integration limits which were derived in appendix B.4.4. A chain of simple changes of the integration region allows a derivation of the

boundary values for Jaquet-Blondel variables:

$$\begin{aligned}
\Gamma_3 &= \int_0^S dQ_h^2 \int_{Q_h^2/S}^1 dy_h \int_0^{(1-y_h)Q_h^2/y_h} dz_2 \quad = \int_0^1 dy_h \int_0^{y_h S} dQ_h^2 \int_0^{(1-y_h)Q_h^2/y_h} dz_2 \\
&= \int_0^1 dy_h \int_0^{(1-y_h)S} dz_2 \int_{y_h z_2/(1-y_h)}^{y_h S} dQ_h^2 \quad = \int_0^1 dy_{\rm JB} \int_0^{(1-y_h)S} dz_2 \int_0^{y_h S - y_h z_2/(1-y_h)} dQ_{\rm JB}^2 \\
&= \int_0^1 dy_{\rm JB} \int_0^{y_h S} dQ_{\rm JB}^2 \int_0^{(1-x_{\rm JB})(1-y_{\rm JB})S} dz_2 \quad = \int_0^S dQ_{\rm JB}^2 \int_{Q_{\rm JB}^2/S}^1 dy_{\rm JB} \int_0^{(1-x_{\rm JB})(1-y_{\rm JB})S} dz_2 .
\end{aligned} \tag{B.103}$$

Thus, we derived:

$$0 \le \quad Q_{\rm JB}^2 \quad \le S, \tag{B.104}$$

$$\frac{Q_{\rm JB}^2}{S} \le \quad y_{\rm JB} \quad \le 1, \tag{B.105}$$

$$\begin{aligned}
m^2 + 2m\epsilon \le \quad \tau \quad &\le m^2 + (1-x_{\rm JB})(1-y_{\rm JB})S \\
&\approx (1-x_{\rm JB})(1-y_{\rm JB})S.
\end{aligned} \tag{B.106}$$

Here we took into account that the lower bound for the τ integration is modified in case of the hard contribution to the infrared singular part; see the corresponding remarks in the foregoing appendix.

The physical region $\mathcal{E}_{\rm JB} = (Q_{\rm JB}^2, y_{\rm JB})$ is shown in figure 42.

C The phase space volume

In the above appendices, many boundaries for external variable sets and for integration variables have been introduced in different combinations of variables and in different order. A useful tool for numerical checks of the correctness of all these boundaries is the integral over the phase space volume, which must be identical for all the different presentations.

The phase space volume (3.9) is calculated now in terms of the variables which were introduced for the study of the photoproduction process:

$$\begin{aligned}
\Gamma &= \frac{\pi S^2}{4\sqrt{\lambda_S}} \int dy_l \, dQ_l^2 \, dy_h \, dQ_h^2 \frac{dz_{2(1)}}{\sqrt{R_z}} \\
&= \frac{\pi}{4\sqrt{\lambda_S}} \int_{(M+m_\pi)^2}^{(\sqrt{s}-m)^2} dW^2 \int_{Q_l^{2\,\min}}^{Q_l^{2\,\max}} dQ_l^2 \int_{(M+m_\pi)^2}^{W^2} dM_h^2 \int_{Q_h^{2\,\min}}^{Q_h^{2\,\max}} dQ_h^2 \int_{z_2^{\min}}^{z_2^{\max}} \frac{dz_2}{\sqrt{R_z}}.
\end{aligned} \tag{C.1}$$

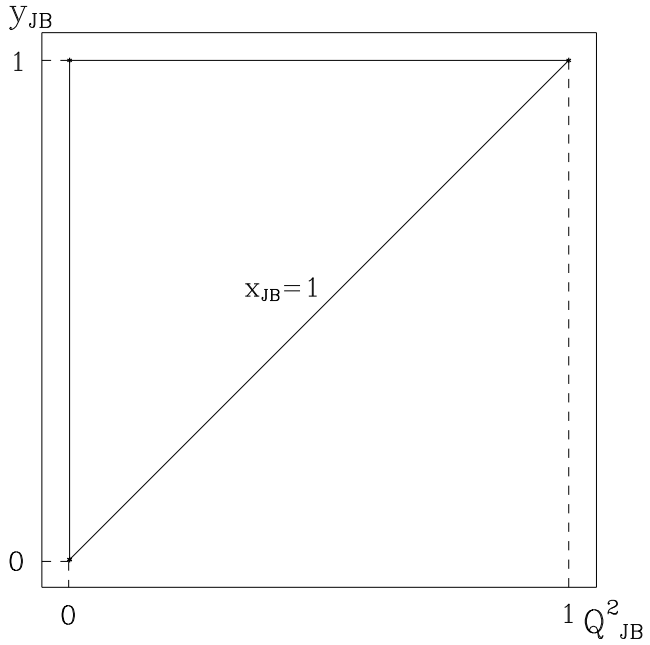

Figure 42: *Physical region $(Q^2_{\rm JB}, y_{\rm JB})$ for the cross-section in Jaquet-Blondel variables.*

The boundaries for z_2 are (B.9), those for Q_h^2 are (B.46), and those for Q_l^2 are (B.25). We first apply (D.2). Next, the integration over Q_h^2 yields

$$\int dQ_h^2 = Q_h^{2\,\max} - Q_h^{2\,\min}, \tag{C.2}$$

which together with the result of the first integration and with (A.29), $A_2 = \lambda_q$, leads to fortunate cancellations:

$$\Gamma \;=\; \frac{\pi}{4\sqrt{\lambda_S}} \int dW^2\, dQ_l^2\, dM_h^2 \frac{W^2 - M_h^2}{W^2}. \tag{C.3}$$

The two subsequent integrals over M_h^2 and Q_l^2 are also trivial; after neglecting m_π:

$$\Gamma \;=\; \frac{\pi}{8s} \int dW^2 \frac{(W^2 - M^2)^2}{W^2} \sqrt{(s - W^2 + M^2)^2 - 4m^2 W^2}. \tag{C.4}$$

The last integration yields

$$\begin{aligned}
\Gamma \;=\; & \frac{\pi^2}{8S} \Bigg\{ \frac{\sqrt{\lambda_S}}{6} \left[s^2 + 10m^2 s - 5M^2 s + m^4 - 5m^2 M^2 - 2M^4 \right] \\
& - \left[m^2 s (s + m^2 - 2M^2) + \frac{1}{2}(s + m^2) M^4 \right] \ln \frac{s + m^2 - M^2 + \sqrt{\lambda_S}}{s + m^2 - M^2 - \sqrt{\lambda_S}} \\
& + \frac{1}{2}(s - m^2) M^4 \ln \frac{\left(s - m^2 + M^2 + \sqrt{\lambda_S}\right)\left(s - m^2 - M^2 + \sqrt{\lambda_S}\right)}{\left(s - m^2 + M^2 - \sqrt{\lambda_S}\right)\left(s - m^2 - M^2 - \sqrt{\lambda_S}\right)} \Bigg\},
\end{aligned} \tag{C.5}$$

with $s = S + m^2 + M^2$. Neglecting the electron mass m one gets

$$\Gamma \approx \frac{\pi^2}{8s}\left[\frac{1}{6}(s^2 - 5sM^2 - 2M^4)(s - M^2) + sM^4 \ln\frac{s}{M^2}\right], \tag{C.6}$$

and after a subsequent neglection of the proton mass

$$\Gamma \approx \frac{\pi^2}{48}s^2. \tag{C.7}$$

D Tables of integrals for the approach of section 3

D.1 First series of $z_{1(2)}$-integrals

This first series of integrals over z_1 or z_2 is used for the common treatment of the cross-section in leptonic, mixed, and hadronic variables. The first integration is over z_1 or z_2. It corresponds to the angular integration over the angle φ of the photon in the rest system of the proton as discussed in A.1. At this stage of the integration, there is no infrared problem. The necessary integrals are:

$$[\mathcal{A}]_z = \frac{1}{\pi}\int_{z_{1(2)}^{\min}}^{z_{1(2)}^{\max}} \frac{dz_{1(2)}}{\sqrt{R_Z}}\mathcal{A}, \tag{D.1}$$

$$[1]_z = \frac{1}{\sqrt{A_{1,2}}}, \tag{D.2}$$

$$\left[\frac{1}{z_{1(2)}}\right]_z = \frac{1}{\sqrt{C_{1(2)}}}, \tag{D.3}$$

$$\left[\frac{1}{z_{1(2)}^2}\right]_z = \frac{B_{1(2)}}{C_{1(2)}^{3/2}}. \tag{D.4}$$

Using the relation $z_1 = z_2 + Q_h^2 - Q_l^2$, one may derive

$$\frac{1}{z_1 z_2} = \frac{1}{Q_h^2 - Q_l^2}\left(\frac{1}{z_2} - \frac{1}{z_1}\right), \tag{D.5}$$

and thus reduce the corresponding integral type to known ones. The functions A, B, C are defined in (A.29)–(A.31). The integration boundaries $z_{1(2)}^{\max(\min)}$ may be found in (B.9).

In appendix B.1.2, we perform the integration over $z_{1(2)}$ with dedicated cuts for the photonic energy and scattering angle. In this case, the above table of integrals becomes modified:

$$[1]_{\hat{z}} = -\frac{1}{\pi\sqrt{\lambda_q}}\mathrm{asin}\frac{B_{1(2)} - z_{1(2)}\lambda_q}{\sqrt{D_z}}\,|_{\hat{z}}, \tag{D.6}$$

$$\left[\frac{1}{z_{1(2)}}\right]_{\hat{z}} = \frac{1}{\pi\sqrt{C_1}}\mathrm{asin}\frac{z_{1(2)}B_{1(2)} - C_{1(2)}}{z_{1(2)}\sqrt{D_z}}\,|_{\hat{z}}, \tag{D.7}$$

$$\left[\frac{1}{z_{1(2)}^2}\right]_{\hat{z}} = \frac{1}{\pi C_1}\frac{\sqrt{R_z(z_{1(2)})}}{z_{1(2)}}\,|_{\hat{z}} + \frac{B_{1(2)}}{C_{1(2)}}\left[\frac{1}{z_{1(2)}}\right]_{\hat{z}}. \tag{D.8}$$

In the table, the abbreviation

$$\Big|_{\hat{z}} \equiv \Big|_{\hat{z}_{1(2)}^{\min}}^{\hat{z}_{1(2)}^{\max}} \tag{D.9}$$

is used, where the boundaries $\hat{z}_{1(2)}^{\min,\max}$ have been derived in B.1.2. Further, we use (A.28) in the slightly rewritten form (B.8) and a similar relation holds for D_z:

$$\begin{aligned} D_z &= 4sW^2 \left[Q_l^{2\max}(W^2) - Q_l^2\right] \left[Q_l^2 - Q_l^{2\min}(W^2)\right] \\ &\times \left[Q_h^{2\max}(W^2, Q_l^2, M_h^2) - Q_h^2\right] \left[Q_h^2 - Q_h^{2\min}(W^2, Q_l^2, M_h^2)\right]. \end{aligned} \tag{D.10}$$

D.2 The integrals for the infrared problem

For the angular integration,

$$[\mathcal{A}]_\xi = \frac{1}{2}\int_{-1}^{1} d\xi \mathcal{A}, \tag{D.11}$$

one needs the following integrals which are calculated with account of the exact kinematics:

$$[1]_\xi = 1, \tag{D.12}$$

$$\left[\frac{1}{1-\beta_i\xi}\right]_\xi = \frac{1}{2\beta_i}\ln\frac{1+\beta_i}{1-\beta_i}, \tag{D.13}$$

$$\left[\frac{1}{(1-\beta_i\xi)^2}\right]_\xi = \frac{1}{1-\beta_i^2}, \tag{D.14}$$

$$\left[\ln(1-\xi^2)\right]_\xi = 2\ln 2 - 2, \tag{D.15}$$

$$\left[\frac{\ln(1-\xi^2)}{1-\beta_i\xi}\right]_\xi = \ln 2\frac{1}{\beta_i}\ln\frac{1+\beta_i}{1-\beta_i} + \frac{1}{2\beta_i}\left[\mathrm{Li}_2\left(\frac{2\beta_i}{\beta_i-1})\right) - \mathrm{Li}_2\left(\frac{2\beta_i}{\beta_i+1})\right)\right], \tag{D.16}$$

$$\left[\frac{\ln(1-\xi^2)}{(1-\beta_i\xi)^2}\right]_\xi = \frac{1}{1-\beta_i^2}\left(2\ln 2 - \frac{1}{\beta_i}\ln\frac{1+\beta_i}{1-\beta_i}\right). \tag{D.17}$$

Since the definition of the velocities β_i depends on the lorentz system, some of the above integrals do so.

Further, integrals over the Feynman parameter α are used:

$$[\mathcal{A}]_\alpha = \int_0^1 d\alpha \mathcal{A}. \tag{D.18}$$

The first one is

$$\left[\frac{1}{-k_\alpha^2}\right]_\alpha = 2\mathrm{L_m}. \tag{D.19}$$

with

$$-k_\alpha^2 = Q^2\alpha(1-\alpha) + m^2, \tag{D.20}$$

and the $\mathrm{L_m}$ is defined in (4.29). Due to the invariance of $-k_\alpha^2$, the integral (D.19) is relativistic invariant.

A second integral of the type (D.18) occurs in (4.23). It depends on the system in which it is calculated:

$$\left[\frac{1}{\beta_\alpha(-k_\alpha^2)}\ln\frac{1-\beta_\alpha}{1+\beta_\alpha}\right]_\alpha = \frac{2}{Q^2+2m^2}\mathcal{S}_\Phi, \tag{D.21}$$

$$\mathcal{S}_\Phi = \frac{1}{2}\left(Q^2+2m^2\right)\int_0^1 \frac{d\alpha}{\beta_\alpha(-k_\alpha^2)}\ln\frac{1-\beta_\alpha}{1+\beta_\alpha}. \tag{D.22}$$

The exact answer for this type of integrals may be found following the hints in [6]. For the proton rest system, the explicit result in the ultra-relativistic limit is (4.31). For the case of photoproduction, which was calculated in another rest system, the exact expression has been calculated numerically. Finally, we mention that for the case of the (γe) rest frame, which was used e.g. in the case of Jaquet-Blondel variables, the kinematical simplifications are such that the S_Φ-function need not be introduced; see section 7.3.

D.3 The second and third integrations for $\delta_{\rm hard}^{\rm IR}$

In this appendix, integrals over (first) Q^2 and (then) y are collected. They are used for the calculation of the hard part of the infrared divergent cross-section contribution.

D.3.1 Leptonic variables

The necessity to work out the absolute values in (B.39)–(B.40) explicitly for a subsequent integration over y_h forces us to perform the integrations in the following four regions separately:

$$\begin{array}{lccccccccc}
\text{Region I :} & y_h^{\min} & < & y_h & < & y_{h1}, & Q^2_{h\,\rm II} & \le & Q^2_h & \le & y_h S, \\
\text{Region II :} & y_{h1} & < & y_h & < & y_{h2}, & Q^2_{h\,\rm II} & \le & Q^2_h & \le & y_h S, \\
\text{Region III :} & y_{h2} & < & y_h & < & y_{hd}, & Q^2_{h\,\rm II} & \le & Q^2_h & \le & y_h S, \\
\text{Region IV :} & y_{hd} & < & y_h & < & y_h^{\max}(\epsilon), & Q^2_{h\,\rm II} & \le & Q^2_h & \le & Q^2_{h\,\rm I}.
\end{array}$$

We introduce now the operation

$$\{\mathcal{A}\}_{Qz} = S\int_{Q^2_{h\,\rm II}}^{\min\{Q^2_{h\,\rm I}, y_h S\}} dQ^2_h [\mathcal{A}]_z, \tag{D.23}$$

where the operation $[\mathcal{A}]_z$ is defined in (D.1).

The integrals $\{\mathcal{A}\}_{Qz}$ in the regions I–IV are:

$$\left\{\frac{Q_l^2}{z_1 z_2}\right\}^{\rm I}_{Qz} = \frac{1}{y_{lh}}\ln\frac{b}{(-a_1)(-a_2)}, \tag{D.24}$$

$$\left\{\frac{m^2}{z_1^2}\right\}^{\rm I}_{Qz} = \left\{\frac{m^2}{z_2^2}\right\}^{\rm I}_{Qz} = 0, \tag{D.25}$$

$$\left\{\frac{Q_l^2}{z_1 z_2}\right\}^{\rm II}_{Qz} = \frac{1}{y_{lh}}\left(\ln\frac{Q_l^2}{m^2}+\ln\frac{a_1}{-a_2}\right), \tag{D.26}$$

$$\left\{\frac{m^2}{z_1^2}\right\}^{\rm II}_{Qz} = \frac{1}{y_{lh}}, \tag{D.27}$$

$$\left\{\frac{m^2}{z_2^2}\right\}^{\rm II}_{Qz} = 0, \tag{D.28}$$

$$\left\{\frac{Q_l^2}{z_1 z_2}\right\}^{\rm III}_{Qz} = \frac{1}{y_{l_h}}\left(2\ln\frac{Q_l^2}{m^2} + \ln\frac{a_1 a_2}{b}\right), \tag{D.29}$$

$$\left\{\frac{m^2}{z_1^2}\right\}^{\rm III}_{Qz} = \left\{\frac{m^2}{z_2^2}\right\}^{\rm III}_{Qz} = \frac{1}{y_{l_h}}, \tag{D.30}$$

$$\left\{\frac{Q_l^2}{z_1 z_2}\right\}^{\rm IV}_{Qz} = \frac{2}{y_{l_h}}\ln\frac{Q_l^2}{m^2}, \tag{D.31}$$

$$\left\{\frac{m^2}{z_1^2}\right\}^{\rm IV}_{Qz} = \left\{\frac{m^2}{z_2^2}\right\}^{\rm IV}_{Qz} = \frac{1}{y_{l_h}}, \tag{D.32}$$

with

$$\begin{aligned} a_1 &= (1-y_l x_l)(y_h - y_{h1}), \\ a_2 &= [1-y_l(1-x_l)](y_h - y_{h2}), \\ b &= (y_h - x_l y_l)^2(1-y_l - x_l y_l r), \\ y_{l_h} &= y_l - y_h. \end{aligned} \tag{D.33}$$

Now we define the third integration over y_h:

$$(\mathcal{A})_{yQz} = \int_{y_h^{\min}}^{y_{h1}} dy_h \{\mathcal{A}\}^{\rm I}_{Qz} + \int_{y_{h1}}^{y_{h2}} dy_h \{\mathcal{A}\}^{\rm II}_{Qz} + \int_{y_{h2}}^{y_{hd}} dy_h \{\mathcal{A}\}^{\rm III}_{Qz} + \int_{y_{hd}}^{y_h^{\max(\epsilon)}} dy_h \{\mathcal{A}\}^{\rm IV}_{Qz}. \tag{D.34}$$

The result of this:

$$\begin{aligned} \left(\frac{Q_l^2}{z_1 z_2}\right)_{yQz} &= \ln\frac{Q_l^2}{m^2}\ln\frac{y_l^2(1-x_l)^2(1-y_l)S^2}{4M^2\epsilon^2(1-y_l x_l)[1-y_l(1-x_l)]} \\ &+ \frac{1}{2}\ln^2(1-y_l) - \frac{1}{2}\ln^2\left[\frac{1-y_l(1-x_l)}{1-y_l x_l}\right] \\ &- {\rm Li}_2\left[\frac{1-y_l}{(1-y_l x_l)[1-y_l(1-x_l)]}\right] - {\rm Li}_2(1), \end{aligned} \tag{D.35}$$

$$\left(\frac{m^2}{z_1^2}\right)_{yQz} = \ln\frac{y_l(1-x_l)S}{2M\epsilon(1-y_l x_l)}, \tag{D.36}$$

$$\left(\frac{m^2}{z_2^2}\right)_{yQz} = \ln\frac{y_l(1-x_l)(1-y_l)S}{2M\epsilon[1-y_l(1-x_l)]}. \tag{D.37}$$

From (D.35)–(D.37), (4.35) follows immediately.

D.3.2 Leptonic variables. Photoproduction

The first integration of (4.5) with $Q^2 = Q_l^2$, is over z_2. Then, one has to integrate (4.12), which becomes (5.4) for leptonic variables, over Q_h^2 within the integration region as shown in figure 36. We begin with these two integrations:

$$\{\mathcal{A}\}_{Qz} \equiv \int_{Q_h^{2\,\min}}^{Q_h^{2\max}} dQ_h^2 [\mathcal{A}]_z, \tag{D.38}$$

where the boundaries of the integration over Q_h^2 are (B.46), and the $[\mathcal{A}]_z$ is defined and calculated in appendix D.1. Two such twofold integrals have to be performed:

$$\left\{\frac{Q_l^2}{z_1 z_2}\right\}_{Qz} = \frac{1}{W^2 - M_h^2}\frac{1}{\beta}\,\mathrm{L}_\beta, \tag{D.39}$$

$$\left\{\frac{m^2}{z_1^2}\right\}_{Qz} = \left\{\frac{m^2}{z_2^2}\right\}_{Qz} = \frac{1}{W^2 - M_h^2}. \tag{D.40}$$

The L_β and β are defined in (6.8). There is only one third integration:

$$\begin{aligned}\left\{\frac{1}{W^2 - M_h^2}\right\}_M &\equiv \int_{M_h^{2\min}}^{M_h^{2\max}} dM_h^2 \frac{1}{W^2 - M_h^2} \\ &= \ln\frac{W^2 - (M + m_\pi)^2}{2\epsilon\sqrt{W^2}}.\end{aligned} \tag{D.41}$$

The boundaries for this integration are (B.45). After three integrations, we finally arrive at (6.7).

D.3.3 Mixed variables

W consider the case $x_m \leq 1$. From the discussion of the roots of C_1 and C_2 in appendix B.3.2 it may be seen that there are three integration regions:

Region I :	$y_l^{\min}(\epsilon)$	$<$	y_l	$<$	y_{l_d},	$Q_{h\,\mathrm{II}}^2$	$\leq$	Q_h^2	$\leq$	$Q_{h\,\mathrm{I}}^2$,
Region II :	y_{l_d}	$<$	y_l	$<$	y_{l_2},	$Q_{h\,\mathrm{II}}^2$	$\leq$	Q_h^2	$\leq$	$y_h S$,
Region III :	y_{l_2}	$<$	y_l	$<$	$y_l^{\max}$,	$Q_{h\,\mathrm{II}}^2$	$\leq$	Q_h^2	$\leq$	$y_h S$,

with $Q_{h\,\mathrm{I,II}}^2$ given by (B.27).

Using the definition (D.23) for $\{A\}_{Qz}$, one gets the following results in the three regions I–III:

$$\left\{\frac{Q_l^2}{z_1 z_2}\right\}_{Qz}^{\mathrm{I}} = \frac{2}{y_{l_h}}\ln\frac{Q_l^2}{m^2}, \tag{D.42}$$

$$\left\{\frac{m^2}{z_1^2}\right\}_{Qz}^{\mathrm{I}} = \left\{\frac{m^2}{z_2^2}\right\}_{Qz}^{\mathrm{I}} = \frac{1}{y_{l_h}}, \tag{D.43}$$

$$\left\{\frac{Q_l^2}{z_1 z_2}\right\}_{Qz}^{\mathrm{II}} = \frac{1}{y_{l_h}}\left[2\ln\frac{Q_l^2}{m^2} + \ln\frac{[1 - x_m(1 + y_h - y_l)](y_{l_2} - y_l)}{(1 - x_m)^2(1 - y_l - x_l y_l r)}\right], \tag{D.44}$$

$$\left\{\frac{m^2}{z_1^2}\right\}_{Qz}^{\mathrm{II}} = \left\{\frac{m^2}{z_2^2}\right\}_{Qz}^{\mathrm{II}} = \frac{1}{y_{l_h}}, \tag{D.45}$$

$$\left\{\frac{Q_l^2}{z_1 z_2}\right\}_{Qz}^{\mathrm{III}} = \frac{1}{y_{l_h}}\left[\ln\frac{Q_l^2}{m^2} + \ln\frac{1 - x_m(1 + y_h - y_l)}{y_l - y_{l_2}}\right], \tag{D.46}$$

$$\left\{\frac{m^2}{z_1^2}\right\}_{Qz}^{\mathrm{III}} = \frac{1}{y_{l_h}}, \tag{D.47}$$

$$\left\{\frac{m^2}{z_2^2}\right\}_{Qz}^{\mathrm{III}} = 0. \tag{D.48}$$

The third integration is defined by

$$(\mathcal{A})_{yQz} = \int_{y_l^{\min}(\epsilon)}^{y_{l_d}} dy_l \{\mathcal{A}\}^{\rm I}_{Qz} + \int_{y_{l_d}}^{y_{l_2}} dy_l \{\mathcal{A}\}^{\rm II}_{Qz} + \int_{y_{l_2}}^{y_l^{\max}} dy_l \{\mathcal{A}\}^{\rm III}_{Qz}. \tag{D.49}$$

The results of the integrations are:

$$\begin{aligned}\left(\frac{Q_l^2}{z_1 z_2}\right)_{yQz} &= \ln\frac{Q_l^2}{m^2}\ln\frac{(1-y_h)^2(1-x_m)S^2}{4\epsilon^2 M^2} + \ln(1-y_h)\ln(1-x_m) \\ &\quad -\frac{1}{2}\ln^2(1-x_m) - {\rm Li}_2\left[\frac{x_m(1-y_h)}{x_m-1}\right], \qquad \text{(D.50)}\\ \left(\frac{m^2}{z_1^2}\right)_{yQz} &= \ln\frac{(1-y_h)S}{2\epsilon M}, \qquad \text{(D.51)}\\ \left(\frac{m^2}{z_1^2}\right)_{yQz} &= \ln\frac{(1-y_h)(1-x_m)S}{2\epsilon M}. \qquad \text{(D.52)}\end{aligned}$$

From (D.50)–(D.52), (4.36) immediately follows.

D.3.4 Hadronic variables

For the hadronic variables one has to integrate $\delta^{\rm IR}_{\rm hard}$ over the kinematical region of figure 41. With the aid of the boundary conditions which are derived in appendix B.4.2 the integration region may be split into the following three subregions:

$$\begin{array}{lllllllll}
\text{Region I:} & y_l^{\min}(\epsilon) & \le & y_l & \le & y_{l3}, & Q^2_{l\,\rm II} & \le & Q_l^2 \le Q^2_{l\,\rm I}, \\
\text{Region II:} & y_{l3} & \le & y_l & \le & y_{l2}, & Q^2_{l\,\rm IV} & \le & Q_l^2 \le Q^2_{l\,\rm I}, \\
\text{Region III:} & y_{l2} & \le & y_l & \le & \bar{y}_l, & Q^2_{l\,\rm IV} & \le & Q_l^2 \le Q^2_{l\,\rm III}.
\end{array}$$

The operation $\{\mathcal{A}\}_{Qz}$ is defined as follows:

$$\{\mathcal{A}\}_{Qz} = S\int_{\max\{Q^2_{l\rm II}, Q^2_{l\rm IV}\}}^{\min\{Q^2_{l\rm I}, Q^2_{l\rm III}\}} dQ_l^2 [\mathcal{A}]_z. \tag{D.53}$$

The integrals $\{\mathcal{A}\}$ in the three regions I–III are:

$$\begin{aligned}\left\{\frac{Q_h^2}{z_1 z_2}\right\}^{\rm I}_{Qz} &= \frac{2}{y_{lh}}\ln\frac{Q_h^2}{m^2}, \qquad \text{(D.54)}\\ \left\{\frac{m^2}{z_1^2}\right\}^{\rm I}_{Qz} &= \frac{1}{y_{lh}(1-y_{lh})}, \qquad \text{(D.55)}\\ \left\{\frac{m^2}{z_2^2}\right\}^{\rm I}_{Qz} &= \frac{1-y_l}{y_{lh}(1-y_h)}, \qquad \text{(D.56)}\\ \left\{\frac{Q_h^2}{z_1 z_2}\right\}^{\rm II}_{Qz} &= \frac{1}{y_{lh}}\left[2\ln\frac{Q_h^2}{m^2} + \ln\frac{(1-y_l)(2+\sqrt{\lambda_h}/S - y_h)}{[2(1-y_l)+\sqrt{\lambda_h}/S + y_h](1-y_h - x_h y_h r)}\right], \qquad \text{(D.57)}\\ \left\{\frac{m^2}{z_1^2}\right\}^{\rm II}_{Qz} &= \frac{1}{y_{lh}(1-y_{lh})}, \qquad \text{(D.58)}\end{aligned}$$

$$\left\{\frac{m^2}{z_2^2}\right\}^{\rm II}_{Qz} = \frac{1-y_l}{y_{lh}(1-y_h)}, \tag{D.59}$$

$$\left\{\frac{Q_h^2}{z_1 z_2}\right\}^{\rm III}_{Qz} = \frac{1}{y_{lh}}\left[\ln\frac{Q_h^2}{m^2} + \ln\frac{(1-y_l)^2}{x_h y_h r - (1-y_l)(1-y_{lh})}\right], \tag{D.60}$$

$$\left\{\frac{m^2}{z_1^2}\right\}^{\rm III}_{Qz} = 0, \tag{D.61}$$

$$\left\{\frac{m^2}{z_2^2}\right\}^{\rm III}_{Qz} = \frac{1-y_l}{y_{lh}(1-y_h)}. \tag{D.62}$$

The third integration is:

$$(\mathcal{A})_{yQz} = \int_{y_l^{\min}(\epsilon)}^{y_{l_3}} dy_l \{\mathcal{A}\}^{\rm I}_{Qz} + \int_{y_{l_3}}^{y_{l_2}} dy_l \{\mathcal{A}\}^{\rm II}_{Qz} + \int_{y_{l_2}}^{\bar{y}_l} dy_l \{\mathcal{A}\}^{\rm III}_{Qz}. \tag{D.63}$$

And the results of the integrations are

$$\left(\frac{Q_h^2}{z_1 z_2}\right)_{yQz} = \ln\frac{Q_h^2}{m^2}\ln\frac{(1-y_h)^2 S^2}{4\epsilon^2 M^2} + {\rm Li}_2(1-y_h) - {\rm Li}_2(1), \tag{D.64}$$

$$\left(\frac{m^2}{z_1^2}\right)_{yQz} = \ln\left(\frac{S}{2\epsilon M}\frac{1-y_h}{y_h}\right), \tag{D.65}$$

$$\left(\frac{m^2}{z_2^2}\right)_{yQz} = \ln\frac{(1-y_h)S}{2\epsilon M} - 1. \tag{D.66}$$

From (D.64)–(D.66), (4.37) follows immediately.

D.4 The second integration for $\delta_{\rm R}^{\rm F}$. Mixed and hadronic variables

When performing the integration over y_l at given values of y_h, Q_h^2, and Q_l^2 within the limits ${y_l}^{min}$ and ${y_l}^{max}$, one faces eleven types of integrals which should be treated separately in regions I and II of figure 39.

For details of their definitions see the appendices B.3.3 for the case of mixed and B.4.3 for hadronic variables.

The integrals are:

$$[\mathcal{A}]_y = S\int_{y_l^{\min}}^{y_l^{\max}} dy_l\, \mathcal{A}. \tag{D.67}$$

Integrals for region I with $Q_l^2 > Q_h^2$:

$$\left[\frac{1}{\sqrt{\lambda_q}}\right]^{\rm I}_y = \ln\left(\frac{Q_h^2}{y_h Q_l^2}\right), \tag{D.68}$$

$$\left[\frac{1}{\sqrt{C_1}}\right]^{\rm I}_y = \frac{1}{Q_l^2}\ln\left[\frac{Q_l^2}{m^2}\frac{\left(1-\frac{y_h Q_l^2}{Q_h^2}\right)}{\left(1-\frac{Q_h^2}{Q_l^2}\right)}\right], \tag{D.69}$$

$$\left[\frac{1}{\sqrt{C_2}}\right]_y^{\rm I} = \frac{1}{Q_h^2}\ln\left[\frac{1-y_h}{1-\frac{Q_h^2}{Q_l^2}}\right], \tag{D.70}$$

$$\left[\frac{y_l}{\sqrt{C_1}}\right]_y^{\rm I} = \frac{Q_h^2-y_hQ_l^2}{Q_l^4}\left(2-\frac{Q_l^2}{Q_h^2}\right)+\frac{Q_l^2-Q_h^2+y_hQ_l^2}{Q_l^2}\left[\frac{1}{\sqrt{C_1}}\right]_y^{\rm I}, \tag{D.71}$$

$$\left[\frac{y_l}{\sqrt{C_2}}\right]_y^{\rm I} = \frac{Q_h^2-y_hQ_l^2}{Q_h^4}+\frac{Q_h^2-Q_l^2+y_hQ_l^2)}{Q_h^2}\left[\frac{1}{\sqrt{C_2}}\right]_y^{\rm I}, \tag{D.72}$$

$$\left[\sqrt{C_1}\right]_y^{\rm I} = S^2(Q_h^2-y_hQ_l^2)^2\left(\frac{Q_l^2}{2Q_h^4}+\frac{1}{Q_l^2}-\frac{1}{Q_h^2}\right), \tag{D.73}$$

$$\left[\sqrt{C_2}\right]_y^{\rm I} = S^2(Q_h^2-y_hQ_l^2)\left(-\frac{y_hQ_l^2}{2Q_h^2}+\frac{Q_l^2}{Q_h^2}-\frac{1}{2}\right), \tag{D.74}$$

$$\left[\frac{m^2}{C_1^{3/2}}\right]_y^{\rm I} = \frac{Q_l^2}{2S^2(Q_h^2-y_hQ_l^2)(Q_l^2-Q_h^2)^2}, \tag{D.75}$$

$$\left[\frac{m^2}{C_2^{3/2}}\right]_y^{\rm I} = 0, \tag{D.76}$$

$$\left[\frac{m^2y_l}{C_1^{3/2}}\right]_y^{\rm I} = \frac{Q_l^2-Q_h^2+y_hQ_l^2}{2S^2(Q_h^2-y_hQ_l^2)(Q_l^2-Q_h^2)^2}, \tag{D.77}$$

$$\left[\frac{m^2y_l}{C_2^{3/2}}\right]_y^{\rm I} = 0. \tag{D.78}$$

Integrals for region II with $Q_l^2 < Q_h^2$:

$$\left[\frac{1}{\sqrt{\lambda_q}}\right]_y^{\rm II} = \ln\left(\frac{1}{y_h}\right), \tag{D.79}$$

$$\left[\frac{1}{\sqrt{C_1}}\right]_y^{\rm II} = \frac{1}{Q_l^2}\ln\left[\frac{1-\frac{y_hQ_l^2}{Q_h^2}}{1-\frac{Q_l^2}{Q_h^2}}\right], \tag{D.80}$$

$$\left[\frac{1}{\sqrt{C_2}}\right]_y^{\rm II} = \frac{1}{Q_h^2}\ln\left[\frac{Q_l^2(1-y_h)}{m^2\left(1-\frac{Q_l^2}{Q_h^2}\right)}\right], \tag{D.81}$$

$$\left[\frac{y_l}{\sqrt{C_1}}\right]_y^{\rm II} = \frac{1-y_h}{Q_l^2}+\frac{Q_l^2-Q_h^2+y_hQ_l^2}{Q_l^2}\left[\frac{1}{\sqrt{C_1}}\right]_y^{\rm II}, \tag{D.82}$$

$$\left[\frac{y_l}{\sqrt{C_2}}\right]_y^{\rm II} = \frac{(1-y_h)(2Q_l^2-Q_h^2)}{Q_h^4}+\frac{Q_h^2-Q_l^2+y_hQ_l^2}{Q_h^2}\left[\frac{1}{\sqrt{C_2}}\right]_y^{\rm II}, \tag{D.83}$$

$$\left[\sqrt{C_1}\right]_y^{\rm II} = (1-y_h)S^2\left[Q_h^2-\frac{(1+y_h)Q_l^2}{2}\right], \tag{D.84}$$

$$\left[\sqrt{C_2}\right]_y^{\rm II} = (1-y_h)^2S^2\left[\frac{Q_l^4}{Q_h^2}-Q_l^2+\frac{Q_h^2}{2}\right], \tag{D.85}$$

$$\left[\frac{m^2}{C_1^{3/2}}\right]_y^{\rm II} = 0, \tag{D.86}$$

$$\left[\frac{m^2}{C_2^{3/2}}\right]_y^{\rm II} = \frac{1}{2(1-y_h)(Q_l^2-Q_h^2)^2S^2}, \tag{D.87}$$

$$\left[\frac{m^2y_l}{C_1^{3/2}}\right]_y^{\rm II} = 0, \tag{D.88}$$

$$\left[\frac{m^2y_l}{C_2^{3/2}}\right]_y^{\rm II} = \frac{Q_h^2-Q_l^2+y_hQ_l^2}{2Q_h^2(1-y_h)(Q_l^2-Q_h^2)^2S^2}. \tag{D.89}$$

E Tables of integrals for section 7

E.1 The $\cos\vartheta_R, \varphi_R$-integrals

The integrals are defined as follows:

$$[\mathcal{A}]_{\varphi_R} = \frac{1}{2\pi}\int_0^{2\pi} d\varphi_R \mathcal{A}, \tag{E.1}$$

$$[1]_{\varphi_R} = 1, \tag{E.2}$$

$$[1-y_l]_{\varphi_R} = A, \tag{E.3}$$

$$\left[(1-y_l)^2\right]_{\varphi_R} = A^2+\frac{1}{2}B^2. \tag{E.4}$$

The following abbreviations are used:

$$A = \frac{1}{2\tau}\left\{(1-y_h)(\tau+m^2)+\frac{z_2}{\sqrt{\lambda_1}}\left[Q_h^2-z_2-y_h(Q_h^2+\tau+m^2)\right]\cos\vartheta_R\right\}, \tag{E.5}$$

$$B = \frac{z_2}{2\tau S}\sqrt{\lambda_\tau}\sin\vartheta_p\sin\vartheta_R. \tag{E.6}$$

After applying these exact formulae, in a second step the following integrals are applied:

$$[\mathcal{A}]_{\vartheta_R} = \frac{1}{2}\int_{-1}^{1}\mathcal{A}, \tag{E.7}$$

$$[1]_{\vartheta_R} = 1, \tag{E.8}$$

$$[\cos\vartheta_R]_{\vartheta_R} = 0, \tag{E.9}$$

$$\left[\frac{1}{z_1}\right]_{\vartheta_R} = \frac{\tau}{z_2}\frac{1}{\sqrt{\lambda_1}}\ln\frac{Q_h^2+\tau+m^2+\sqrt{\lambda_1}}{Q_h^2+\tau+m^2-\sqrt{\lambda_1}}, \tag{E.10}$$

$$\left[\frac{1}{z_1^2}\right]_{\vartheta_R} = \frac{\tau}{z_2}\frac{1}{m^2z_2}. \tag{E.11}$$

In ultra-relativistic approximation:

$$\ln\frac{Q_h^2+\tau+m^2+\sqrt{\lambda_1}}{Q_h^2+\tau+m^2-\sqrt{\lambda_1}} \approx \mathrm{L}_\tau, \tag{E.12}$$

and

$$\left[\frac{1}{z_1}\right]_{\vartheta_R} \approx \frac{1}{Q_\tau^2}\mathrm{L}_\tau. \tag{E.13}$$

The L_τ and Q_τ^2 are defined in (7.16) and (7.17), respectively.

The twofold integrals over the two photon angles, $\mathcal{J}^R[\mathcal{A}] = (\tau - m^2)/(4\pi\tau)\int d\Omega_R \mathcal{A}$, with $\mathcal{A} = 1/z_1$ and $\mathcal{A} = 1/z_1^2$ agree exactly with those which have been calculated for bremsstrahlung problems in e^+e^- annihilation in [76].

E.2 The third integration for $\delta_{\mathrm{hard}}^{\mathrm{IR}}$

In the integration of the infrared divergent part of the cross-section we use the following regularized integrals for the integration of the hard, finite contributions in hadronic variables:

$$[\mathcal{A}]_z^h = \int_{\bar{z}_2}^{\tau^{\max}} dz_2 \mathcal{A}, \tag{E.14}$$

with $\bar{z}_2 = 2m\epsilon$, and $\tau^{\max} = Q_h^2(1-y_h)/y_h$, see (B.94).

In the case of Jaquet-Blondel variables, the upper boundary differs:

$$[\mathcal{A}]_z^{\mathrm{JB}} = \int_{\bar{z}_2}^{\tau^{\max}} dz_2 \mathcal{A}, \tag{E.15}$$

with $\tau^{\max} = (1-x_{\mathrm{JB}})(1-y_{\mathrm{JB}})S$, see (B.106).

The integrals are:

$$\left[\frac{1}{z_2}\right]_z^h = \ln\left(\frac{Q_h^2}{2m\epsilon}\frac{1-y_h}{y_h}\right), \tag{E.16}$$

$$\left[\frac{\mathrm{L}_\tau}{z_2}\right]_z^h = 2\ln\frac{Q_h^2}{m^2}\ln\left(\frac{Q_h^2}{2m\epsilon}\frac{1-y_h}{y_h}\right) - \frac{1}{2}\ln^2\left(\frac{Q_h^2}{m^2}\frac{1-y_h}{y_h}\right) - 2\mathrm{Li}_2\left(1-\frac{1}{y_h}\right) - \mathrm{Li}_2(1), \tag{E.17}$$

$$\left[\frac{1}{z_2}\right]_z^{\mathrm{JB}} = \ln\frac{(1-x_{\mathrm{JB}})(1-y_{\mathrm{JB}})S}{2m\epsilon}, \tag{E.18}$$

$$\left[\frac{\mathrm{L}_\tau}{z_2}\right]_z^{\mathrm{JB}} = 2\ln\frac{Q_{\mathrm{JB}}^2}{m^2}\ln\frac{(1-x_{\mathrm{JB}})(1-y_{\mathrm{JB}})S}{2m\epsilon} - \frac{1}{2}\ln^2\frac{(1-x_{\mathrm{JB}})(1-y_{\mathrm{JB}})S}{m^2} - 2\mathrm{Li}_2\left(1-X_{\mathrm{JB}}\right) - \mathrm{Li}_2(1), \tag{E.19}$$

where

$$X_{\mathrm{JB}} = \frac{1-x_{\mathrm{JB}}(1-y_{\mathrm{JB}})}{x_{\mathrm{JB}}y_{\mathrm{JB}}}. \tag{E.20}$$

The regular integrals may be found in appendix E.3.

E.3 The third integration for $\delta_{\mathrm{R}}^{\mathrm{F}}$

A second series of integrals over z_2 is used in order to perform analytically even the last, third integration in case of hadronic variables. Here, this integration corresponds to an integral over the invariant mass τ; see the discussion in section 7.4.

The finite integrals over z_2 or, equivalently, over τ, are defined as follows:

$$[\mathcal{A}]_\tau^h = \int_{m^2}^{\tau^{\max}} d\tau \mathcal{A}, \tag{E.21}$$

$$[\mathcal{A}]_\tau^{\rm JB} = \int_{m^2}^{\tau^{\max}} d\tau \mathcal{A}. \tag{E.22}$$

Here, at the upper integration limit the ultra-relativist approximation may be applied: $\tau^{\max} \approx z_2^{\max} = Q_h^2(1-y_h)/y_h$ in the case of hadronic variables, and $\tau^{\max} \approx z_2^{\max} = (1-x_{\rm JB})(1-y_{\rm JB})S$ in the case of Jaquet-Blondel variables.

The integrals are:

$$[1]_\tau^h = Q_h^2 \frac{1-y_h}{y_h}, \tag{E.23}$$

$$\left[\frac{1}{\tau}\right]_\tau^h = \ln\left(\frac{Q_h^2}{m^2}\frac{1-y_h}{y_h}\right), \tag{E.24}$$

$$\left[\frac{1}{\tau^2}\right]_\tau^h = \frac{1}{m^2}, \tag{E.25}$$

$$\left[\frac{1}{Q_\tau^6}\right]_\tau^h = \frac{1}{2}(1-y_h^2)\frac{1}{Q_h^4}, \tag{E.26}$$

$$\left[\frac{1}{Q_\tau^4}\right]_\tau^h = (1-y_h)\frac{1}{Q_h^2}, \tag{E.27}$$

$$\left[\frac{1}{Q_\tau^2}\right]_\tau^h = \ln\frac{1}{y_h}, \tag{E.28}$$

$$[\mathrm{L}_\tau]_\tau^h = \frac{Q_h^2}{y_h}\left\{2\ln\frac{1}{y_h} + (1-y_h)\left[2\ln\frac{Q_h^2}{m^2} - \ln\left(\frac{Q_h^2}{m^2}\frac{1-y_h}{y_h}\right) - 1\right]\right\}, \tag{E.29}$$

$$\left[\frac{\mathrm{L}_\tau}{Q_\tau^2}\right]_\tau^h = \ln^2 y_h - \ln y_h \ln\frac{Q_h^2}{m^2} + \mathrm{Li}_2\left(\frac{1}{y_h}\right) - \mathrm{Li}_2(1), \tag{E.30}$$

$$\left[\frac{\mathrm{L}_\tau}{Q_\tau^4}\right]_\tau^h = \frac{1}{Q_h^2}\left[-(1-2y_h)\ln y_h + (1-y_h)\left(\ln\left(\frac{Q_h^2}{m^2}\frac{y_h}{1-y_h}\right) + 2\right)\right], \tag{E.31}$$

$$\left[\frac{\mathrm{L}_\tau}{Q_\tau^6}\right]_\tau^h = \frac{1}{2Q_h^4}\left[-(1-2y_h^2)\ln y_h + (1-y_h^2)\ln\left(\frac{Q_h^2}{m^2}\frac{y_h}{1-y_h}\right) + (1-y_h)(2+y_h)\right]. \tag{E.32}$$

Further,

$$\left[\frac{1}{\tau}\right]_\tau^{\rm JB} = \ln\frac{(1-x_{\rm JB})(1-y_{\rm JB})S}{m^2}, \tag{E.33}$$

$$\left[\frac{\mathrm{L}_\tau}{Q_\tau^2}\right]_\tau^{\rm JB} = (1-y_{\rm JB})\left[\ln^2 X_{\rm JB} + \ln X_{\rm JB}\ln\frac{Q_{\rm JB}^2}{m^2(1-y_{\rm JB})} + \mathrm{Li}_2(X_{\rm JB}) - \mathrm{Li}_2(1)\right], \tag{E.34}$$

where the $X_{\rm JB}$ is defined in (E.20).

F Leading logarithmic approximations

In the leading logarithmic approximation, the $\mathcal{O}(\alpha)$ corrections consist of initial state radiation, final state radiation, and the Compton peak contribution,

$$\frac{d^2\sigma^{\mathrm{R}}}{dxdy} = \frac{d^2\sigma^i}{dxdy} + \frac{d^2\sigma^f}{dxdy} + \frac{d^2\sigma^C}{dxdy}, \tag{F.1}$$

where the latter contribution exists only for leptonic and mixed variables. For leptonic variables it is numerically important:

$$\frac{d^2\sigma^C}{dx_l dy_l} = \frac{\alpha^3}{x_l S}\left[1+(1-y_l)^2\right]\ln\frac{Q_l^2}{M^2}\int\limits_{x_l}^1 \frac{dz}{z^2}\frac{z^2+(x_l-z)^2}{x_l(1-y_l)}\sum_f\left[q_f(z,Q_l^2)+\bar{q}_f(z,Q_l^2)\right]. \tag{F.2}$$

The other two cross-sections have the following structure:

$$\frac{d^2\sigma^a}{dxdy} = \int\limits_0^1 dz\left[\frac{\alpha}{2\pi}\left(\ln\frac{Q_a^2}{m^2}\right)\frac{1+z^2}{1-z}\right]\left\{\theta(z-z_0)\mathcal{J}(x,y,Q^2)\left.\frac{d^2\sigma^0}{dxdy}\right|_{x=\hat{x},y=\hat{y},S=\hat{S}} - \frac{d^2\sigma^0}{dxdy}\right\}. \tag{F.3}$$

For the different sets of variables, the definitions of the $\hat{x},\hat{y},\hat{S}$, as well as the lower integration boundary z_0, differ. For leptonic variables, they are well-known since long; see, e.g. [15, 73]. For the cases of mixed and Jaquet-Blondel variables, they have been derived in [70] and for further sets of variables in [72] where also the formulae for higher order LLA corrections with soft photon exponentiation are collected and numerically discussed.

The formulae which were used for our comparisons in section 8.2 may be found in table 1.

In the case of Jaquet-Blondel variables, the hadronic final state is treated totally inclusive. Thus, in accordance with the Kinoshita-Lee-Nauenberg theorem [77] there is no LLA correction from final state radiation. One should also mention that a gauge invariant separation of initial and final state radiation is possible for the leading logarithmic corrections but not for the complete order $\mathcal{O}(\alpha)$.

In (F.3), it is

$$\hat{x} = \frac{\hat{Q}^2}{\hat{y}\hat{S}}, \tag{F.4}$$

$$\mathcal{J}(x,y,Q^2) = \left|\frac{\partial(\hat{x},\hat{y})}{\partial(x,y)}\right|, \tag{F.5}$$

$$\hat{x}(z_0) = 1. \tag{F.6}$$

From the last equation, the lower integration boundary derives. In the case of mixed variables, e.g., one gets $z_0 = y$ for initial state radiation and $z_0 = x$ for final state radiation.

	Initial state radiation			Final state radiation		
Variables	leptonic	Jaquet-Blondel	mixed	leptonic	Jaquet-Blondel	mixed
$\hat{y}$	$\frac{z+y-1}{z}$	$\frac{y}{z}$	$\frac{y}{z}$	$\frac{z+y-1}{z}$	–	y
$\hat{S}$	zS	zS	zS	S	–	S
$\hat{Q}^2$	zQ^2	$\frac{1-y}{1-y/z}Q^2$	zQ^2	$\frac{Q^2}{z}$	–	$\frac{Q^2}{z}$

Table 1: The definition of scaling variables for the different leading logarithmic cross-sections.

References

[1] E. Bloom et al., *Phys. Rev. Letters* **23** (1969) 930;
M. Breidenbach et al., *Phys. Rev. Letters* **23** (1969) 935;
R. Taylor, in: Proceedings of the 4th Int. Conference on Electron and Photon Interactions at High Energies, Liverpool, 1969 (Daresbury Nuclear Physics Lab., Daresbury, 1969), p. 251; *Rev. Mod. Phys.* **63** (1991) 573.

[2] L. Mo and Y. Tsai, *Rev. Mod. Phys.* **41** (1969) 205;
Y.S Tsai, preprint SLAC-Pub-848 (1971).

[3] BCDMS Collaboration, A. Benvenuti et al., *Phys. Letters* **B195** (1987) 91; **B223** (1988) 485; **B237** (1990) 592.

[4] A. Akhundov and D. Bardin, JINR Dubna preprint P2-9587 (1976).

[5] A. Akhundov, D. Bardin and N. Shumeiko, JINR Dubna preprint E2-10147 (1976); ibid., E2-10205 (1976); *Sov. J. Nucl. Phys.* **26** (1977) 660.

[6] D. Bardin and N. Shumeiko, *Nucl. Phys.* **B127** (1977) 242.

[7] N. Shumeiko, *Sov. J. Nucl. Phys.* **29** (1979) 807.

[8] A. Akhundov, D. Bardin and N. Shumeiko, *Sov. J. Nucl. Phys.* **32** (1980) 234.

[9] A. Akhundov, D. Bardin and N. Shumeiko, *Sov. J. Nucl. Phys.* **44** (1986) 988.

[10] E. Derman, *Phys. Rev.* **D7** (1973) 2755.

[11] A. Akhundov, D. Bardin and W. Lohmann, Fortran program `TERAD86` and JINR Dubna preprint E2-86-104 (1986);
A. Akhundov and W. Lohmann, IfH Zeuthen preprint PHE 90-32 (1990).

[12] B. Badelek, D. Bardin, K. Kurek and C. Scholz, Uppsala Univ. preprint TSL/ISV-94-0092 (1994);
see also: P. Kuzhir and N. Shumeiko, *Sov. J. Nucl. Phys.* **55** (1992) 1086.

[13] D. Bardin and N. Shumeiko, *Sov. J. Nucl. Phys.* **29** (1979) 499;
D. Bardin, O. Fedorenko and N. Shumeiko, *J. Phys.* **G7** (1981) 1331;
D. Bardin, P. Christova and O. Fedorenko, Fortran program `ASYMETR`.

[14] D. Bardin, C. Burdik, P. Christova and T. Riemann, contribution to the 1987 Workshop on Physics at HERA, JINR Dubna preprint E2-87-595 (1987); *Z. Physik* **C42** (1989) 679; Fortran program `DISEPNC`, which is a branch of the Fortran program `TERAD91` [38].

[15] M. Consoli and M. Greco, *Nucl. Phys.* **B186** (1981) 519.

[16] D. Bardin, C. Burdik, P. Christova and T. Riemann, *Z. Physik* **C44** (1989) 149; Fortran program `DISEPCC`, which is a branch of the Fortran program `TERAD91` [38].

[17] A. Akhundov, D. Bardin, P. Christova, S. Riemann, T. Riemann, M. Sachwitz and H. Vogt, Fortran program `DIZET` version 4.04 (21 Aug. 1991), which is a branch of the Fortran program `TERAD91` [38]; version 2 was described in: D. Bardin, M. Bilenky, T. Riemann, M. Sachwitz and H. Vogt, *Comput. Phys. Commun.* **59** (1990) 303.

[18] T. Sloan, G. Smadja and R. Voss, *Phys. Repts.* **C162** (1988) 45;
BCDMS Collaboration, A. Benvenuti et al., *Phys. Letters* **B237** (1990) 592;
NMC Collaboration, P. Amaundruz et al., *Phys. Letters* **B295** (1992) 159.

[19] E665 Collaboration, M. Adams et al., preprint Fermilab-Pub-93-171 (1993), subm. to *Phys. Rev. Letters.*

[20] U. Amaldi (ed.), Proceedings of the Study of an *ep* Facility for Europe, DESY 79-48 (1979) 391.

[21] R. D. Peccei (ed.), Proceedings of the Workshop *Physics at HERA*, Hamburg, October 12-14, 1987 (DESY, Hamburg, 1988).

[22] W. Buchmüller and G. Ingelman (eds.), Proceedings of the Workshop *Physics at HERA*, Hamburg, October 29-30, 1991 (DESY, Hamburg, 1992).

[23] CHARM Collaboration, J. Allaby et al., *Phys. Letters* **B213** (1988) 554;
CDHSW Collaboration, A. Blondel et al., *Z. Physik* **C49** (1991) 187;
CCFR Collaboration, S. A. Rabinowitz et al., *Phys. Rev. Letters* **70** (1993)134.

[24] F. Brasse, in: J. Sanford (ed.), Proceedings of the XXVIth International Conference on High Energy Physics, Aug. 6–12 1992, Dallas (Texas) (American Institute of Physics, New York, 1993), AIP Conference Proceedings No. 272, p. 1849, and preprint DESY 92–140 (1992);
H1 Collaboration, I. Abt et al., *The H1 detector at HERA*, preprint DESY 93–103 (1993), subm. to *Nucl. Instr. Meth.*.

[25] ZEUS Collaboration, M. Derrick et al., *Phys. Letters* **B293** (1992) 465.

[26] J. Blümlein and M. Klein, in: E. Berger (ed.), Proceedings of the Workshop on Research Directions of the Decade, Snowmass 1990 (World Scientific, Singapore, 1992), p. 549.

[27] S. Bentvelsen, J. Engelen and P. Kooijman, in: W. Buchmüller and G. Ingelman (eds.), Proceedings of the Workshop on Physics at HERA, Oct. 29–30, 1991, Hamburg (DESY, Hamburg, 1992), Vol. 1, p. 23.

[28] A. Blondel and F. Jaquet, in: U. Amaldi (ed.), Proceedings of the Study of an *ep* Facility for Europe, DESY 79-48 (1979) 391.

[29] H. Spiesberger et al., in: W. Buchmüller and G. Ingelman (eds.), Proceedings of the Workshop on Physics at HERA, Hamburg (1991), Vol. 2, p. 798;
G. Kramer and H. Spiesberger, ibid., p. 789.

[30] W. Beenakker, F. Berends and W. van Neerven, in: J. Kühn (ed.), Proceedings of the Workshop on Radiative Corrections for e^+e^- Collisions, Schloß Ringberg, Tegernsee, April 1989 (Springer, Berlin, 1989), p. 3.

[31] G. Montagna, O. Nicrosini and L. Trentadue, *Nucl. Phys.* **B357** (1991) 390.

[32] J. Blümlein, *Z. Physik* **C47** (1990) 89.

[33] J. Blümlein, Fortran program `HELIOS`; a short write-up may be found in: W. Buchmüller and G. Ingelman (eds.), Proceedings of the Workshop on Physics at HERA, Hamburg (1991), Vol. 3, p. 1270.

[34] J. Kripfganz, H. Möhring, H. Spiesberger, *Z. Physik* **C49** (1991) 501.

[35] A. Kwiatkowski, H. Möhring and H. Spiesberger, Fortran program `HERACLES`, *Comput. Phys. Commun.* **69** (1992) 155; a short write-up of v. 4.1 (1991) in: W. Buchmüller and G. Ingelman (eds.), Proceedings of the Workshop on Physics at HERA, Hamburg (1991), Vol. 3, p. 1294.

[36] W. Placzek, Fortran program `LESKO`, in: W. Buchmüller and G. Ingelman (eds.), Proceedings of the Workshop on Physics at HERA, Hamburg (1991), Vol. 3, p. 1433.

[37] H. Anlauf, H. Dahmen, P. Manakos, T. Mannel and T. Ohl, Fortran program `KRONOS`, in: J. Blümlein and T. Riemann (eds.), Proceedings of the Zeuthen Workshop on Elementary Particle Theory – Deep Inelastic Scattering, Teupitz, April 1992, *Nucl. Phys.* **B** (Proc. Suppl.) **29A** (1992) 247.

[38] A. Akhundov, D. Bardin, L. Kalinovskaya and T. Riemann, Fortran program `TERAD91`; a short write-up may be found in: W. Buchmüller and G. Ingelman (eds.), Proceedings of the Workshop on Physics at HERA, Hamburg (1991), Vol. 3, p. 1285; see also [44].

[39] A. Akhundov, D. Bardin, C. Burdik, P. Christova and L. Kalinovskaya, *Z. Physik* **C45** (1990) 645.

[40] M. Böhm and H. Spiesberger, *Nucl. Phys.* **B294** (1987) 1081; ibid., **B304** (1987) 749; see also the corrected numerical results in [42].

[41] H. Spiesberger, Fortran program `EPRC91`, *Nucl. Phys.* **B349** (1991) 109 .

[42] W. Hollik, in: N. Dombey and F. Boudjema (eds.), Proceedings of the Workshop on Radiative Corrections: Results and Perspectives, Brighton, July 10-14, 1989 (Plenum Press, New York, 1990), p. 467.

[43] A. Akhundov, D. Bardin, L. Kalinovskaya and T. Riemann, *Phys. Letters* **301B** (1993) 447.

[44] D. Bardin, A. Akhundov, L. Kalinovskaya and T. Riemann, in: J. Blümlein and T. Riemann (eds.), Proceedings of the Zeuthen Workshop on Elementary Particle Theory – Deep Inelastic Scattering, Teupitz, April 1992, *Nucl. Phys.* **B** (Proc. Suppl.) **29A** (1992) 209.

[45] G. Jarlskog and D. Rein (eds.), Proceedings of the Large Hadron Collider Workshop, Aachen, 4–9 Oct. 1990, CERN 90–10 (1990).

[46] S.M. Bilenky, *Introduction to the Physics of Electroweak Interaction* (Pergamon Press, 1982).

[47] W. Hollik et al., in: W. Buchmüller and G. Ingelman (eds.), Proceedings of the Workshop on Physics at HERA, Hamburg (1991), Vol. 2, p. 923.

[48] J. Blümlein, A. Leike and T. Riemann, in: G. Jarlskog and D. Rein (eds.), Proceedings of the Large Hadron Collider Workshop, Aachen, 4–9 Oct. 1990, CERN 90–10 (1990), Vol. II, p. 1010.

[49] J. Blümlein, lecture held at the St. Petersburg Winter School on Theoretical High Energy Physics, Gatchina, Russia, 1993, in: *Surveys in High Energy Physics* **7** (1994) 181;
G. Wolf, lectures held at the 42nd Scottish Universities Summer School in Physics, 1993, preprint DESY 94–022 (1994).

[50] C. Callan and D. Gross, *Phys. Rev. Letters* **22** (1969) 156.

[51] A. Martin, W. Stirling and R. Roberts, *Phys. Letters* **306B** (1993) 145, E: ibid. **309B** (1993) 492.

[52] A. Martin, W. Stirling and R. Roberts, in: H. Plothow-Besch, PDFLIB: Nucleon, Pion and Photon Parton Density Functions and α_s Calculations, version 4.17 (1994), CERN Program Library entry W5051, Item 1-3-34.

[53] M. Veltman, program for analytical manipulations `SCHOONSCHIP`.

[54] H. Spiesberger, private communication.

[55] F. Low, *Phys. Rev.* **110** (1958) 974.

[56] W. Marciano and A. Sirlin, *Nucl. Phys.* **B88** (1975) 86.

[57] D. Bardin and V. Dokuchaeva, *Nucl. Phys.* **B246** (1984) 221.

[58] G. Schuler, in: W. Buchmüller and G. Ingelman (eds.), Proceedings of the Workshop on Physics at HERA, Hamburg (1991), Vol. 1, p. 461.

[59] J. Jersak, E. Laermann and P. Zerwas, *Phys. Rev.* **D25** (1981) 1218; *Phys. Letters* **B98** (1981) 363; A. Arbuzov, D. Bardin and A. Leike, *Mod. Phys. Letters* **A7** (1992) 2029.

[60] N. Volkonsky and L. Prokhorov, *Sov. J. Exp. Theor. Phys. Letters* **21** (1975) 389.

[61] D. Duke and J. Owens, *Phys. Rev.* **D30** (1984) 49.

[62] D. Duke and J. Owens, in: H. Plothow-Besch, PDFLIB: Nucleon, Pion and Photon Parton Density Functions and α_s Calculations, version 4.17 (1994), CERN Program Library entry W5051, Item 1-1-6.

[63] CTEQ Collaboration: J. Botts, J. Morfin, J. Owens, J. Qiu, Wu-Ki Tung and H. Weerts, *Phys. Letters* **B304** (1993) 159; preprint MSU-HEP 93/24 (1993).

[64] CTEQ Collaboration, in: H. Plothow-Besch, PDFLIB: Nucleon, Pion and Photon Parton Density Functions and α_s Calculations, version 4.17 (1994), CERN Program Library entry W5051, Item 1-4-22.

[65] A. Martin, W. Stirling and R. Roberts, Durham preprint DTP-93-86 (1993).

[66] A. Martin, W. Stirling and R. Roberts, in: H. Plothow-Besch, PDFLIB: Nucleon, Pion and Photon Parton Density Functions and α_s Calculations, version 4.17 (1994), CERN Program Library entry W5051, Item 1-3-36.

[67] CTEQ Collaboration, in: H. Plothow-Besch, PDFLIB: Nucleon, Pion and Photon Parton Density Functions and α_s Calculations, version 4.17 (1994), CERN Program Library entry W5051, Item 1-4-24.

[68] CTEQ Collaboration, in: H. Plothow-Besch, PDFLIB: Nucleon, Pion and Photon Parton Density Functions and α_s Calculations, version 4.17 (1994), CERN Program Library entry W5051, Item 1-4-17.

[69] J. Blümlein, G. Levman and H. Spiesberger, in: E. Berger (ed), Proceedings of the Workshop on Research Directions of the Decade, Snowmass 1990 (World Scientific, Singapore, 1992), p. 554; *J. Phys.* **G19** (1993) 1695.

[70] J. Blümlein, *Phys. Letters* **B271** (1991) 267.

[71] D. Bardin , P. Christova, L. Kalinovskaya and T. Riemann, Fortran program `TERAD91`, publication in preparation.

[72] J. Blümlein, preprint DESY 94-044 (1994).

[73] E. Kuraev, V. Fadin and N. Merenkov, *Sov. J. Nucl. Phys.* **41** (1985) 466 ;
E. Kuraev, N. Merenkov and V. Fadin, *Sov. J. Nucl. Phys.* **47** (1988) 1009.

[74] A. Arbuzov et al., Fortran program `HECTOR`. This program comprises `HELIOS` [33] and `TERAD` [38] within one interface, but also new options; a long write-up is in preparation.

[75] E. Byckling and K. Kajanti, *Particle Kinematics* (Mir, Moscow, 1975).

[76] A. Akhundov, D. Bardin, O. Fedorenko and T. Riemann, *Sov. J. Nucl. Phys.* **42** (1985) 762; JINR Dubna preprint E2-84-777 (1984).

[77] T. Kinoshita, *J. Math. Phys.* **B271** (1962) 267;
T.D. Lee and M. Nauenberg, *Phys. Rev.***133** (1964) B1549.